POLYMER-ZEOLITE NANOCOMPOSITES: PREPARATION, CHARACTERIZATION AND APPLICATION IN HEAVY-METAL REMOVAL

by

SYDNEY THABO MTHOMBO

Student Number: 200918170

Dissertation in fulfilment of the requirement for the degree

MASTER OF SCIENCE

in

CHEMISTRY

in the

FACULTY OF SCIENCE

of the

UNIVERSITY OF JOHANNESBURG

Supervisor	**:**	**PROF B.B. MAMBA**
Co-supervisor(s)	**:**	**DR A.K. MISHRA**
		DR S.B. MISHRA

DECLARATION

I hereby declare that this dissertation, which I herewith submit for the research qualification

MASTERS DEGREE IN CHEMISTRY

To the University of Johannesburg, Department of Chemical Technology, is, apart from the recognised assistance of my supervisors, my own work and has not previously been submitted by me to another institution to obtain a research diploma or degree.

_____ on this ____ day of _____

(Candidate)

_____ on this ____ day of _____

(Supervisor)

_____ on this ____ day of _____

(Co-supervisor)

_____ on this ____ day of _____

(Co-supervisor)

DEDICATION

This work is dedicated to my late mom, whom I wish could have lived longer... *“usheshe walala Mavundla ungakadli titselo tebatukulu”*

ACKNOWLEDGEMENTS

I owe my deepest gratitude to God Almighty for His unconditional love and guidance… To Thee Be Thy Glory!!

Financial support from the University of Johannesburg (UJ) National Research Fund (NRF) and the DST/Mintek Nanotechnology Innovation Centre (NIC) is greatly appreciated.

In putting together work of this magnitude, one needs encouragement, advice and assistance from everyone, and I wish to acknowledge the following persons for their contributions towards the success of this project:

1. My supervisors, Prof B.B. Mamba, Dr A.K. Mishra and Dr S.B. Mishra for their supervision, advice and technical guidance throughout the duration of this work.

2. UJ staff from the Departments of Chemical Technology, Metallurgy, Spectrau and Physical Chemistry for their assistance with the instruments that were required for the success of this study.

3. Mr James from Mintek and Ms Onica from the Sasol Polymer Technology Centre for their assistance and guidance in their different areas of expertise.

4. My postgraduate colleagues and friends from UJ's Department of Chemical Technology who were always willing to assist in the laboratory, and also read parts of this work and offered many helpful suggestions and constructive criticism.

5. My family and girlfriend, who have always been so supportive of my career and hobbies – the two, although often indistinguishable.

The work presented in this dissertation has already been submitted and accepted for publication in peer reviewed journals and presented in both national and international oral and poster presentation conferences.

Conferences attended

1. S.T. Mthombo, A.K. Mishra, S.B. Mishra & B.B. Mamba. *A study of the adsorption behaviour of Cu(II), Pb(II) and Co(II) onto novel ethylene vinyl acetate-clinoptilolite nanocomposites*: **Oral presentation**. 11th WaterNet/WARFSA/GWP-SA 27th – 29th October 2010*,* Victoria Falls, Zimbabwe*.*

2. S.T. Mthombo, A.K. Mishra, S.B. Mishra & B.B. Mamba. *Ethyl vinyl acetate-clinoptilolite nanocomposites for the removal of lead from water*: **Poster presentation**. 1st Young Water Professionals Conference in Southern Africa, 18th – 23rd January 2010, CSIR, Pretoria, South Africa

3. S.T. Mthombo, A.K. Mishra, S.B. Mishra & B.B. Mamba**.** *Synthesis and characterization of polymer-zeolite composites for the removal of heavy metals from water* – **Poster Presentation***.* 1st BIOMATASA Conference, 23rd – 25th September 2009, CSIR, Pretoria, South Africa.

Publications

1. S.T. Mthombo, A.K. Mishra, S.B. Mishra & B.B. Mamba. A study of the adsorption behaviour of Cu(II), Pb(II) and Co(II) onto novel ethylene vinyl acetate-clinoptilolite nanocomposites*.* (Accepted for publication in the *Journal of Applied Polymer Science*).

2. S.T., A.K. Mishra, S.B. Mishra & B.B. Mamba. Fabrication and characterization of natural and HCl-activated clinoptilolite filled ethylene vinyl acetate (EVA) nanocomposite films. (Submitted for publication in *Polymer Bulletin Journal*).

ABSTRACT

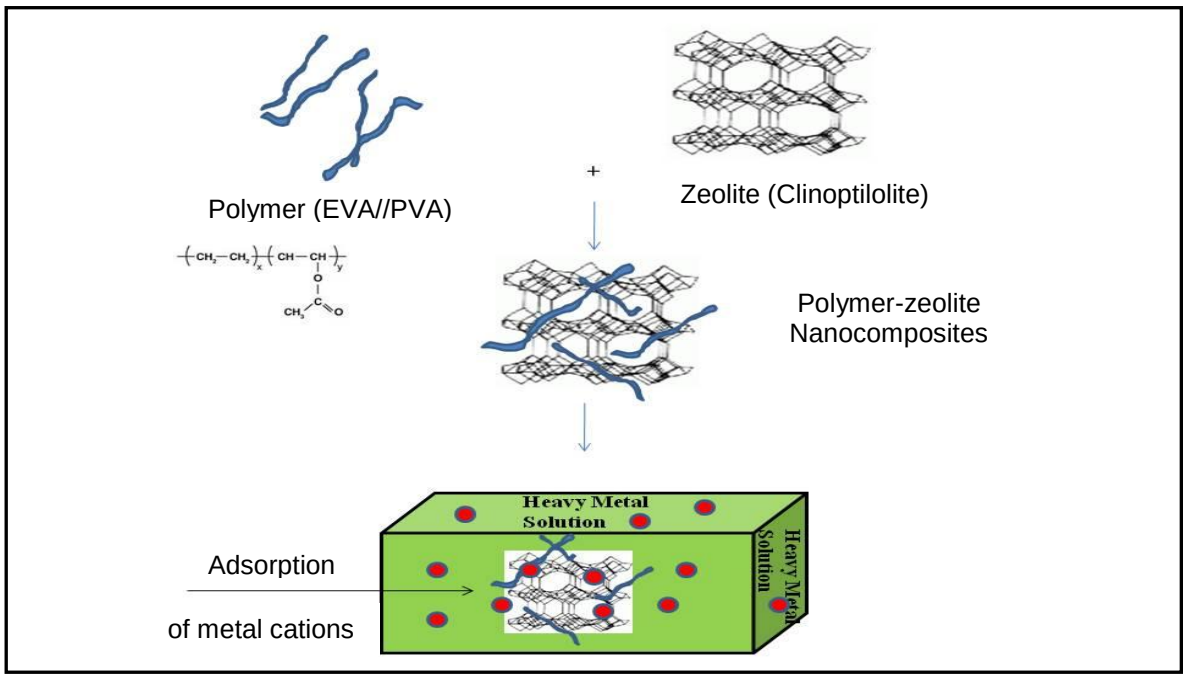

Polymer nanocomposites are a new class of composites in which at least one dimension of the particles dispersed in the polymer matrix is in the nanometer range. Recently, different types of zeolite minerals, either natural (Clinoptilolite, chabazite, modernite) or synthetic (A-type, X-type, Y-type) are being employed as particulate fillers into the polymer matrix. Owing to their unique ion exchange phenomenon, zeolites have been widely studied as heavy metal adsorbents, but very few researchers have focused on the sorption of heavy metal ions on zeolite-filled polymer nanocomposites.

In this study, the characteristics and application in wastewater treatment of PVA and EVA polymer nanocomposites filled with a natural zeolite, clinoptilolite (C), are discussed. The PVA/EVA-C were fabricated using the melt mixing technique in a rheomixer, then extruded at 130^{o}C to obtain 0.5 mm thick nanocomposite strips. The strips were then characterised for their morphology and chemical composition using SEM-EDS, XRD, XRF and FT-IR. Thermal properties were determined using TGA and DSC, while mechanical tests were carried out on an Instron machine. Heavy metal adsorption was studied in batch mode using single and mixed synthetic solutions of Cu(II), Pb(II), Co(II).

TABLE OF CONTENTS

Section ***Page***

LIST OF FIGURES

Figure ***Description*** ***Page***

No table of figures entries found.

LIST OF TABLES

LIST OF ABBREVIATIONS

AAS	Atomic absorption spectrometry
BET	Brunauer-Emmett-Teller
CEC	Cation-exchange capacity
DSC	Differential scanning calorimetry
EDX	Energy dispersive X-ray
EVA	Ethylene vinyl acetate
FT-IR	Fourier Transform Infrared
MMT	Montmorillonite
PLSN	Polymer-layered silicate nanocomposite
PVC	Polyvinyl chloride
SEM	Scanning electron microscopy
TEM	Transmission electron microscopy
TGA	Thermogravimetric analysis
XRD	X-ray diffraction
XRF	X-ray fluorescence

CHAPTER 1

INTRODUCTION

1.1 Background

Pollutants present in aquatic systems are often as a result of extensive agricultural and industrial activities such as mining, electroplating and petroleum refining.[1] These waters often contain, amongst other (organic) pollutants, toxic metals such as cadmium, silver and lead, as well as other non-metallic elements such as arsenic and selenium. Owing to the detrimental effects of these cationic species on the environment, several remediation techniques such as chlorination and chemical coagulation have been developed.[2] However, most of these techniques either produce toxic by-products or tend to precipitate the metal as one or two products. For example, chlorination results in the formation of chlorinated compounds that are toxic to living organisms. In view of these problems, an efficient treatment method has become imperative, in order to prevent contamination of the receiving waters to a degree which might interfere with their use, be it for drinking water supply, irrigation, recreation or any other required purpose.

1.2 Problem statement

Over the past decades, attention has been focused on the various adsorbents which have metal-binding capabilities and are capable of removing heavy metals from contaminated water at a generally low cost. Because of their low cost and natural availability, natural minerals such as chitosan, zeolites, clays and fly ash are often considered to be low-cost adsorbents.[4] Amongst these, zeolites have attracted more interest perhaps due to their ion-exchange capabilities and high affinity for divalent sorbates.[5] However, the existence of zeolites in powder form at nanoscale has been a major limitation. The aggregation of particles under different electrolytes leads to variations in the flow properties of the mineral, and this is an undesired feature for their use as sorbents. It therefore becomes imperative to

incorporate particular additives to counter-act this characteristic behaviour. In particular, incorporation of polymers enables the application of the mineral itself as an adsorbent confined in an isolated and practically usable medium in aquatic systems.[6] In this study, clinoptilolite, a zeolite, was incorporated into poly(vinyl alcohol) (PVA) and ethylene vinyl acetate (EVA) polymer matrices in the fabrication of PVA/EVA-zeolite composites. It was anticipated that the resultant nanocomposites would have enhanced adsorption properties more suitable for heavy-metal decontamination from aqueous media.

1.3 Justification

Particulate-filled polymer composites are a new class of composites with the ultimate goal of enhanced adsorption properties. Although an extensive amount of research work has been done in the fields of polymer-based composites, most of the studies were conducted with calcium carbonate, silver nanoparticles and clay, and very few studies have been reported with zeolites as the filler material.[7] PVA and EVA, though non-biodegradable, are highly hydrophilic polymers with excellent cohesive strength and adhesion to a wide range of substrates. Combining a zeolite having excellent mechanical, thermal and chemical properties, with a polymer, should result in a composite material with remarkably improved mechanical, thermal and physicochemical properties when compared with the pristine materials.

1.4 Objectives of the study

The principal objectives of this study were to investigate the potential of EVA/PVA-zeolite composites in the removal of Cu(II), Pb(II) and Co(II) from synthetic solutions for application in wastewater treatment. The mechanical and thermal properties of the composite materials were also studied. The specific objectives were as follows:

i. To investigate the optimum operational conditions for the removal of Cu(II), Pb(II) and Co(II) from aqueous solutions by means of a series of batch experiments

ii. To determine the effects of chemical conditioning of the filler material on the removal capacities of the zeolite-filled polymer composites in both single and mixed metal solutions

iii. To investigate the effects of zeolite loading and pretreatment on the thermal, mechanical and structural properties of the EVA/PVA-zeolite composite films

iv. To assess the applicability of the composites filled with natural and chemically conditioned zeolites on the removal of Cu(II), Pb(II) and Co(II) from real water samples obtained from a wastewater effluent.

v. To investigate the desorption capacity of the EVA/PVA-zeolite composites and their reusability in heavy-metal removal

1.5 Outline of the dissertation

A brief description and summary of each chapter are given in the dissertation outline below.

Chapter 2 (Literature Review)

This chapter covers most of the background literature related to this study. A review of the wastewater treatment techniques, and the detrimental effects caused by the presence of heavy metals in the environment is included. Furthermore, the preparation methods and characterization techniques of particulate-filled polymer composites are also discussed. Finally, the potential use of zeolite-based polymer composites as an additional treatment option during the tertiary stages of water treatment is explored.

Chapter 3 (Fabrication and Characterization of Natural and HCl-activated Zeolite-Filled Nanocomposite Films)

In this chapter, the experimental and analytical procedures used in the preparation and characterization of the zeolite and the EVA-zeolite composite materials are described. The results, discussions and conclusions drawn are also included.

Chapter 4 (Characterization of Natural Zeolite-Filled PVA Melt Extruded Nanocomposite Films)

This chapter discusses the structural, physicochemical and thermal properties of the PVA films filled with natural zeolite. The conclusions drawn from the discussion of results thus obtained are also included.

Chapter 5 (A Comparative Study on the adsorption of Cu(II), Pb(II) and Co(II) on Clinoptilolite-Filled EVA/PVA Nanocomposite Films)

Studies on the sorption of the Pb(II), Cu(II) and Co(II) by the composite materials are outlined in this chapter. The desorption and reusability of the materials in heavy-metal recovery are also discussed. The sorption data are given and conclusions are drawn.

Chapter 6 (General Conclusions and Recommendations)

The conclusions from Chapters 3, 4 and 5 are summarized in this chapter. Also included here are the recommendations for future work.

References: All literature sources cited in each chapter of the dissertation are listed at the end of the relevant chapter.

1.6 References

1. Kesraouni-Ouki S., Cheeseman C.R., Perry R. *J. Chem. Technol. Biotechnol,* **59** (2) (1994) 121-126.

2. Volesky B. *Microb. Rev.* **14** (1994) 291-392.

3. Reed S.C., Middlebrooks E.J., Crites R.W. *Natural Systems for Waste Management and Treatment*. McGraw-Hill, 1988.

4. Babel S and Kurniawan T.A. *J. Hazard. Mater. B* **97**: 219-243.

5. Erdem E., Karapinar N., Donat D. *J. Colloid Interface Sci.* **280** (2004) 309–314.

6. Ulosoy U. and Simsek S. *J. Hazard. Mater. B* **127** (2004) 309-314.

7. Pehlivan H., Balkose D., Ulku S., Tihminlioglu F. *Comp. Sci. Technol.* **65** (2005) 2049-2058.

CHAPTER 2

LITERATURE REVIEW

2.1 Introduction

This chapter reviews some of the detrimental effects caused by the presence of heavy metals in the environment, particularly in water systems. A brief review is given of the conventional methods used for heavy-metal recovery, as well as their limitations, and how the current study seeks to address these. Background information is given and the synthesis, properties and applications of polymer nanocomposites and their precursors are described in detail. In conclusion, the chapter highlights some of the principles behind characterization techniques that have been used in this study.

2.2 Heavy-metal toxicity

The accumulation of heavy metals in the environment, thereby causing heavy-metal poisoning has remained a major concern for the process industry. A heavy metal is described as a metallic element with specific gravity four or five times that of water[1], and they include metals such as arsenic, cadmium, copper, cobalt, iron, lead, mercury, silver, zinc, etc. Most heavy metals are non-toxic, unless ingested in large amounts. However, lead, cadmium, mercury and inorganic arsenic, often referred to as 'the big four' are amongst the most toxic metals, even at low concentrations.[2] Heavy-metal toxicity entails the alteration, removal or impartation of the production of specific molecules needed in the bodies of living organisms. Toxic metals target sites such as proteins, enzymes, and DNA molecules. At these sites, they can displace a specific molecule from its binding site, under the 'disguise' of being this molecule, a phenomenon called molecular mimicry.[3] The specific effects of the heavy metals investigated in this study are described in the sections that follow.

2.2.1 Copper

Copper is an essential trace element for all living organisms. The main source of copper for humans is dietary intake via foodstuffs and drinking water. In soft water regions, copper can be leached out in water pipes and therefore ingested via drinking water. In addition, carbonated drinks may contain appreciable amounts of copper.[4] In the blood, copper exists in two forms:

- About 85% to 95% is bound to the ceruloplasmin
- The remaining portion is loosely bound to albumin and other small molecules

It is this loosely bound copper that causes toxicity as it has the ability to accept and donate single electrons as it changes its oxidation state, and in essence, catalyzes the production of reactive species such as hydrogen peroxide and hydroxyl radicals. These charged species then cause severe damage to the proteins, lipids and DNA.[5]

2.2.2 Lead

Lead is a naturally occurring bluish-gray metal and is often present in the environment as a result of extensive practices of petroleum refining, electroplating, halogenations, etc., and is introduced into bodies of living organisms through inhalation of lead fumes or ingestion of lead salts in solution.[6] When it enters the bloodstream as Pb^{2+}, lead interferes with a variety of body processes, and is toxic to many organs and tissues including the heart, bones, kidneys and the nervous system. For example, Pb^{2+} interacts with the sulfhydryl groups in human protein and also impairs the synthesis of haemoglobin, resulting in severe disruptions in the metabolism and function of the brain, liver and kidneys. Other chronic effects include increased blood pressure, kidney malfunction and interference with the metabolism of vitamin D.[4] In plants, lead accumulates within the cell walls and intermolecular spaces, resulting in plant growth retardation.[6,7]

2.2.3 Cobalt

Cobalt is an essential element for health in animals in acceptable amounts as a component of vitamin B_{12}. However, like all other 'potentially harmless' heavy metals, excessive cobalt amounts in living organisms can be lethal. Cobalt commonly enters the environment via metal industries which recycle scrap metal that contains cobalt, as well as from the fabrication of tungsten. Pure cobalt is a steel-gray, shiny hard metal.[8] Although its toxicity is not well documented, cobalt has been implicated in dermatitis, as well as affecting the respiratory system in animals.[9]

For these reasons, the remediation, treatment and removal of heavy-metal ions from water has remained a major concern for many process industries, and the methods that have been used in wastewater treatment are summarised in the next section.

2.3 Summary of wastewater treatment methods

The conventional methods of wastewater treatment involve the collection of water in a central, segregated location (the wastewater treatment plant) in which the water is subjected to various treatment methods. These methods can be grouped, based on the nature of the treatment method being used, into physical, chemical or biological. Some of the physical methods include sedimentation, aeration and filtration. In these processes, no gross changes are implemented on the chemical state of the water. Instead, pollutants (mainly solids) are removed by physical means. The most common method is sedimentation, whereby solids are allowed to settle by means of gravity. In filtration, wastewater is passed through a filtration medium (e.g. sand filter) to remove entrained solids from the wastewater.[10]

Chemical methods involve the use of a chemical or a chemical process to remove pollutants from water. The most commonly used process is chlorination, whereby chlorine, an oxidizing agent, is used to kill bacteria and also to retard the rate of decomposition of the water.[11] Other oxidizing disinfectants that have been used

include ozone. Coagulation is another chemical process in which a coagulant, mainly polyvalent metals such as ferric sulphate [$Fe_2(SO_4)_3$ $3H_2O$], aluminium sulphate [$Al_2(SO_4)_3$ $14H_2O$] and lime will interact with particulates to form precipitates that can be removed from the water.[12] In biological processes however, microorganisms, in particular bacteria, are used to purify water by means of biodegradation mechanisms. Depending on the utilization of air, biological processes can either be aerobic or anaerobic.

In spite of their prolific use, these aforementioned processes have major limitations. For example, the physical treatment methods produce large amounts of sludge, which are difficult to dispose of. Moreover, the use of chemicals, in particular chlorine, results in the formation of by-products which can be toxic to living organisms. Still, most of the heavy metals are resistant to the biological treatment methods; hence there remains a need for the development of a method that would be cost-effective and efficient, while being less of a health hazard. The use of zeolite-filled polymer nanocomposites as an additional treatment option during the tertiary stages of water treatment holds great potential in this regard.

2.4 Polymer-layered silicate nanocomposites

Particulate-filled nanocomposites are a new class of composites in which at least one dimension of the dispersed particles is in the nanometer range, i.e. less than 100 nm. Depending on how many dimensions of the dispersed particles are within the nanometer range, nanocomposites can be distinguished into three types: isodimensional particles are obtained when all three dimensions of the dispersed particles are in the order of nanometers[13] such as spherical silica nanoparticles obtained by *in situ* sol-gel methods as well as semiconductor nanoclucters.[14] When two dimensions are in the meter range, while the third is larger, and often forming an elongated structure, they are often nanotubes (e.g. carbon nanotubes) as well as whiskers such as cellulose whiskers.[15,16] The third type, and of particular interest in this study, is characterized by one dimension in the nanometer scale, in which the filler is present in the form of sheets which are a few nanometers long. These types of composites are obtained almost exclusively by

the intercalation of the polymer into the galleries of the layered silicate host, and can be collectively referred to as polymer-layered silicate nanocomposites (PLSNs).[17] A wide variety of both natural and synthetic crystalline fillers have been employed in PLSNs, and a few are listed in Table 2.1.

Table 2.1: A non-exhaustive list of examples of layered host crystals susceptible to intercalation by a polymer

Chemical Nature	Examples	Reference
Carbon oxides	Graphite oxide	[18]
Layered double hydroxide	$Mg_6Al_2(OH)_{16}CO_3\ nH_2O$	[19]
Clays	Montmorillonite	[20,21]
Metal chalcogenides	$(TiS_2)_2MoS_2$	[22,23]
Zeolites	Clinoptilolite	[24]

Amongst all the potential nanocomposite precursors, those based on layered silicates have been widely investigated perhaps due to the abundant availability of the starting materials and because their intercalation chemistry has been well documented.[25] A typical layered silicate structure is shown in Figure 2.1. Owing to the nanometre-size particles obtained by dispersion, the resulting nanocomposites exhibit markedly improved mechanical, thermal and physicochemical properties when compared with the pristine polymer. The section below describes some of the techniques used in the synthesis of PLSNs.

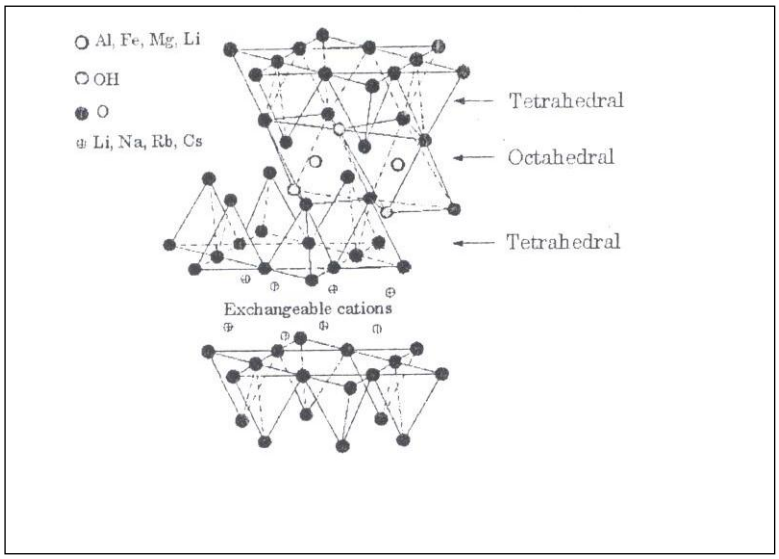

Figure 2.1: A typical phyllosilicate structure (reproduced from [30]).

2.4.1 Nanocomposite preparation methods

One of the most widely used methods in the synthesis of PLSNs is *in situ* intercalative polymerization. In this technique, the layered silicate is swollen within the liquid monomer such that the polymerization occurs in between the intercalated sheets. Polymerization can be initiated by heat or radiation, or by the fusion of a suitable (organic) initiator or catalyst fixed through cation exchange inside the interlayer, prior to the swelling step by the monomer.[26] In the exfoliation-adsorption technique, the layered silicate is exfoliated into single layers using a solvent in which the polymer is soluble. Owing to the weak forces that stack the layered silicate together, they are easily dispersed in an adequate solvent. The polymer then adsorbs onto the delaminated sheets and upon evaporation of the solvent (or precipitation of the mixture), the sheets sandwich the polymer, resulting in an ordered multilayer structure.[26] This method has also been widely used for polymeric materials such as poly(imides) and other conjugated polymers that are infusible and insoluble in organic solvents. In this case, a soluble precursor is intercalated in the layered silicate and then chemically or thermally converted in the desired polymer.[27]

Melt intercalation is another method by which PLSNs can be prepared, and has been explored in this study. In this technique, the layered silicate is mixed with the polymer matrix in the molten state.[26,28] Under these conditions, depending on the degree of compatibility between the layer surfaces and the polymer, the latter can penetrate and fill the interlayer spaces of the filler, forming an ordered structure. This method has been preferred in the preparation of particulate-filled nanocomposites mainly due to its simplicity, convenience and up-scalability for industrial uses. Furthermore, no solvent is required in this method. Depending on the degree of penetration of the polymer into the layered silicate galleries, the resulting nanocomposites will have either an exfoliated or intercalated structure.[29] These two structures are described in detail in the section below**.**

2.4.2 Polymer-layered silicate nanocomposite structures

Depending on the method of preparation, which in turn determines the degree of penetration of the polymer into the silicate layers, two main types of PLSNs can be obtained, and these are intercalated and exfoliated structures. However, when the polymer is completely un-intercalated into the silicates sheets, a phase-separated composite is obtained, and the properties of such composites are normally similar to those of traditional microcomposites. In an intercalated structure, the polymer chains are intercalated between the silicate layers, forming an ordered multilayer of polymeric and inorganic sheets. An exfoliated structure results when the silicate layers are completely and uniformly dispersed in a polymer matrix (Figure 2.2). X-ray diffraction is normally used to differentiate between the two structures. The intercalation of the polymer chains tends to increase the interlayer (*d*-) spacing of the silicate, resulting in lower angle (2θ) values; while in the exfoliated structure, diffraction peaks of the silicate disappear in the diffractograms of the nanocomposite. This could be due to excessive *d*-spacing in between the layers (i.e. >8 nm).[17] The angle and *d*-spacing are collated through Bragg's equation,[31]:

$$\lambda = 2d \sin \theta \qquad (2.1)$$

where:

λ is the wavelength of the X-ray radiation

d is the spacing between diffractional lattice planes

θ is the measured diffraction angle

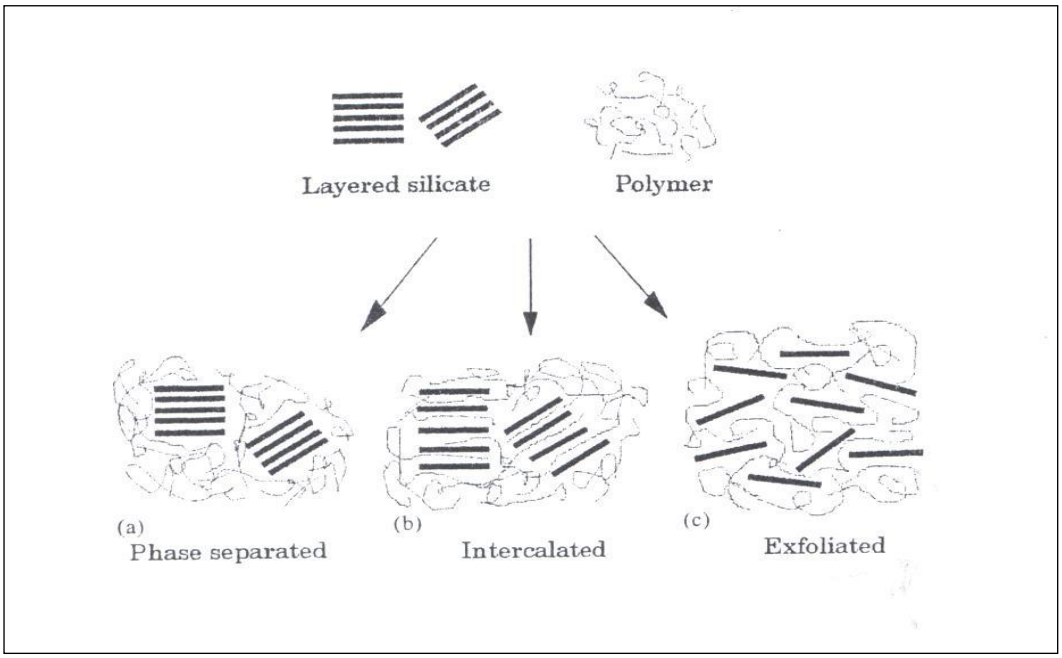

Figure 2.2: The different types of nanocomposites than can be obtained from the interaction of a layered silicate and a polymer

2.4.3 Application of PLSNs

Although the chemistry of polymers when mixed with layered silicates has been known for a long time now, two recent findings have stimulated the revival of interest in these materials. The first was the finding published in a report by the Toyota research[32] group which when working on nylon-6/montmorillonite (MMT), observed that very small amounts of the silicate loadings resulted in pronounced improvements on the thermal and mechanical properties of the nanocomposite; and secondly, the discovery by Vaia et al. that it is possible to melt intercalate

polymers with layered silicates without the use of an organic solvent.[33] As a result, efforts are being made globally to develop similar materials with all types of polymer matrices.

Alexandre and his group used ethylene vinyl acetate (EVA) of varying vinyl acetate contents as a matrix for the preparation of EVA-MMT nanocomposites. A partially intercalated and exfoliated structure was observed, as evidenced by the presence of peaks characteristic of the intercalation process in the X-ray diffraction (XRD) as well as silicate layers in Transmission Electron Microscopy (TEM) micrographs. They also concluded that the presence of polar, ester groups on the vinyl acetate moieties along the EVA chain improved the intercalation ability of EVA, and that the intercalation-exfoliation morphology occurs even at low vinyl acetate content.[34] In another study, Ren et al. investigated the use of vinyl acetate (VAc) as a compatibilizer between a hydrophilic MMT and a hydrophobic polyvinyl chloride (PVC) by the Masterbatch Process. Their results confirmed the formation of exfoliated PVC/VAc/MMT, which exhibited improved mechanical properties, when compared with the conventional (PVC/MMT) without the compatibilizer.[21]

Although there have been several reports on polymer-clay composites,[35-39] it has remained extremely difficult to achieve 100% pure, controlled aspect ratio, and particle size distribution of the filler. Inspired by these challenges, Yang et al. recently investigated the use of exfoliated α-zirconium phosphate (α-ZrP) as an alternative filler in a polyvinyl alcohol (PVA) polymer matrix.[40] Although similar to MMT (in terms of crystalline structure), the α-ZrP has the layers formed by zirconium atoms connected to each other by the oxygen atoms of the phosphate group. Thus in the formation of these layers, each phosphate molecule donates three oxygen atoms, leaving one OH group oriented towards the interlayer space, which can be exchanged reversibly with both mono- and divalent cations.[41] Consequently, this material has a high aspect ratio and cation exchange capacity (CEC), perfect particle size and ease of surface functionality. From their results it was evident that the hydrogen bonding enhanced the miscibility of PVA and α-ZrP. They also reported that tensile strength and elongation at break of the

nanocomposite films increased by 17.3% and 26.65% respectively, compared to the virgin polymer.

Because of their outstanding properties, these types of materials possess a great potential in the production of tailor-made properties for application in other fields. However, most of the studies carried out on PLSNs focused on the use of materials such as clays, carbon oxides and layered double hydroxides, and only recently both natural and synthetic zeolites have been employed as particulate fillers into polymer matrices.[42,43] Pehlivan et al. have studied the characteristics of pure and silver-exchanged natural zeolite-filled polypropylene (PP) composite films. In their investigations, they observed that PP is more susceptible to thermal degradation in the presence of silver-exchanged zeolites, compared to pure zeolites. The composite films were also found to be brittle at higher zeolite loading; hence the optimum conditions thus obtained were 2% wt to 4% wt of the zeolite, treated with 4.36 mg Ag^{+}/g zeolite.[24]

However, most of the studies found in the literature and highlighted above have focused mainly on the mechanical and thermal properties of the materials, and very few studies have explored the physicochemical aspects, and hence the application of these materials in the removal of pollutants from water. The use of zeolites as alternative low-cost adsorbents for the removal of heavy-metal cations has been well documented,[44-47] but the adsorption of these heavy metals onto polymer-zeolite nanocomposites has not been explored. In this study therefore, we investigated the use of zeolite-filled EVA/PVA nanocomposites in the removal of Cu(II), Pb(II) and Co(II) from aqueous solutions.

2.5 Zeolites

Zeolites are naturally occurring crystalline aluminosilicate minerals belonging to the subclass, Tectosilicates.[48] The word zeolite was first coined by a Swedish mineralogist, Axel Fredrik Cronstedt, who upon heating the mineral stilbite, noticed that it produced large amounts of steam from water that had been absorbed by the mineral. Thus, the mineral was called zeolite (meaning, ‘boiling stone’), from the

Greek *zeo* meaning 'boil' and *lithos* meaning 'stone'.[49] Structurally, zeolites consist of a framework of tetrahedral molecules linked to each other by corner-sharing oxygen atoms. Isomorphic substitution of, for example, Al^{3+} for Si^{4+} within the framework, generates negative charges that are counter balanced by alkali or alkaline cations situated in the interlayer. These cations are coordinated with a defined number of water molecules, and are bound to the aluminosilicate framework by weaker electrostatic bonds, allowing the intercalation of small particles in between the particles to occur.[25,50] Consequently, these hydrated cations can be exchanged with either inorganic or organic cationic species (e.g. alkylammonium) for use in various environmental remediation applications. Naturally, zeolites are formed by the alternation of volcanic rocks with freshwater in lakes or by sea water.[51] Today, both natural and synthetic zeolites (A-type, X-type and Y-type) are used in industry for water purification, as catalysts, detergents as well as in nuclear processing.[52]

The application of zeolites in water purification is made possible by their ability to undergo ion exchange. The ion exchange reactions involve an exchange of two or more ions which are loosely bound to two phases, one of which is liquid (or molten), a phenomenon which can be represented by the equilibrium reaction below:[53]

$$nZ - Y^{+}_{zeolite} + M^{n+}_{solution} \rightarrow nZ - M^{n+}_{zeolite} + nY^{+}_{solution} \qquad (2.2)$$

where:

Z represents the zeolite phase

M is the cationic group in solution

n is an integer representing the oxidation state and number of metal ions

Clinoptilolite, although not the most well known, is the most abundant zeolite in the heulandite family. It has the complex formula:[54] $(Na,K,Ca)_{2-3}Al_3(Al,Si)_2Si_{13}O_{36}\cdot 12(H_2O)$, and its typical model structure is shown in Figure 2.3.

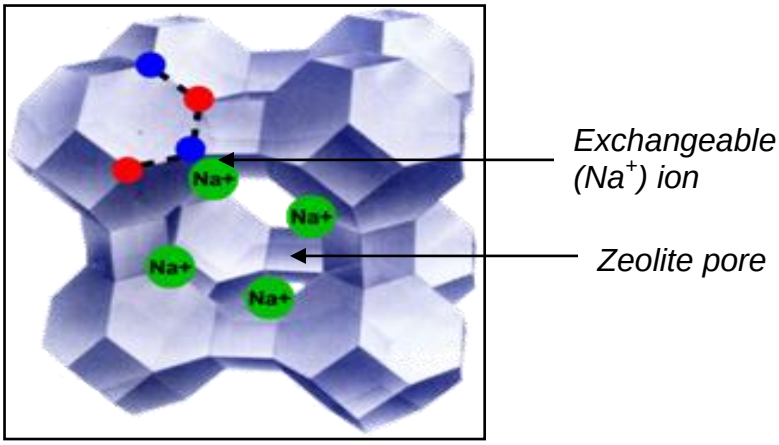

Figure 2.3: A typical model structure of clinoptilolite showing hydrated cations on the 'cages' of the framework.

Like all zeolitic materials, clinoptilolite has the ability to lose and gain water reversibly as well as exchange the hydrated cations (with ions in solution), without a change in the crystal structure.[55] In particular, clinoptilolite has a high affinity for divalent cations. It is also very stable in terms of dehydration and has a high thermal stability of 700^{o}C in air, the highest of all other natural zeolites with a similar structure.[25,56] Moreover, on a mass basis, clinoptilolite as an adsorbent has a larger surface area than bulk particles and can be pretreated with various conditioning agents (acids, bases, surfactants, etc.) to increase its affinity for targeted compounds. Pretreatment is aimed at replacing exchangeable cations on the pore surface with a cation that is more willing to undergo cation exchange with ions in solution.[57,58]

2.6 Polymer matrices

In polymer nanocomposite materials, the continuous polymeric phase, which is often present in larger proportions, is called the matrix. The role of the matrix is to adhere and to bind to the inorganic nanofillers. Since the properties of the resulting nanocomposite will depend not only on the properties of the individual starting materials, but also on the interfacial interactions between them, it becomes imperative to understand the chemistry of the matrix. In this study, ethylene vinyl acetate (EVA) and polyvinyl alcohol (PVA) were used as the matrices.

EVA is a copolymer of ethylene and vinyl acetate in which the larger portion is ethylene, while the vinyl acetate constitutes between 10% and 40%. The chemical structural formula of EVA is shown in Figure 2.4. Industrially, EVA is prepared mainly through the reaction of ethylene and acetic acid with oxygen, in the presence of palladium as catalyst,[59] but it can also be prepared during the gas phase addition of acetic acid to acetylene.[60] EVA has been used in many applications as a clinginess-enhancing additive, as well as a drug-delivery device in biomedical engineering. Although non-biodegradable, the polymer is quite inert, with relatively high mechanical strength. It is flexible and delivers high cohesion strength and compatibility. EVA ensures excellent adhesion to a wide variety of substrates, and is highly resistant to rupture.[61]

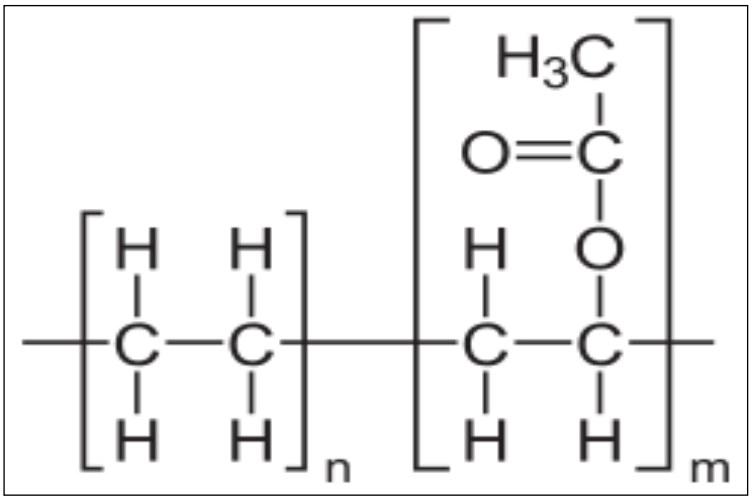

Figure 2.4: Structural formula of ethylene (vinyl alcohol)

PVA was first prepared by Hermann and Haehnell in 1924, via the hydrolysis of polyvinyl acetate in ethanol, with potassium hydroxide. Today, PVA is produced commercially through ester-interchange with methanol in the presence of anhydrous sodium methylate or aqueous sodium hydroxide.[62] The structure of PVA is given in Figure 2.5. PVA can be classified as being partially hydrolyzed or fully hydrolyzed, depending on the degree of hydrolysis. PVA is a highly hydrophilic and fully degradable polymer. It has a high tensile strength and flexibility, as well as excellent adhesive and film-forming properties.[63]

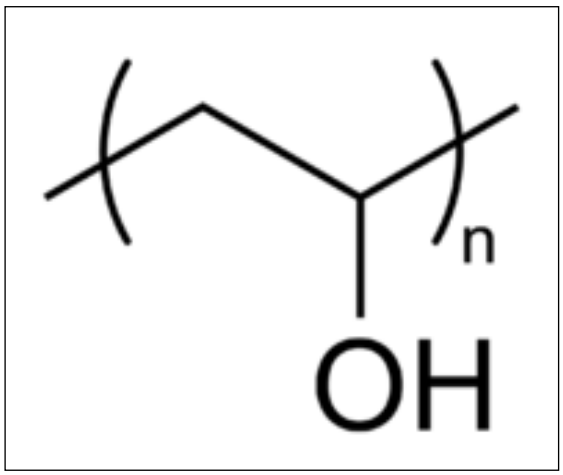

Figure 2.5: Structural formula of polyvinyl alcohol

Other than their mechanical strength and film-forming properties, the hydrophilic nature of these polymers, made possible by the presence of polar hydroxyl groups in the polymer chains, will, upon interaction with the silica-oxygen-layers on the surface of the filler, result in an entirely polar surface. Thus, the dipole-dipole interactions between the polymer chains and the silicate layers may act as the driving force for the polymer chains to intercalate into the silicate layers.[21] The section that follows below summarizes the underlying principles in the techniques that have been used to characterize the materials.

2.7 Characterization techniques

2.7.1 Scanning electron microscopy

The scanning electron microscope (SEM) images the surface of a sample, giving valuable information on its morphology and topography. The principle of the SEM is based on a high-energy beam of electrons that constantly interact with the sample under study, giving signals which allow the scanning to occur.[64] Unlike an optical microscope, the SEM micrographs have a large depth of field, yielding a characteristic three-dimensional appearance, useful for the understanding of the structure of the sample. SEMs are normally equipped with an X-ray detector, from

which X-ray spectral measurements are performed using a solid-state energy dispersive X-ray (EDX) spectrometer. These characteristic X-rays are used to quantify the composition of the sample.[65]

2.7.2 X-ray fluorescence

The X-ray fluorescence (XRF) technique is derived from the emission of X-rays from a sample that has been excited with fluorescent or secondary X-rays.[66] When the energy of radiation is sufficient enough to dislodge an inner, tightly held electron, a loosely held outer electron will replace the inner one, and this will result in energy being released due to a decreases in binding energy between the inner and outer orbital. This results in the radiation of lower energy-fluorescence X-rays, which can be used to determine the abundance of elements present in the sample.[67]

2.7.3 Fourier Transform Infrared

Covalent bonds in a sample absorb infrared (IR) radiation at a specific amplitude characteristic to that type of bond, due to decreased frequency, which is dependent on the geometry and weights of the atoms present in the vibrating covalent bonds.[68] An IR spectrum of a given compound is therefore unique, and this can serve as a fingerprint for that compound as it gives the specific functional groups present in the compound. The IR region of the electromagnetic spectrum runs from 1 400 cm^{-1} to 10 cm^{-1}, but of interest is the mid-IR region (40 cm^{-1} to 400 cm^{-1}), which corresponds to changes in the vibrational energies within the molecules.[69]

2.7.4 X-ray diffractometry

X-ray diffraction (XRD) is based an elastic scattering of X-rays from an electron cloud of individual atoms. Powder XRD is a technique used to characterize the crystallographic structure, crystalline size and preferred orientation of powdered solids. In XRD, a monochromatic X-ray generated from a cathode tube is directed

towards a sample to produce unique X-rays against a scattering angle characteristic of its crystalline atomic structure. Qualitative analyses are carried out by comparing the diffraction data (of the unknown sample) against a database of known patterns.[66]

2.7.5 Brunauer-Emmett-Teller

Surface area and pore volume measurements are of key importance in adsorption studies by ion exchangers. This is because during adsorption and ion exchange, the size of the pore will determine which ions will be hindered or allowed to pass through the pores of the adsorbent. The Brunauer-Emmett-Teller (BET) technique was invented by Stephen Brunauer, Paul Hugh Emmett and Edward Teller in 1938, and based on the Langmuir theory of monolayer gas adsorption, provides valuable information on the surface area, pore size and distribution of solid materials.[70] The total surface area ($S_{BET,\ total}$) and specific surface area (S_{BET}) are evaluated by the following equations:[71]

$$S_{total} = \frac{V_m NS}{V} \qquad (2.3)$$

$$S_{BET}\ \frac{S_{total}}{a} \qquad (2.4)$$

where;

V_m is the molar volume of adsorbed gas.

N: Avogadro's number

S: cross-section of the adsorbing species

V: volume of the adsorbent gas

a: mass of adsorbent (g)

2.7.6 Thermogravimetric analysis

Physical changes as a result of heat in a particular material are often characteristic of the components of that material. Thermogravimetric analysis (TGA), is a

technique used to measure the change in mass of a material in a specified atmosphere, with a change in temperature.[68] This technique does not only measure the degradation temperatures of materials, but can also be used to estimate the adsorbed moisture, as well as the level of inorganic components present in a sample. During analysis, the sample material is placed in a high alumina cup suspended on an analytical balance. The balance then sends a weight signal, along with the sample temperature and elapsed time, to a computer for programming.

2.7.7 Differential scanning calorimetry

The differential scanning calorimetry (DSC) is a thermo-analytical technique which measures the amount of heat required to increase the temperature of a sample and reference, for which both their temperatures are kept the same, throughout the experiment.[72] The reference temperature should have a well-defined heat capacity over the investigated temperature range. The DSC can be used to measure a number of characteristic properties of a material, including fusion, crystallization, glass transition (T_g) as well as other chemical reactions.[73,74] The principle behind the phase transition detection in DSC is that, when a sample undergoes a phase transition, more or less heat will need to flow to it than the reference, in order to maintain both at the same temperature; this depends on whether the process is endothermic or exothermic.[75,76]

2.7.8 Instron extensometer

The extensometer is an instrument designed to evaluate the mechanical properties of materials. It measures such properties as tensile strength, strain, Young's modulus, stress and elongation at break.[77] A schematic representation of a tensile test is shown in Figure 2.6. During a tensile test, a 'test specimen' is firmly gripped at either ends, and an axial pull is slowly exerted until the material breaks.

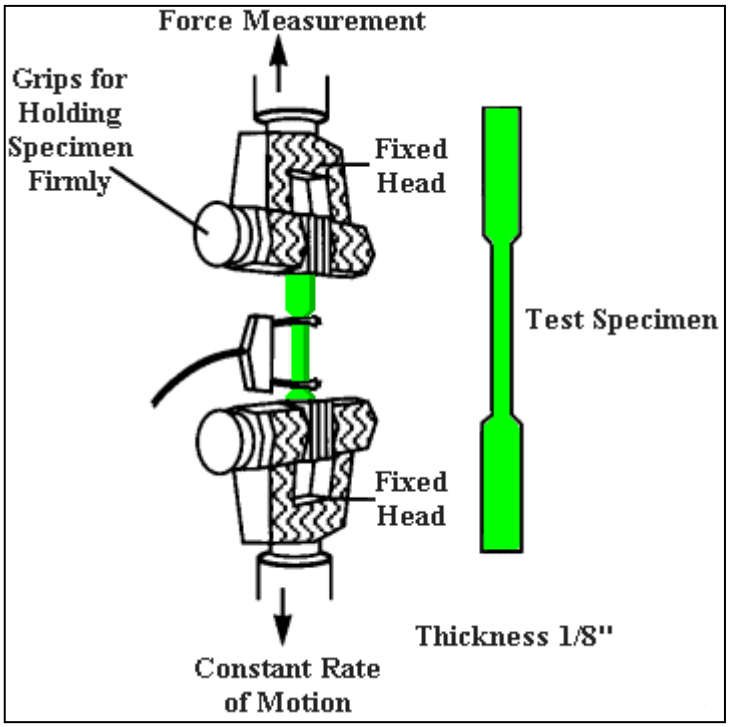

Figure 2.6: A schematic representation of a tensile test

2.7.9 Flame atomic absorption spectroscopy

The atomic absorption spectroscopy (AAS) is a spectroanalytical technique used for the quantitative determination of chemical elements, employing the absorption of light by free atoms in the gaseous state.[78] It has been widely used in analytical chemistry for the determination of the concentration of elements (analytes) in solution. This requires standards with known analyte content, in order to establish a relation between the measured absorbance and the analyte concentration. In flame AAS, the solution is automised into a flame to produce automated vapour. When monochromatic light of the same wavelength is passed through the sample from a hallow cathode tube, the element's atoms will absorb the radiant light, and the degree of absorption expresses the amount of sample present in solution.[68,79] Commonly used flame automizers are principally air-acetylene and the nitrous oxide (N_20)-acetylene flame. The latter flame, in addition, is used ideally for analytes with a high affinity for oxygen.[80]

2.8 Conclusion

In view of the litrature cited in this chapter, it is evident that the excellent mechanical and thermal properties of PLSNs have been intensively utilized in the manufacturing, clothing, packaging, etc., industries, while their physicochemical properties have not been fully explored. Also, there are still existing shortcomings in the conventional methods of metal removal, especially for multi-component solutions. It is therefore of utmost interest to us to develop cost-effective and easy-to-recover zeolite-filled polymer nanocomposites, in an attempt to 'fill the gaps' within the conventional methods of heavy-metal recovery from aqueous solutions.

2.9 References

1. Bock S. *Journal of Integrative Medicine* **1** (6) (1999) 7-12.
2. ATSDR *Draft Toxicological Profile for Cobalt. Agency for Toxic Substances and Registry*, U.S. Department of Health and Human Services. Atlanta GA, 2001.
3. Bralley J.A., Lord R.S. *Laboratory Evaluations in Molecular Medicine.*The Institute for Advances in Molecular Medicine, Norcross GA, 2001.
4. Brewer G.D. *Clin. Neurophysiol.* **121** (4) (1999) 459-460.
5. Markowitz M. *Pediatrics in Review* **10** (2000) 327-335.
6. Kopittke P.M., Asher C.J., Kopittke R.A. Menzies N.W. *Environmental Pollution,* **150** (2007) 280-286.
7. Inglezakis V.J., Loizidou M.D., Grigoropoulou H.P. *J. Colloid Interface Sci.* **261** (2003) 49-53.
8. Donaldson J.D., and Beyersmann D. Cobalt and cobalt compounds. *Ullman's Encyclopedia of Industrial Chemistry*. Wiley-VCH, Weinheim, Germany, 2005.
9. Quing D. *Alternative Medicine Review* **3** (1998) 262-270.
10. Reed S.C., Middlebrooks E.J., Crites R.W. *Natural Systems for Waste Management and Treatment*, McGraw-Hill, New York, 1998.

11. Tchobanoglous G., Burton F.L., Stensel H.D. *Wastewater Engineering: Treatment Disposal Reuse*, 4th edn., McGraw-Hill, New York, 2003.
12. Faist S.D., Aly O.M., *Chemistry of Water Treatment*, 2nd edn., Lewis Publishers, London, 1998.
13. Mark J.E. *Polym. Eng. Sci.* **36** (1996) 2905-2930.
14. Herron N. and Thorn D.L. *Adv. Mater.* **10** (1998) 1173-1184.
15. Calvert P. Potential Application of Nanotubes. In: T.W. Ebbesen (Ed.) *Carbon Nanotubes*, CRC Press, Boca Raton, 1997.
16. Favier V., Canova G.R., Shrivastava S.C., Cavaille J.Y. *Polym. Eng. Sci.* **37** (1997) 1732-1739.
17. Alexandre M. and Dubios P. *Mater. Sci. Eng.* **28** (2000) 1-63.
18. Ding Y., Jones D.J.,Maireles-Torres P. *Chem. Mater.* **7** (1995) 562-571.
19. Wilson O.C., Olorunyolemi T., Jaworski A., Borum L., Young D., Siriwat A., Dickens E., Oriakhi C., Lerner M. *Appl. Clay Sci.* **15** (1999) 265-279.
20. Ogata N., Kawakage S., Ogihara T. *J. Appl. Polym. Sci.* **66** (1997) 573-581.
21. Ren J., Huang Y., Liu Y., Tang X. *Polymer Testing* **24** (2005) 316-323.
22. Herman L., Morales J., Santos J. *J. Solid State Chem.* **141** (1998) 327-329.
23. Harris D.T., Bonagamba T.J., Schmidt-Rohr K. *Macromolecules* **32** (1999) 6718-6724.
24. Pehlivan H., Balkose D., Ulku S., Tihminlioglu F. *Comp. Sci. Technol.* **65** (2005) 2049-2058.
25. Theng B.K.G. *The Chemistry of Clay-Organic Reactions,* Wiley, New York, 1974.
26. Oriakhi C. *Chem. Br.* **34** (1998) 59-62.

27. Yano K., Usuki A., Okada A., Kurauchi T., Kamigaito O. *J. Polym. Sci.* **31** (1993) 2493-2498.
28. Supraka S.R., Pralay M., Masami O. *Macromolecules* **35** (2002) 3104-3131.
29. Giannelis E.P. *Appl. Organometal. Chem.* **12** (10) (1998) 675-682.
30. Giannelis E.P., Khrishnamoorti R., Manias E. *Adv. Polym. Sci*. **118** (1999) 108-147.
31. Cullity B.D., Stock S.R. *Elements of X-Ray Diffraction*, 3rd edn., Prentice-Hall, New Jersey, 2001.
32. Okada A., Kawasumi M., Usuki A., Kojima Y., Karauchi T., Kamagaito O. *MRS Symposium Proceedings, Pittsburg* **171** (1990) 45-50.
33. Vaia R.A., Vasudevan S., Kraweic W., Scanlon L.G., Giannelis E.P. *Adv. Mater.* **7** (1995) 109-115.
34. Alexandre M., Beyer G., Henrist C., Cloots R., Rulmont A., Dubois P. *Macromolecular Rapid Communications.* **22** (8) (2001) 643-646.
35. Chang T.C., Yang H.S., Chao K.Y. *Chen. Chem. Soc.* **39** (1992) 209.
36. Zhu Z.K., Yang Y., Yin J., *J. Appl. Polym. Sci.* **73** (1999) 2063-2077.
37. Masaya K., Naoki H., Makoto K., *Macromolecules* **30** (1997) 6333.
38. Ren J., Gu S.Y., *China Plast.* **17** (2002) 26.
39. Kornmann X., Bergland L.A., Sterte J., *Polym. Eng. Sci.* **38** (8) (1998) 1351-1358.
40. Yang Y., Liu C., Wu H. *Polymer Testing* **28** (2009) 371-377.
41. Jung J.H., Sohn H.J. *Micro. Meso. Mater.* **106** (2007) 49-53.
42. Acosta J.L, Morales E., Ojeda M.C., Linares A. *J. Mater. Sci.* **21** (1986) 725-728.
43. Ozmichi F., Balkose D., Ulku S. *J. Appl. Polym. Sci.* **82** (2001) 2913-2921.

44. Gunay A., Arslankaya E., Tosun I. *J. Hazard. Mater.* **146** (2007) 362-371.

45. Battacharyya K.G., Gupta S.S., *J. Colloid Interface Sci.* **310** (2007) 411-424.

46. Zou W., Han R., Chen Z., Jinghua Z., Shi J. *Colloid Surf. A Physicochem. Eng. Aspects* **279** (2006) 238-24.

47. Wang S., Terdkiatburana T., Tade M.O. *Sep. Purif. Technol.* **62** (2008) 64-70.

48. Bärlocher C.H., Meier W.M., Olson D.H., 5th edn., Elsevier, Amsterdam, 2001.

49. International Zeolite Association, *Database of Zeolite Structures*, http://www.iza-structure.org/databases. (Date accessed: 18/07/2010).

50. Rozic M., Cerjan-Stefanovic S., Kurajika S., Vanica V., Hodzic E. *Water Res.* **34** (2000) 3675-3681.

51. Almaraz B. P., Trocellier P. and Rangel D. I. *Nuclear Instruments and Methods in Physics Research* **210** (2003) 424-428.

52. Abd El-Rahman K. M., El-Kamash A. M., El-Sourougy M. R., Abdel-Moniem N. M. *J. Radioanal. Nucl. Chem.* **268** (2006) 221–230.

53. Debrowski A., Hubicki Z., Podkoscielny P. and Robens E. *Chemosphere* **56** (2) (2004) 91-106.

54. International Zeolite Association: *Database of Zeolite Structures,* http://www.IZA-structure.org/databases. (Date accessed: 12/10/2010)

55. Bailey S. E., Olin T. J. Brica R. M. Adrian D. D. *Water Res.* **33** (1999) 2469-2479.

56. Mugan C. and Melek Y. *Sep. Purif. Technol.* **37** (2004) 93-105.

57. Semens M.J. and Martin W.P. *Water Res.* **31**(6) (1997) 1379-1382.

58. Kesraoui-Ouki S. Cheeseman C. and Perry R. *Environ. Sci. Technol.* **27** (6) (1993) 1108-1116.

59. Han Y.F., Kumar D., Sivadinarayana C., Goodman D.W. *Journal of Catalysis* **224** (2004) 60-68.

60. Roscher G. Vinyl Esters. In: *Ullman's Encyclopedia of Chemical Technology.* John Wiley and Sons, New York, 2004.

61. http://www.wikipedia.org./wiki./ethylene-vinyl_acetate. (Date accessed: 13/10/ 2010).

62. El-Kodsi G. and Schurz J. *Chemical and Technical Assessment* **27** (1973) 253-255.

63. http://www.wikipedia.org./wiki./polyvinyl_alcohol. (Date accessed: 13/10/ 2010).

64. Newbury D. E. *Anal. Chem*. 1159A (1990).

65. Danilatos, G. D. *Advances in Electronics and Electron Physics* **71** (1988) 109–250.

66. www.thermo.com/eThermo/CMA/PDFs/Product/productPDF_11602.pdf

67. Thomsen V. and Schatzlein D. *Spectroscopy* **17** (7) (2002) 22–27.

68. Skoog D.A., Holler F. J. and Nieman T.A. *Saunders College of Publishing,* Philadelphia, USA, 1998.

69. Shanov V., Yun Y.H., Schulz M.J. *J. University of Chemical Technology and Metallurgy* **41** (2006) 377-390.

70. Brunauer S., Emmett P.H., Teller E. *J. Am. Chem. Soc.* **60** (1938) **309-319.**

71. http://www.wikipedia.org./wiki./BET_theory (Date accessed: 13/10/2010).

72. Wounderlich B. *Thermal Analysis.* Academic Press, New York, 1990.

73. Dean, John A. *The Analytical Chemistry Handbook*. McGraw Hill, New York, 1995.

74. Pungor E. *A Practical Guide to Instrumental Analysis*.: Boca Raton, Florida, 1995.

75. Skoog, Douglas A., F. James Holler and Timothy Nieman. *Principles of Instrumental Analysis,* 5th Edn., New York, 1998.

76. M. J. O'Neill *Anal. Chem.* **36** (1964) 1238–1245.

77. http://www.istron.us/wa/applicatios/test_types/tension/default.aspx (Date accessed: 10/11/2010).

78. Welz B., Sperling M. *Atomic Absorption Spectrometry*, Wiley-VCH, Weinheim, Germany, 1999.

79. Walsh A. *Spectrochim. Acta* **7** (1955) 108-117.

80. Broekaert J.A.C. *Analytical Atomic Spectrometry with Flames and Plasmas*, 3rd Edn., Wiley-VCH, Weinheim, Germany, 1998.

CHAPTER 3

FABRICATION AND CHARACTERIZATION OF NATURAL AND HCL-ACTIVATED ZEOLITE-FILLED NANOCOMPOSITE FILMS

3.1 Introduction

In recent decades, research has been focused on the production of polymeric materials, with the ultimate goal of producing materials with enhanced performance. Particulate-filled polymer composites have been used in fields such as drug delivery systems, food packaging, automobile and protective coating industries.[1,2] Polymer composites are normally obtained in one of two methods: the most popular is to introduce nanoscale particles into a polymer matrix to produce polymer/nanoparticle composites, while the other entails the fabrication of the polymer materials themselves on the nanoscale.[3] In the former case, incorporation of the particles into the polymer matrix can be achieved by using one of the two following approaches:

- By insertion of suitable monomers into the silicate galleries of the filler, followed by subsequent polymerization
- By direct insertion of the polymer chains into the silicate galleries in molten state.[4]

Recently, the method of melt intercalation has been the most preferred in the preparation of particulate-filled polymer composites, perhaps due to its convenience and up-scalability for industrial uses. The resulting composites will have either exfoliated or interacted structures, depending on the degree of penetration of the polymer into the layered silicate galleries of the filler.[5] Herein, the preparation and characterization of natural and HCl-activated clinoptilolite (C) filled EVA nanocomposites is reported. The acid was chosen because, in the literature, it has been reported that HCl activation of natural zeolites will bring about a change in the zeolite structure even with dilute acid activations.[6] The effects of loading into the polymer matrix and the pre-treatment of the zeolite on

the thermal, mechanical, and structural properties of the composites were investigated.

3.2 Experimental procedure

3.2.1 Materials

The natural zeolite used in this study was supplied by Pratley South Africa and was sourced from the Vulture Creek in the KwaZulu-Natal Province of South Africa. EVA is a commercial product that was bought from Plastamid, South Africa. For acid activation of the zeolite, 32% HCl was used as the conditioning reagent. The reagent was of the highest quality, and was supplied by Sigma Aldrich, South Africa.

3.2.2 Preparation of the zeolite

'As received' (A.R.) samples of the zeolite were ground and washed with deionised water before being oven dried at 105 ^{0}C overnight. The dried particles were then screened through a 38 µm sieve. A portion of the <38 µm particles were subjected to HCl activation. 2M solutions of HCl were used as the conditioning media. Zeolite particles were soaked in 100 mL of the acid solution in a 250 mL volumetric flask and stirred for 24 h at 160 rpm at room temperature. In all the experiments, the solid-to-liquid ratio was kept constant as 10:100 (w/v). The slurry was then filtered via an 0.5 mm filter paper and washed three times with deionised water to remove excess anions.

3.2.3 Characterization of the zeolite material

Both the 'as received' and HCl-activated zeolite samples were then characterized using powder X-Ray diffractrometry (XRD), X-ray fluorescence (XRF) and Fourier Transform Infrared (FT-IR) spectroscopy. Scanning electron microscopy (SEM) was used to determine the morphological characteristics. For SEM, A piece of self

adhesive carbon tape was pasted on a clean microscope slide, on which the sample was then placed. The sample was then coated using an Agar Turbo Carbon Coater, in order to induce conductivity on the sample. Surface analyses were done using the Brunauer-Emmett-Teller (BET) method with an automated gas adsorption analyser (Micromeritics ASAP 2020). Prior to analyses, samples were first degassed (cleaned) under nitrogen atmosphere for 6 h at 150^{o}C at an N_2 flow rate of 60 mL/min.

3.2.4 Fabrication of EVA- zeolite composite materials

All EVA-C nanocomposites were prepared by the melt-mixing technique in a rheomixer (Haake Rheomex OS) at 120^{o}C and at a speed of 60 r/min for 30 min. The mass of polymer or filler required for specific ratios from 100:0 to 70:30 (polymer/zeolite) was calculated using the 'mixing' equation below:

$$m = \rho \times V_c \times f \times Wt \qquad (3.1)$$

where:

m is the mass (g)

ρ is the density of polymer (or zeolite)

V_c and f are constants for the chamber volume and filler rate of the rheomixer, respectively

Wt (%) represents the required weight of polymer or filler

The composite strips were then extruded through a single-screw extruder (Haake OS) at 120^{o}C, to obtain strips from a 50 mm by 0.5 mm sheet die.

3.2.5 Characterization of the composite materials

Optical micrographs of the EVA-C samples with different zeolite loadings were obtained using a SEM (Jeol JSM 5600). XRD analyses were carried out on powder diffraction with Cu K_α scanning from $2\theta = 4^{o}$ to 60^{o} and the data were collected using Philips X'pert software. Thermal studies of the composite films of treated and untreated clinoptilolite were conducted using a Perkin Elmer TGA

(TGA 4000). The experiments were carried out from room temperature up to 900 at a heating rate of 10^{o}C/min. The analyses were performed in air (purged in nitrogen) at a flow rate of 80mL/ min. Tensile (mechanical) tests of the extruded strips of an average width of 0.5 mm were carried out on an Instron extensometer (Instron 4443). All samples were first kept at below 50% humidity for 48 h, and then cut into 'test specimens' (see Fig. 2.6). The tests were carried out at crosshead speed of 50 mm/min at room temperature. Five trials were performed for each sample, and the mean values were used.

3.3 Results and discussion

The following results were obtained from the characterization of the precursors (zeolite and EVA) as well as the resulting EVA-zeolite nanocomposite:

3.3.1 Characterization of the filler

3.3.1.1 Chemical composition

The chemical composition of components (oxides) present in the South African zeolite is shown in Table 3.1The 'as received' zeolite comprised 12.42% Al_2O_3, 71.37% SiO_2, 3.77% K_2O, 1.31% Na_2O, 1.29% CaO, as well as TiO_2 and Fe_2O_3 in trace quantities. Quantities below 0.05% are replaced with a dash (-). From these XRF data, the Si/Al ratio was calculated to be 5.7, which is within the acceptable range characteristic of clinoptilolite.[7]

Table 3.1: Chemical composition from the bulk analysis (XRF) of the 'as-received' (A.R.) zeolite

Composition	% Abundance
Al_2O_3	12.42
CaO	1.29
Cr_2O_3	-
Fe_2O_3	1.22
K_2O	3.77
MgO	0.87
MnO	-
Na_2O	1.31
P_2O5	-
SiO_2	71.37
SO_3	-
TiO_2	0.14
LOI (930^0C)	6.9
Total	**99.29**

(LOI = loss on ignition)

To determine the nature of functional groups associated with the zeolite material, samples of the material were run under IR, and the spectra are shown in Figure 3.1. The stretching bands shown between 1 500 cm^{-1} and 1 000 cm^{-1} are characteristic of zeolitic minerals. The strong IR band at 1 001 cm^{-1} is characteristic of all forms of clinoptilolite, and is representative of the Si-O stretching. The peak at 1 636 cm^{-1} indicates the presence of molecular water in the clinoptilolite sample.[8]

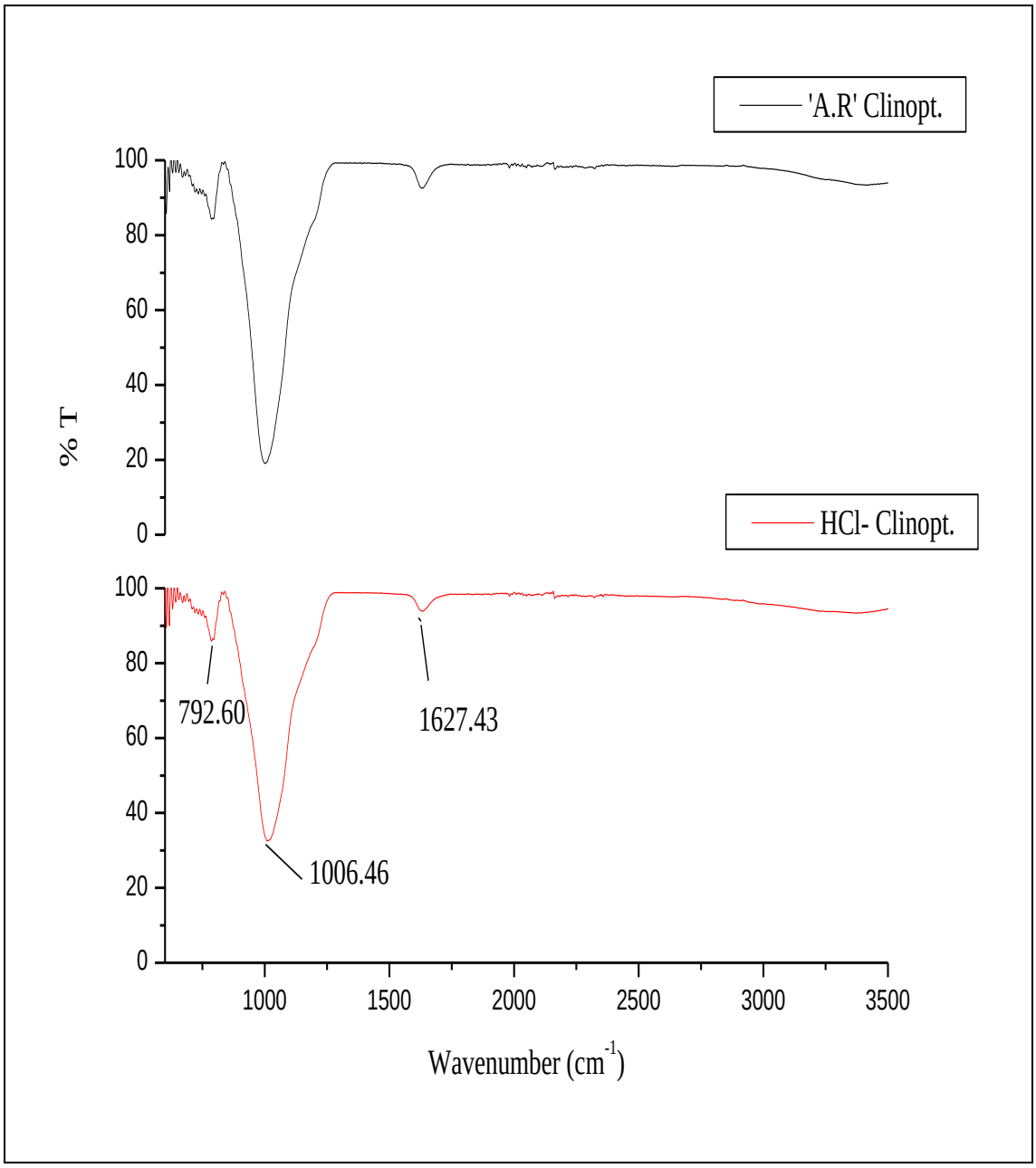

Figure 3.1: FT-IR spectra of 'as received' (A.R.) and HCl-activated zeolite

3.3.1.2 Surface analysis of the filler material

From the BET analysis results a slight increase from 15.96 m^2/g to 20.24 m^2/g was observed in the surface area of the zeolite as a result of acid conditioning. There was also an increase in the pore volume of the acid-activated samples, from 0.061 cm^3/g to 0.668 cm^3/g. This could be attributed to the action of the acid which perhaps washed away particles that were blocking the micropores of the zeolite.

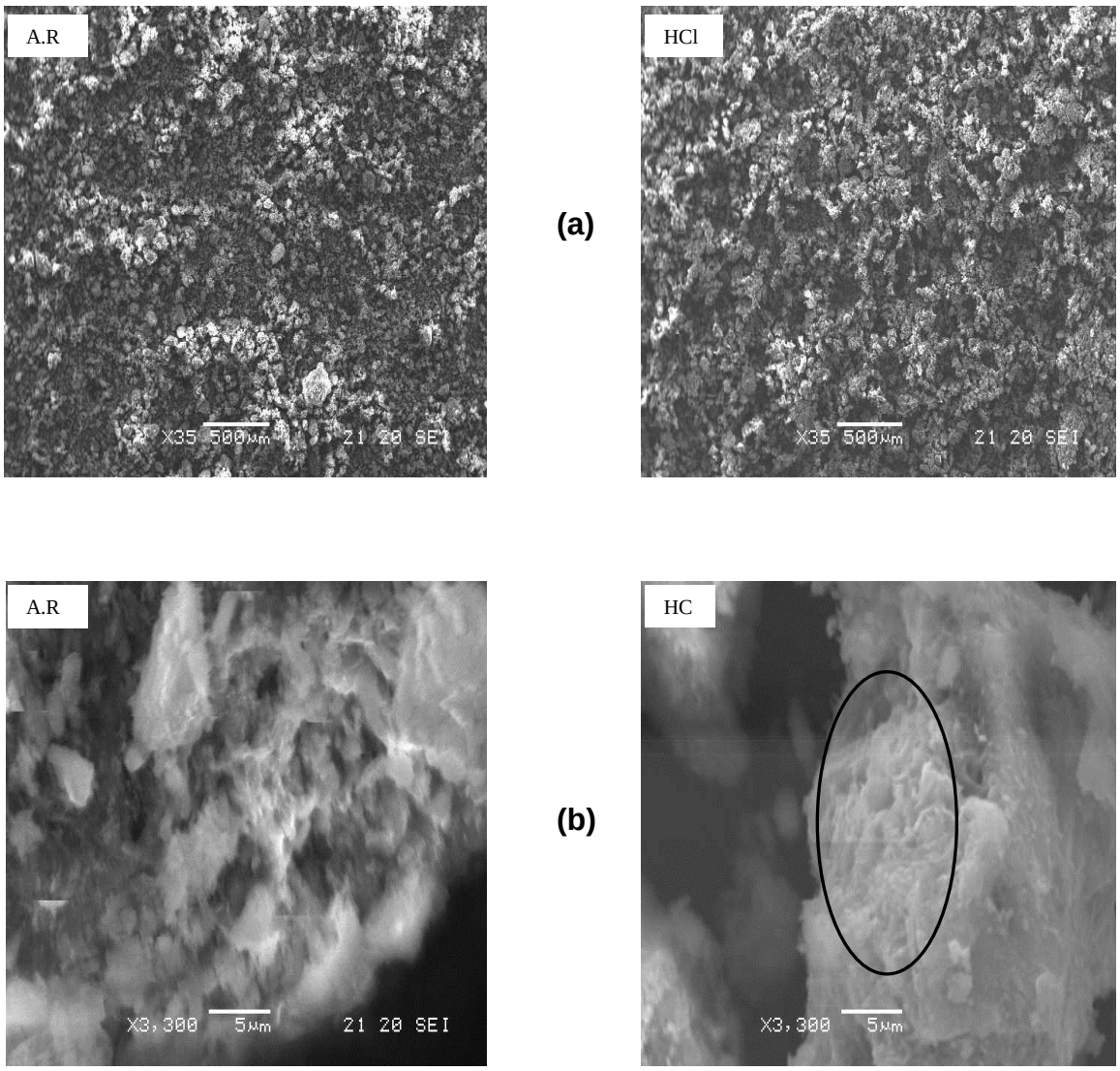

Figure 3.2: SEM micrographs of 'A.R.' and HCl-activated clinoptilolite particles at (a) low magnification(X35) and (b) higher magnification (X3,300)

To ascertain the effect of pretreatment on the surface morphology of the zeolite, samples were observed under SEM, and the micrographs are shown in Fig. 3.2. At low magnification, the clinoptilolite particles are irregularly shaped with no visible difference between the original and chemically conditioned forms of the zeolite. However, a significant change in the morphology is observed between the 'A.R.' and the HCl-activated clinoptilolite at higher magnification. It is evident that conditioning tends to soften and open up the surface yielding some 'flake-like' structures for HCl-activated samples, as compared to the 'rough and compact' structure of the original form. This could be due to the dissolution and decatination of amorphous silica fragments by the acid.[9]

3.3.2 Characterization of the EVA-zeolite composites

3.3.2.1 Crystalline structure and morphology

Powder diffraction measurements of the original zeolite confirmed clinoptilolite as the main component with characteristic peaks observed at $2\theta = 10.4^0$ and 23.4^0. Also present in trace quantities were quartz and sadinine. For comparison, the XRD patterns of the EVA-C filled with 5%, 15% and 30% of the filler are also shown in Figure 3.3. It can be observed that with increasing clinoptilolite loading in the composite, the spacing at the base of the peaks slightly increases, resulting in a shift of the peaks to lower 2θ values, suggesting that the ordered framework of the zeolite is disrupted due to intercalation with the polymer.[10] This intercalation could be largely enhanced by the strong dipole-dipole interaction between the carboxylic groups on the EVA copolymer and the silica-oxygen layers existing on the zeolite framework.[11] The presence of characteristic peaks of the zeolite in the EVA-C composites suggests that clinoptilolite partially keeps its original crystal structure, and exists as primary particles.

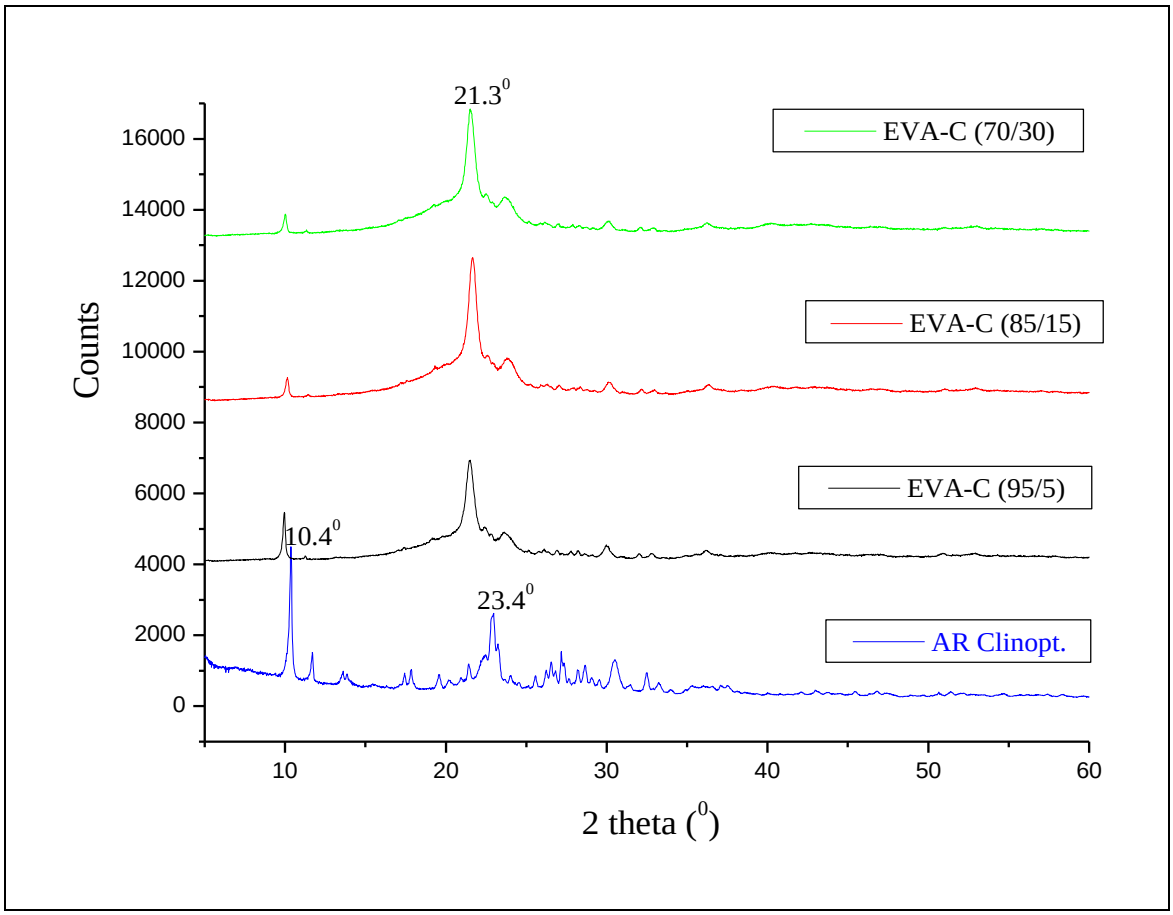

Figure 3.3: X-ray diffraction patterns of EVA-C composites filled with 5%, 15% and 30% of the filler. For comparison, the XRD pattern of the original clinoptilolite is also included.

The XRD data of the EVA-C materials is summarized in Table 3.2. Crystallographic spacing and crystalline size were calculated using Bragg's (Eq. (3.2)) and Scherrer's (Eq. (3.3)) equation cited in [14] respectively, as described below:

$$\lambda = 2d \sin \theta \qquad (3.2)$$

$$\tau = \frac{K\lambda}{\beta \cos\theta} \qquad (3.3)$$

where:

λ is the X-ray wavelength

θ is Bragg's angle

d is the distance between atomic layers in a crystal

τ represents the mean size of the ordered domains

K is the shape factor

ß is the line broadening at half maximum intensity (FWHM)

The percentage crystallinity was calculated from the ratio of the crystallinity of the composite material to that of the 100% crystalline material. From the data in Table 3.2, it can be observed that the *d*-spacing increases with an increase in zeolite content in the composite material, resulting in a decrease in the 2θ values. Addition of the zeolite also increased the crystallinity of the structure, acting as a nucleating agent in the EVA crystallization.

Table 3.2: XRD data for the EVA-C composite materials

EVA/C ratio (wt/wt)	2θ (^{0})	*d*-spacing (Å)	% crystallinity
100/0	21.40	4.15	45.64
95/5	21.48	4.13	50.00
90/10	21.38	4.15	55.81
85/15	21.30	4.17	57.68
80/20	21.30	4.17	60.17
70/30	21.29	4.17	62.66

The surface morphology of the plain polymer and that of the EVA-C composites with varying clinoptilolite loadings is shown in Figure 3.4. The microstructure of the plain EVA film is shown in Figure 3.4(a), from which the uniform orientation of the EVA molecules can be observed. The effect of zeolite loading on the polymer matrix was also examined. Figure 3.4(b) and 3.4(c) show the optical micrographs of EVA-C films filled with 5 and 30% of the filler respectively. Although the particles were sieved through a 38 µm sieve, agglomerates of the zeolite particles (spherical white particles) were visible within the EVA matrix, perhaps due to interface incompatibility between the matrix and the filler phases, leading to a non uniform distribution of the filler on the composite films. These agglomerates then

result in the formation of voids (indicated with an arrow), particularly around the zeolite particles, as seen in Figure 3.4(c).

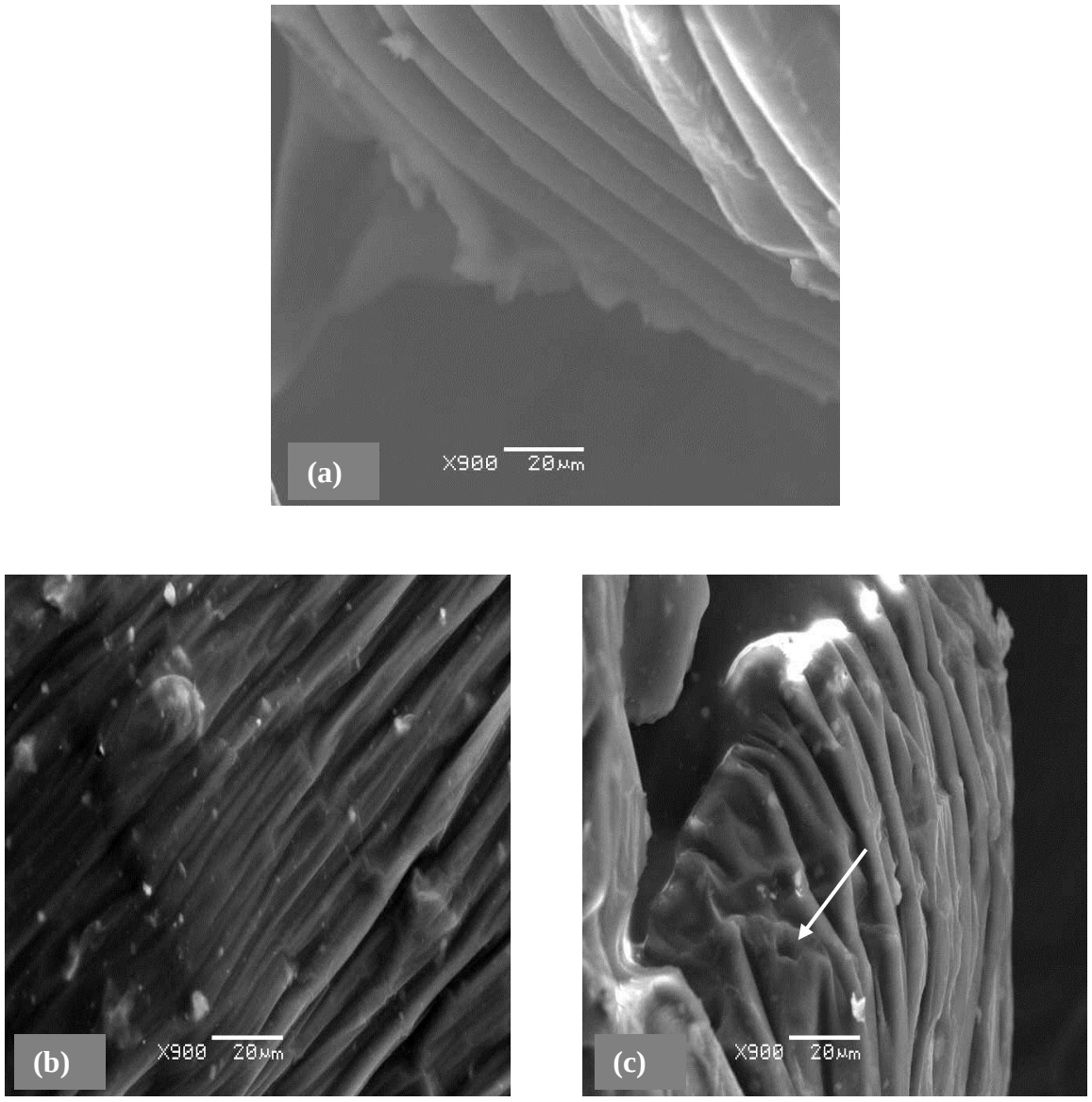

Figure 3.4: Surface morphology of (a) plain EVA, (b) EVA-C filled with 5% 'A.R.' clinoptilolite, and 30% in (c). The arrow in (c) shows a void formed as a result of particle agglomeration.

3.3.3 Mechanical properties

The tensile properties of the extruded films and the plain EVA (control) are summarized in Table 3.3. The results show that addition of the zeolite onto the

polymer matrix increases the Young's modulus initially, but decreases at higher percentage weight (30%) of the filler. This decrease could be attributed to the formation of voids around the filler agglomerates at higher filler dose due to poor interfacial interaction between the polymer matrix and the filler. A decrease was also observed in the stress at break and elongation at break of the composite strips with increasing zeolite dose. The 30% zeolite-containing films had the lowest stress at break (6.2 MPa) compared to the control (11.4 MPa) while the elongation at break decreased by 108.6% from the initial 453.1% of the plain polymer, as seen in Table 3.3. The low elongation at break values indicates the presence of the brittle fracture of the films.

Table 3.3: Tensile test results of the EVA-C composite films filled with 'A.R.' clinoptilolite

EVA/C ratio (% wt)	Young's modulus (MPa)	Tensile stress at break (MPa)	Elongation at break (%)
100/0	420.7	11.4	453.1
95/5	424.1	7.8	446.1
90/10	461.8	9.2	417.3
85/15	498. 1	8.5	369.8
80/20	537.6	7.9	353.7
70/30	447.9	6.2	344.5

The effect of acid activation of the filler on the Young's modulus of the EVA-C composite films as a function of zeolite loading is illustrated in Figure 3.5. A significant decrease in the Young's modulus values is observed for the EVA-C composite films filled with HCl-activated clinoptilolite. This could be attributed to decreased mechanical strength in the reinforcement due to the action of the acid. It has been reported that acid treatment of natural clinoptilolite results in the decatination, dealumination and dissolution of amorphous silica fragments within the framework.[12-14] A study by Korkuna et al. (2006) revealed that there was a

change in the microstructure of the clinoptilolite as a result of dilute acid treatment.[6] It is this effect on the structure that could perhaps result in the poor mechanical strength of the zeolite hence a decrease in the Young's modulus of the EVA-C films filled with acid-activated clinoptilolite.

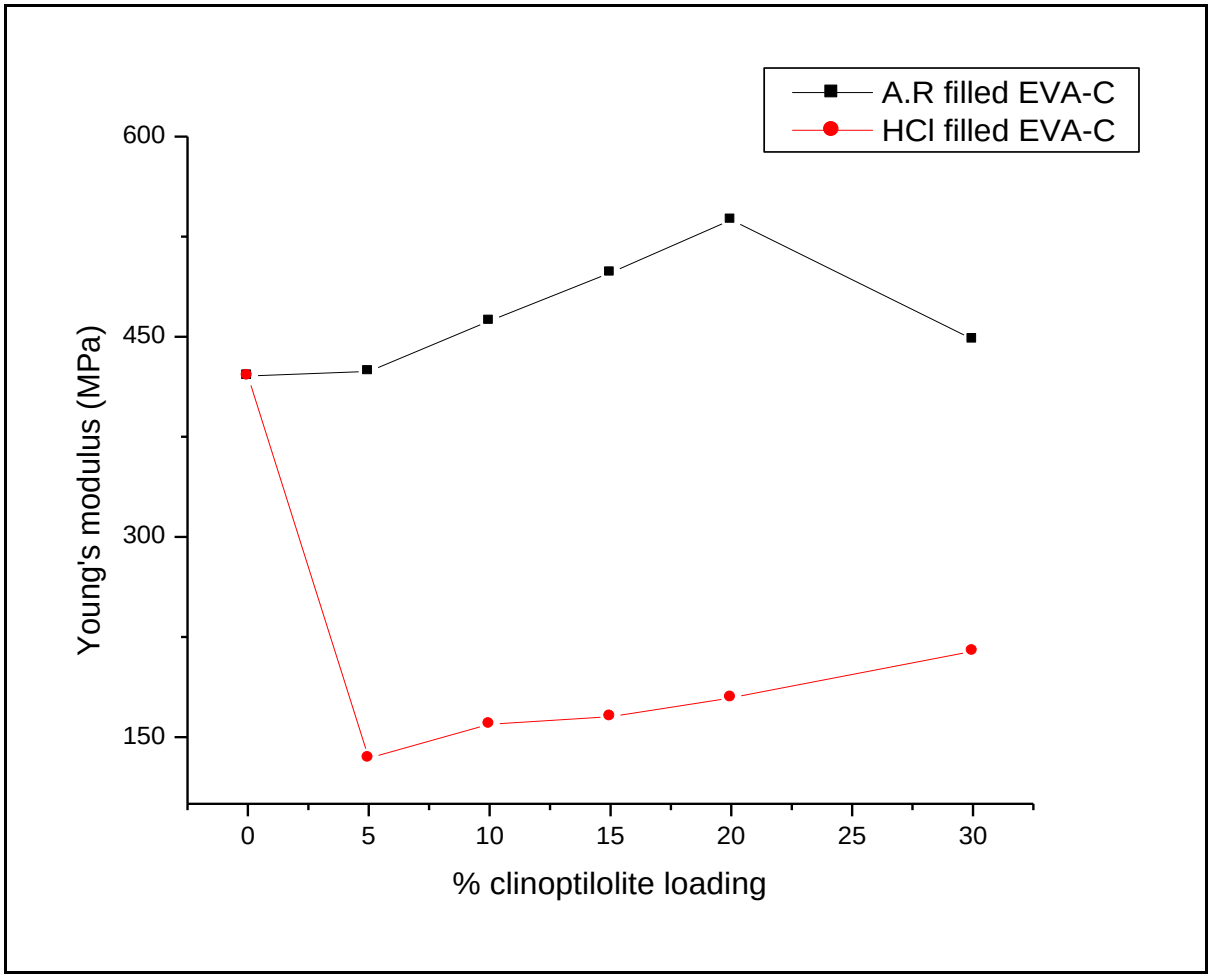

Figure 3.5: The effect of acid activation of the filler on the Young's modulus of the EVA-C composite films

One of the most fundamental factors affecting the mechanical properties of composites is the interfacial compatibility of the polymer matrix with the filler material. To investigate the effect of interfacial interaction, the experimental tensile data of the EVA-C composites were modelled with the Pukanszky model, as shown in Eq. (3.4). Pukanszky's model describes the effect of interfacial interaction and composition on the tensile yield or tensile strength of particulate-filled polymers.

$$\delta_{tc} / \delta_{tm} = \frac{1-\phi_f}{1+2.5\phi_f} \exp B_\sigma \phi_f \qquad (3.4)$$

In Equation (3.4), the interaction parameter *B* is related to the microscopic characteristics of the filler-matrix interface; ϕ_f is the fraction of the filler, while δ_{tc} and δ_{tm} denote the tensile yield (or strength) of the composite and matrix, respectively. Figure 3.6 shows a comparison of the experimental tensile yield data with the Pukanszky model for EVA-C films filled with 'A.R.' and HCl-activated zeolite. It can be observed from Figure 3.6 that the data do not fit the model very well. The first term in Equation (3.4) relates to the decrease in effective load-bearing cross-section, while the second term pertains to interfacial interaction. Parameter *B* in the second term characterizes the interaction between the filler and the matrix, and the higher the value of *B*, the better the compatibility.[15] As depicted in Figure 3.6, the results of the model prediction gave negative *B* values, which was an indication of poor interfacial adhesion between the EVA polymer and the zeolite.

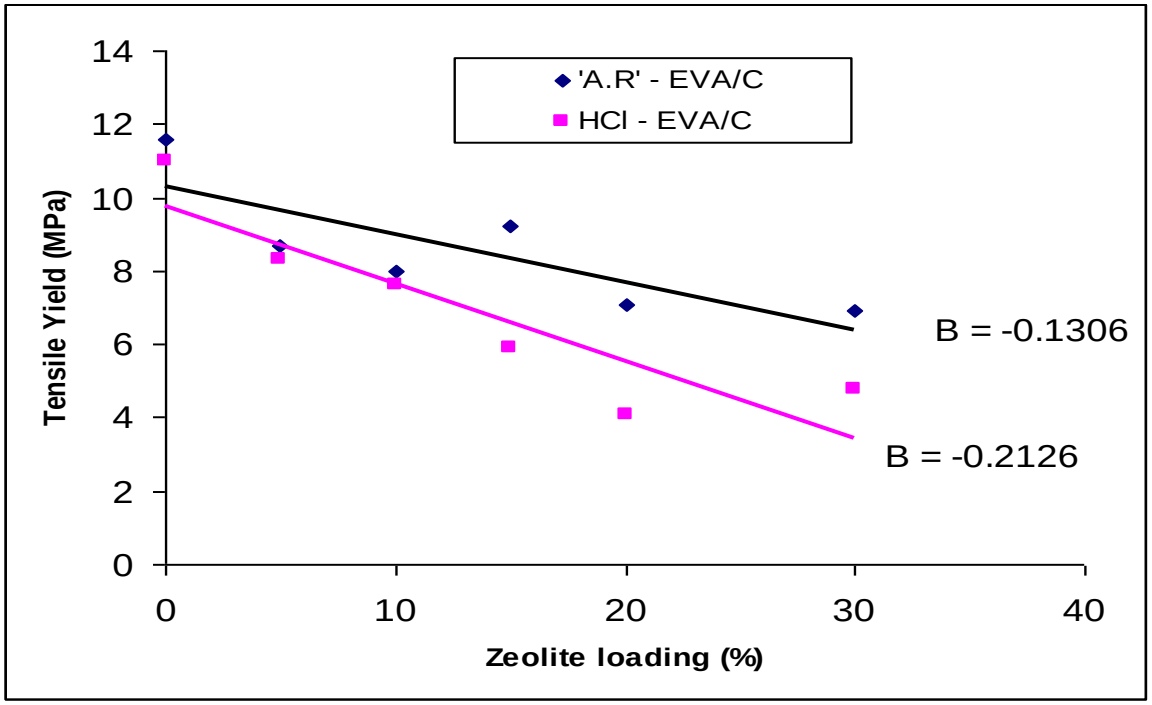

Figure 3.6: A comparison of the experimental tensile yield data with the Pukanszky model for EVA-C films filled with the 'A.R.' and HCl-activated zeolite. *B* is a parameter related to the interfacial interaction of the EVA-C composite system.

3.3.4 Thermal properties

Thermal characteristics of the EVA-C composite films of the 'A.R.' and HCl-activated zeolite were carried out using TGA at a heating rate of 10^{o}C/min. TGA analysis of the HCl and A.R.-filled EVA-C films showed very similar results. On average, degradation started at around 250^{0}C, and terminated at about 540^{0}C. The onset degradation temperature was, to a lesser extent, shifted to lower values with lower filler dosage, an indication that the EVA-C composite was more susceptible to thermal degradation at low zeolite content. The plain EVA is, however, more stable at lower temperatures as its degradation starts at a temperature slightly above those of the EVA-C composite films. Figure 3.7 shows thermograms of the plain EVA and those of A.R. HCl-activated EVA-C films filled with 30% wt of the zeolite.

It can be observed that degradation of the plain polymer occurs in two steps – an initial step from 250^{0}C to 450^{0}C which could be attributed to the removal of the acetyl group, and a final step from 450^{0}C to 540^{0}C, which is indicative of the degradation of the main polymer chain. The filler loses mass continuously throughout the investigated temperature range although this mass is poorly visible in the composite samples, possibly due to its lower content. Although both samples were filled with 30% clinoptilolite, the weight losses at 540^{0}C were 81.64% and 84.95% for the 'A.R.' and HCl-EVA/C films, respectively. This inconsistency further confirms that the distribution of the filler within the polymer matrix was non-uniform. There is no significant shift to higher temperatures of the onset temperature after acid activation. However, the temperature of the maximum rate of weight loss (T_{max}) and the final decomposed temperature (FDT)[16] increased at 30% zeolite loading, compared with the pristine polymer. This is because the degradation of polymers is initiated with the formation of free radicals at weak bonds or chain ends, followed by their transfer to adjacent chains via inter-chain reaction. With an increased zeolite content therefore, the chain-transfer reaction within the polymer is retarded, and as a result, the degradation process will be slowed hence decomposition will take place at higher temperatures.[17]

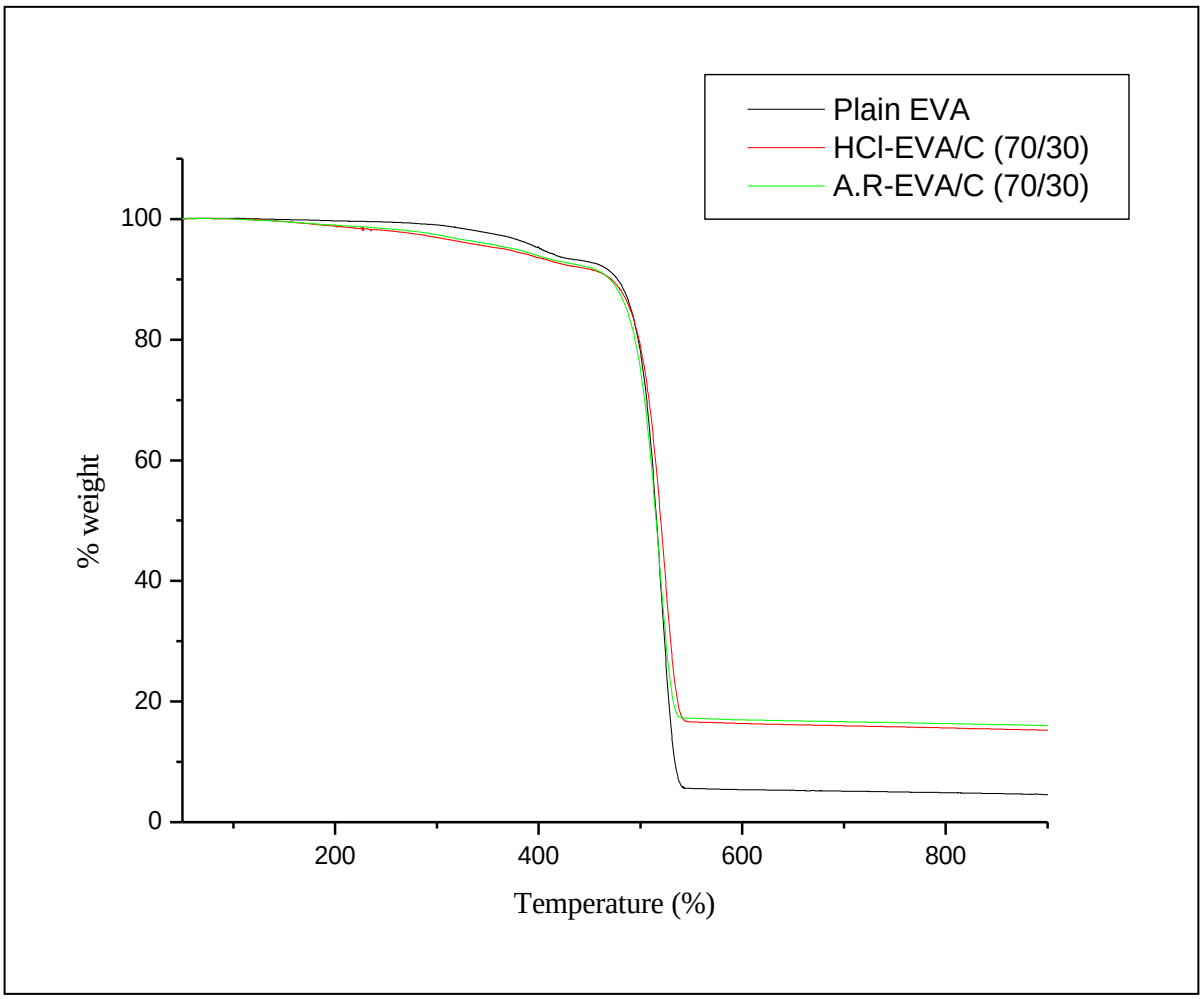

Figure 3.7: TGA curves of plain EVA and 30% wt of A.R. and HCL-activated zeolite filled EVA-C composites

3.4 Conclusion

Natural and HCl-activated-EVA composites were prepared via the melt-mixing technique, and the effects of zeolite loading and HCl activation of the filler on the thermal, mechanical, and structural properties of the composite films were investigated. The results show that addition of the clinoptilolite nanoparticles onto the polymer matrix leads to agglomeration of the particles, resulting in the formation of voids on the surface of the films. Consequently, the films become brittle at higher zeolite loading, resulting in reduced Young's modulus. Acid activation tends to alter the crystal structure of the zeolite, resulting in poor tensile properties of the HCl-activated zeolite-filled EVA films. Addition of the zeolite also increased the crystallinity of the structure, acting as a nucleating agent in the EVA crystallization. Thermal characterization studies showed that addition of the zeolites also retarded the onset degradation temperature of EVA. However, degradation temperatures including T_{max} and FDT were increased, suggesting improved thermal stability, due to reduced inter-chain mobility in the composite materials.

3.5 References

1. Pehlivan H., Balkose D., UlkuS., Tihminlioglu F. *Comp. Sci. Technol.* **65** (2005) 2049-2058.
2. Liu T.B., Burger C., Chu B. *Prog. Polym. Sci.* **28** (2003) 5-11
3. Yang K.K., Wang X.L., Wang Y.Z. *J. Ind. Eng. Chem.* **13** (2007) 485-500.
4. Supraka S.R., Pralay M., Masami O. *Macromolecules* **35** (2002)3104-3131.
5. Gianelis E.P. *Appl. Organometal. Chem*. **12** (10) (1998) 675-682.
6. Korkuna O., Leboda R., Skubiszewska-Zieba J., Vrublevs'ka T., Gun'ko V. M., Ryczkowski J. *Micropor. Mesopor. Mater.* **87** (33) (2006) 243-254.
7. Tsitsishvilli, G.V., Andronikashvili, T.G., Kirov, G.M., Filizova, L.D. *Natural Zeolites*, Ellis Horwood, Chichester, UK, 1992.
8. Madejova J. *Vibrational Spectroscopy* **3** (2003) 1- 6.
9. Kuronen M., Weller M., Townsend R., Harjula R. *React. Funct. Polym.* 66 (2006) 1350-1361.
10. Anirudhan T.S., Suchithra P.S., Rijith S. *Eng. Aspects* **326** (2008) 147-156.
11. Ren J., Huang Y., Liu Yan., Tang X. *Polymer Testing* **24** (2005) 316-323.
12. Al-Degs Y., Tutunji M., Baker H. *Clay Miner.* **38** (2003) 501–509.
13. Inglezakis V. J. and Grigoropoulou H. *J. Hazard. Mater.* B112 (2004) 37-43.
14. Athanasiadis K., Helmreich B. *Water Res*. **39** (2005) 1527-1532.
15. Pukanszky B., Tudos F. *J. Mater. Sci. Lett.* **8** (1989) 1040-1042.
16. Park S.J., Kim H.C. *J. Polym. Sci. Polym. Phys.* **39** (2001) 121-128.
17. Kulijanin J., Comor M.I., Djokovic V., Nedeljkovic J.M. *Mater. Chem. Phys.* **95** (2006) 67-71.

CHAPTER 4

CHARACTERIZATION OF NATURAL ZEOLITE- FILLED PVA MELT EXTRUDED NANOCOMPOSITE FILMS

4.1 Introduction

Over the years, polymeric materials containing both the organic (polymer) and inorganic (reinforcement) components which can either occur naturally or prepared synthetically, have been used for many industrial applications. Fillers are often added to enhance the properties of the polymer, resulting in a homogeneous mixture. If at least one of the dimensions of the filler particles is in the nanometer range, these materials are called polymer nanocomposites. The transition in length scale from micrometer to nanometer yields dramatic properties in the overall properties of the resultant nanomaterial.[1] Layered silicate 'sheet-like' materials are often preferred for the enhancement of polymeric material's properties. Two characteristics of the layered silicates are often considered for polymer-layered silicate nanocomposites (PLSNs):

- The ability of the particles to disperse into individual layers
- The possibility to manipulate their surface chemistry through ion-exchange and hydrophobic bonding mechanisms.

These two characteristics are interrelated since the degree of dispersion of a layered silicate in a polymer matrix depends on the interlayer cation.[2]

This chapter discusses some of the properties of zeolite-filled polyvinyl alcohol (PVA) nanocomposites. PVA, a water-soluble synthetic polymer, has been blended with other natural polymers because of its hydrophilic nature which allows compatibility.[3-7] Herein we report the physical, chemical and thermal properties of melt-blended natural zeolite-PVA films, with varying loadings of the filler.

4.2 Experimental procedure

4.2.1 Materials

The zeolite used in this study was the same as the one described in **Section 3.2.1**. PVA, a creamy white powder with 4% solution viscosity 8mPas at 20^0C and 88% hydrolysis degree was supplied by Sigma Aldrich, South Africa.

4.2.2 Preparation of materials

The zeolite material was prepared as described in **Section 3.2.2**. PVA was used as received without any further purification. PVA-zeolite composites were melt-blended in a rheomixer at 2 200°C at a rotor speed of 60rpm for 30 min. The specific mass ratios of polymer to zeolite were calculated using Eq. (3.1). PVA-zeolite strips of 0.5 mm X 50 mm were extruded at 230^0C from a single- screw extruder rotating at 60rpm.

4.2.3 Characterization of materials

The morphologies of the surface areas and cross-sections of the PVA-C samples were observed under a scanning electron microscope (Jeol JSM 5600) at an accelerating voltage of 5 kV. Samples were mounted on a double-sided adhesive tape, and then coated with carbon under a 4.0 Pa vacuum. The SEM was also coupled to an energy dispersive X-ray (EDX) spectrometer. Fourier Transform Infrared (FT-IR) spectra of the extruded films were recorded on a Perkin Elmer (FT-IR 4000) spectrometer in attenuated total reflection mode in the wavelength range of 4 000 cm^{-1} to 650 cm^{-1}. X-ray diffraction was performed on a Phillips X'pert diffractometer scanning from 4^0 to 60^0 at a current of 20 mA and a voltage of 40 kV. Thermogravimetric analysis (TGA) thermograms of the PVA and PVA-zeolite samples were collected from a Perkin Elmer TGA 4000 between 30^0C and 900^0C at a heating rate of 10^0C. Nitrogen was used as the purge gas at a flow rate of 80 mL/min. Differential scanning calorimetry (DSC)measurements were performed under nitrogen atmosphere on a Shimadzu (DSC 7) in the temperature range from 25^0C to 250 ^{0}C. The heating rate was 20^0C/min. Prior to analysis,

samples were placed into aluminium pans which were crimped closed using the DSC sample press. The swelling behaviour studies were carried out using 40 mm by 20 mm sample strips of the same thickness (0.5 mm). Samples of various zeolite loadings were weighed before and after being placed 100 mL distilled water for 24 h.

4.3 Results and discussion

4.3.1 Scanning electron microscopy (SEM)

SEM micrographs showing the surfaces of the zeolite and the plain PVA are shown in Figure 4.1. The zeolite is composed of regular cubic particles (Figure 4.1a), an indication that the crystallinity of the particles is very high, as can also be observed from the XRD diffractograms in Figure 4.3. Pure PVA films (Figure 4.1b), exhibit a relative smooth cross-section due to its good film-forming properties.

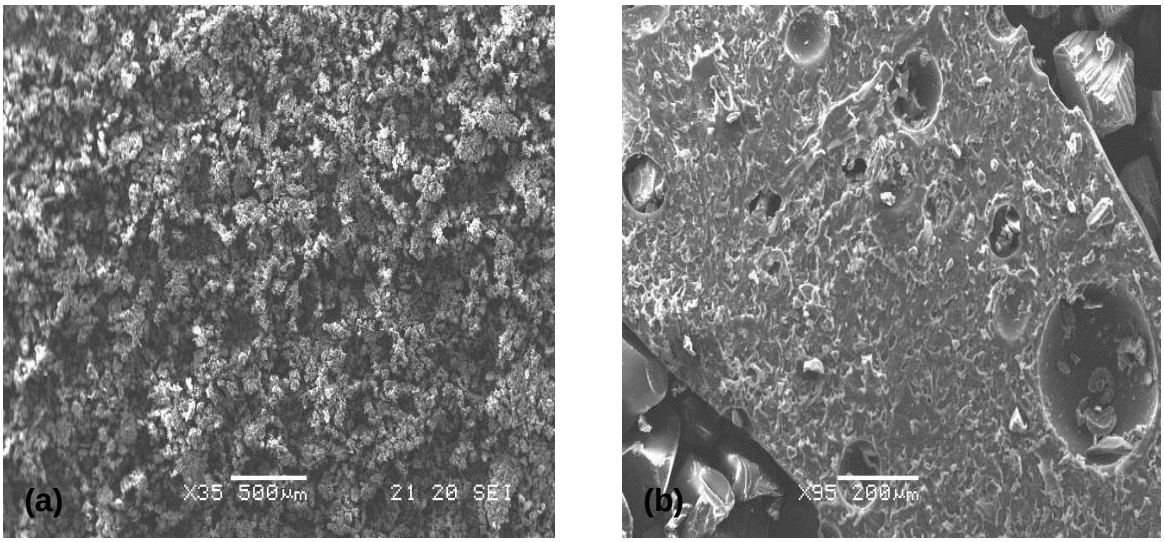

Figure 4.1: SEM micrographs showing the surfaces of (a) the pristine zeolite and (b) the pure PVA polymer

Micrographs of the PVA-zeolite nanocomposites show that the nanoparticles are well dispersed in the PA matrix, as evidenced by the presence of Al and Si peaks in the EDX spectra (Figure 4.2). However, in the PVA-zeolite composites containing 30% of the filler, aggregates of the filler are visible on the surface, as shown in Figure 4.2 (b). This results in a more compact and rough surface of the

composite as compared to the one with less zeolite content, an occurrence which is also expected to increase the crystallinity of the materials. In the PVA-zeolite film containing 5% zeolite (95/5), the surface is smoother, indicating that the nanoparticles formed a stronger interaction with PVA and were dispersed more homogeneously in the polymer matrix. The most intense peaks on the EDX spectra are Al and Si, and are characteristic of all aluminosilicate materials. The C represents carbon possibly from the carbon coating that was used during sample preparation. Hydrated cations on the zeolitic material are also reflected on the EDX spectra, with K and Ca present in significant amounts. Na, which is not present in the composite filled with 30% of the filler, could be both from the zeolite (as an oxide) and the polymer as sodium acetate, a hydrolysis reaction by-product.

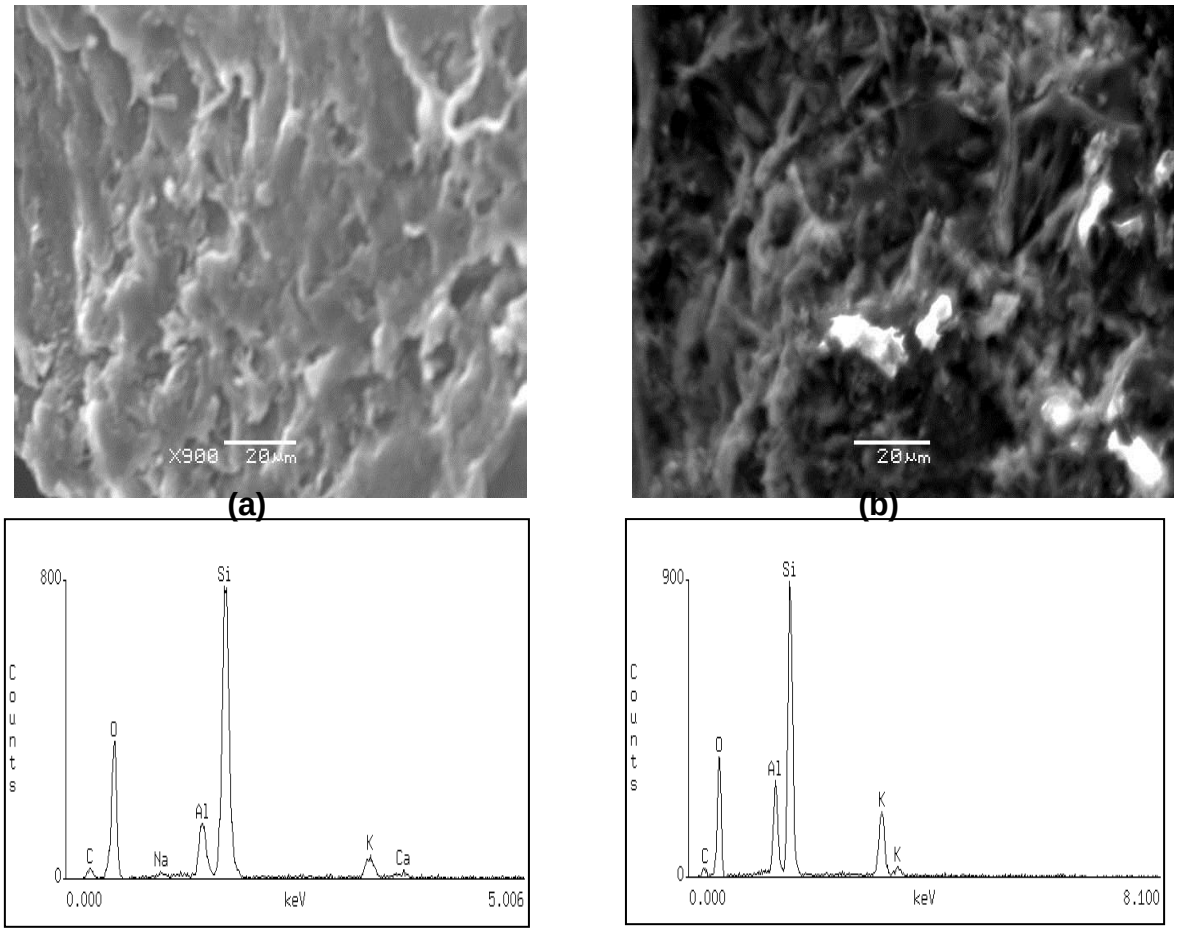

Figure 4.2: SEM-EDX optical micrographs of PVA-zeolite composites filled with (a) 5% and (b) 30% of the filler

4.3.2 X-ray diffractometry (XRD)

The crystalline structure of the PVA/Z composite materials was studied using the X-ray diffraction technique, and the diffractograms are shown in Figure 4.3. Peaks of the zeolitic materials observed at $2\theta = 9^0$ and 23^0 are characteristic of clinoptilolite. From the diffractograms of the plain PVA, an intense peak occurs at $2\theta = 14^0$ which is characteristic of the crystalline phase of PVA.[8] The appearance of this peak could be attributed to strong interactions between PVA chains via the intermolecular hydrogen bond.[9] At higher dosage of the zeolite material (70/30), the intensity of this peak is slightly decreased, an indication that the crystallinity of the PVA is suppressed by the introduction of the zeolite into the polymer matrix.

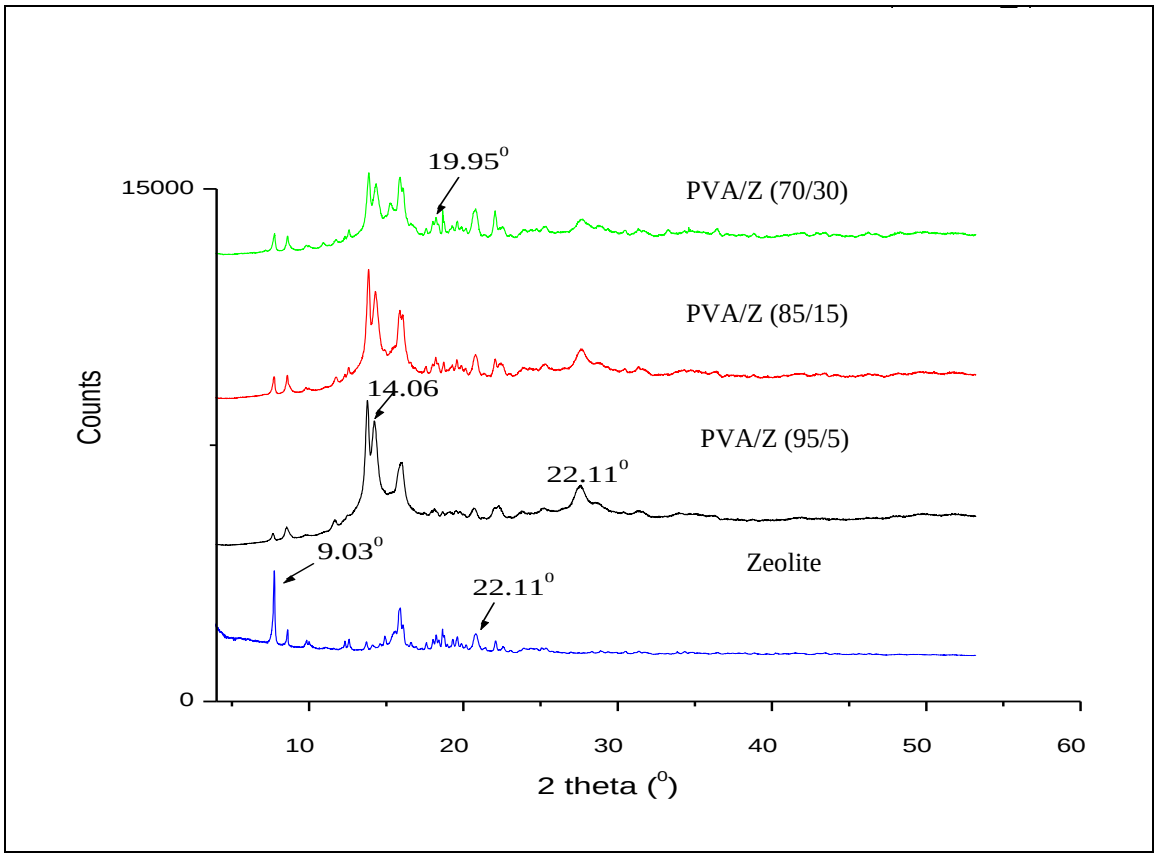

Figure 4.3: X-ray diffraction patterns of the zeolite (Z) and PVA/Z composites filled with 5%, 15% and 30% of the filler

For the plain PVA, another small peak is observed at $2\theta = 22.11^0$, corresponding to an approximately hexagonal ordering of the molecular PVA chains.[10] In the PVA/Z materials, the disappearance of some of the peaks characteristic of the zeolite (e.g. $2\theta = 9^0$) suggests that the silicate layers of the filler are evenly dispersed on the polymer matrix, or perhaps there were too few traces of the crystal to be detected by the XRD. On the other hand, this phenomenon could be evidence of an exfoliated structure of the PVA/Z composites, resulting from an infinite expansion of the zeolite interlayer. Also evident is the fact that the characteristic peaks in the PVA/Z composites are broadened, leading to a shift in the lower-angle values. For example, the characteristic peaks of the zeolite shifted from $2\theta = 22.11^0$ to 19.95^0 in the PVA/Z (70/30). These results confirm that the PVA chains have been intercalated into the zeolite interlayer. Thus PVA/Z composites with partially intercalated and partially exfoliated structures were obtained.

4.3.3 Fourier Transform Infrared (FT-IR) spectroscopy

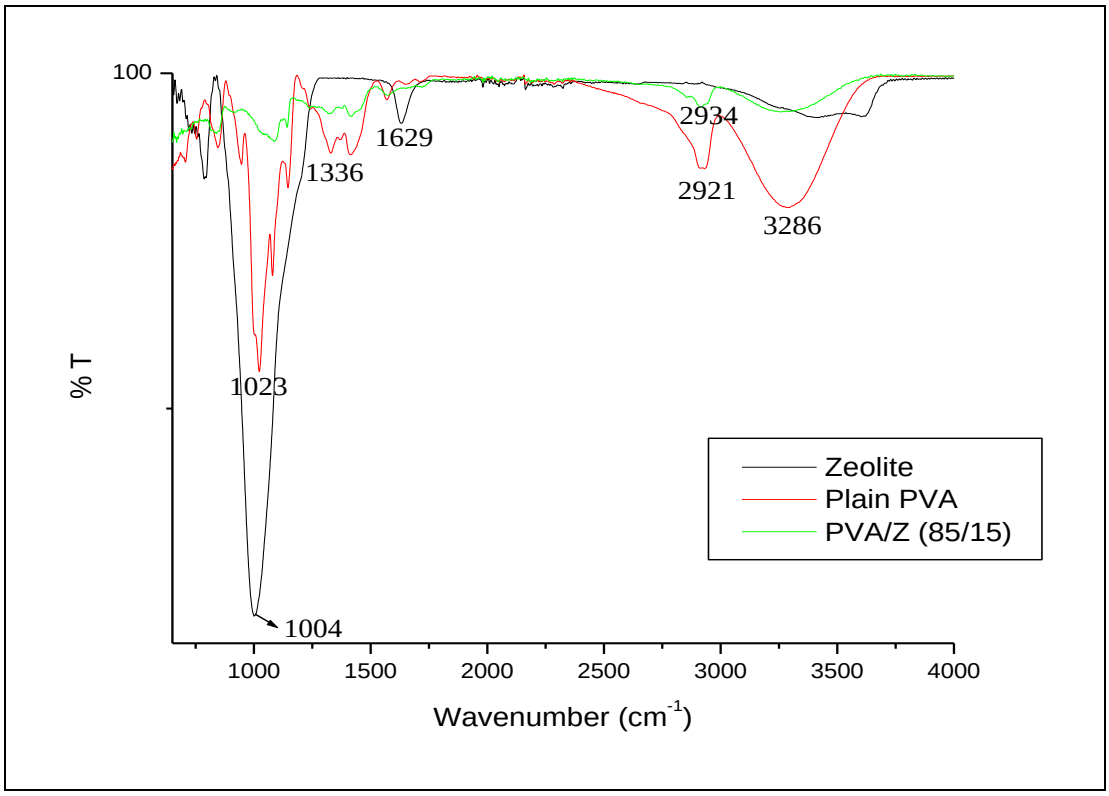

Figure 4.4: A comparison of the FT-IR spectra of a pristine zeolite, a plain polymer and a PVA/Z composite filled with 15% of the filler

The FT-IR spectra of plain PVA, the pristine zeolite and PVA/Z (85/15) are shown in Figure 4.4. The zeolite shows an intense peak at 1 004 cm^{-1}, characteristic of all forms of clinoptilolite, a zeolite, due to Si-O stretching. The peak at 1 629 cm^{-1} is representative of zeolitic water in the sample.[11] In the plain PVA, peaks at 2 921 cm^{-1} and 1 336 cm^{-1} are attributed to the C-H stretching and bending of the PVA chains. The peaks at 840 cm^{-1} and 1 023 cm^{-1} represents C-O stretching of the PVA chains. The broad peak at 3 286 cm^{-1} is assumed to emanate from the O-H stretching frequencies of PVA and hydroxyl groups from molecular water. Slight changes in the characteristic spectral peaks are representative of chemical interaction taking place when two substances are mixed. As seen in the spectra of PVA/Z (85/15), the characteristic peak of PVA at 2 921 cm^{-1} is shifted to 2 934 cm^{-1}. This is an indication that there are hydrogen-bond interactions between the hydroxyl of the zeolite and carbonyl groups of the PVA, an occurrence which possibly contributes to the compatibility between the polymer and matrix.[13]

4.3.4 Thermal analysis (TGA and DSC)

Thermal studies of the PVA/Z composites were carried out using TGA and DSC. The TGA thermograms of the pure PVA, PVA/Z (95/5), (85/15) and (70/30) are shown in Figure 4.5. In all the thermograms, three temperature regions over which weight loss occurs are observed. The first region, at a temperature region of around 100^0C is due to the evaporation of physically weakly bound, yet chemically strongly bound water molecules. The second transition, at around 260 ^{0}C to 380 ^{0}C, corresponds to the side decomposition of PVA. In the third and final degradation step, in the region of 450 ^{0}C to 550 ^{0}C, the transition is due to the cleavage backbone of the main PVA chains, a process also known as carbonation.[14] An improvement in the thermal stability of the nanocomposites can also be observed with an increase in the nanolayer content. For example, the temperature at maximum degradation (T_{max}) for PVA/Z (70/30) increased from 522 ^{0}C (for the pure PVA) to 547 ^{0}C an increase of 4.57%. Other reliable temperatures of degradation such as the onset temperature (T_{on}), for all the nanocomposites are listed in Table 4.1.

Table 4.1: Essential degradation temperatures for the PVA/Z nanocomposites as measured by TGA and DSC

Composite	**TGA (^{0}C)**		**DSC (^{0}C)**	
% wt (PVA/Z)	T_{on}	T_{max}	T_g	T_m
(100/0)	277	522	55.2	227.4
(95/5)	285	532	57.3	228.1
(85/15)	293	529	58.7	228.9
(70/30)	291	547	60.6	229.8

The enhanced thermal resistance of the PVA/Z composites, attributed to the introduction of SiO_2 nanolayers, is present in the zeolite as confirmed in the XRF results listed in Table 3.1. The SiO_2 are distributed homogeneously throughout the PVA matrix, forming high surface area nanoclusters. These nanoclusters have great potential energy and therefore strongly interact with the PVA molecular chains through various effects such as nucleation and the branching effect.[15,16] As a result, the diffusion of decomposition products from the bulk polymer to a gas phase is retarded, hence the nanocomposite will have a significantly improved thermal resistance when compared to the pure PVA.

DSC curves of the PVA and PVAA/Z composites are shown in Fig 4.6. Pure PVA exhibits an endothermic reaction at 55.2^{0}C, corresponding to the glass transition temperature (T_g).[12] For all the zeolite-filled PVA films, the T_g was found to be higher than that of the pure PVA, and also increased with increasing zeolite content (Table 4.1). This is an indication that addition of the zeolitic filler onto the polymer matrix prevents the segmental motion of the polymer chains, thereby increasing the T_g of the PVA/Z when compared to PVA.

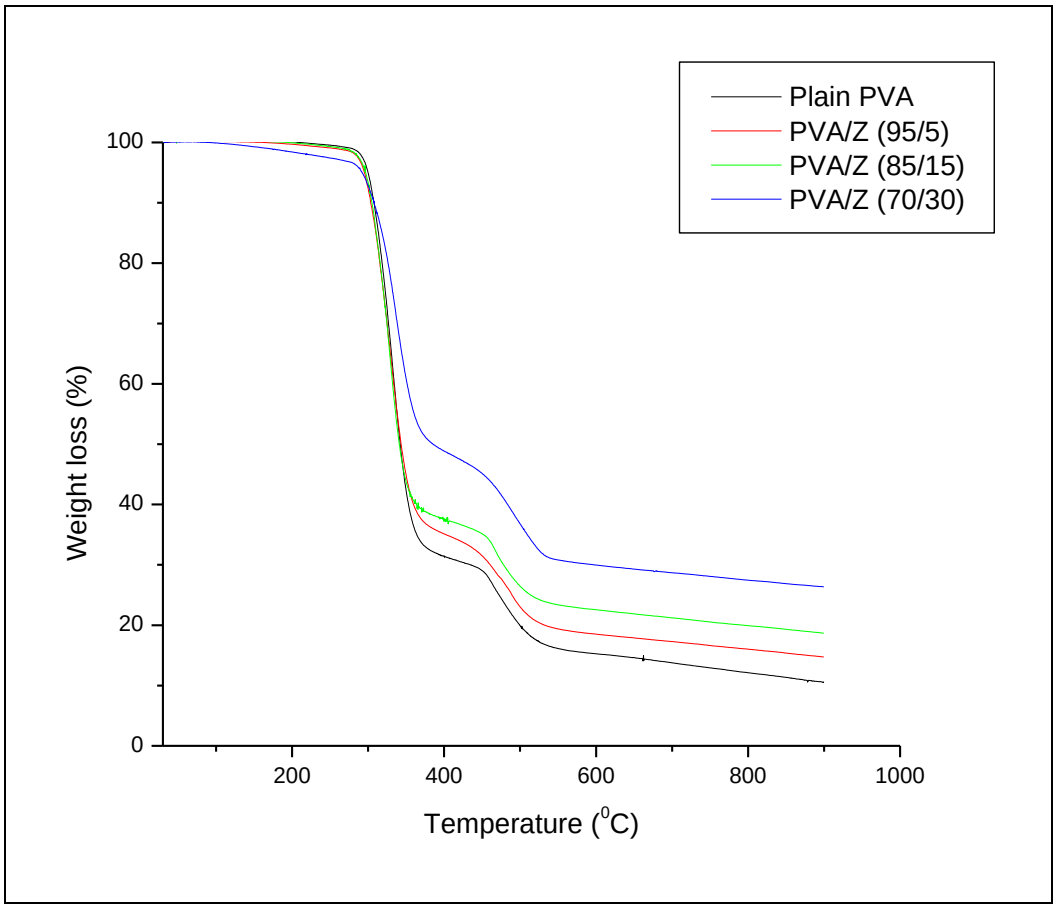

Figure 4.5: TGA thermograms of PVA and PVA/Z composites.

An intense endothermic reaction of PVA is observed at 227.4 ^{0}C, corresponding to the crystalline melting point (T_m) of the polymer.[17] Again when compared with the pure PVA, the T_m values of the PVA/Z composites are higher, as seen in Table 4.1. This observation is due to the fact that hydrogen bonds are generated which, in turn, act as cross-linking points and thus restrict the movement of molecular chains of the polymer.[13]

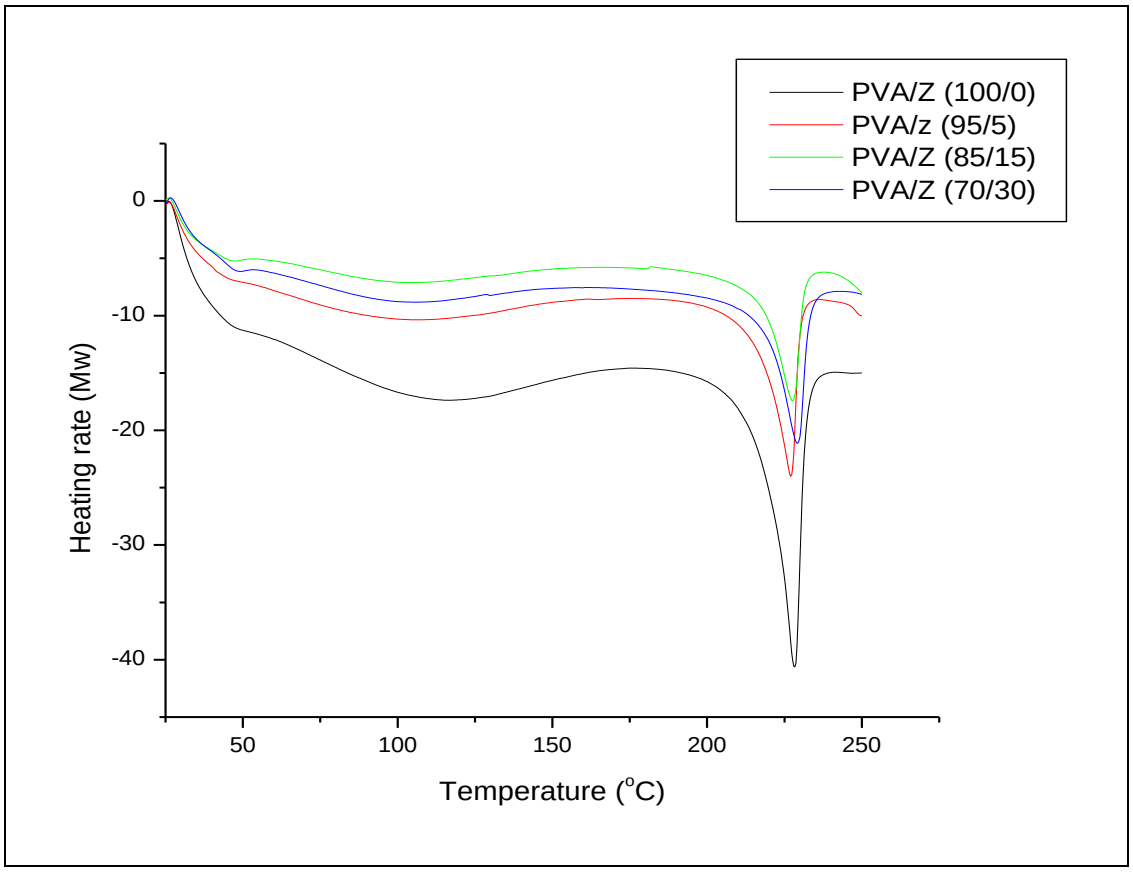

Figure 4.6: DSC curves of the plain PVA and those of PVA/Z filled with 5%, 15% and 30% of the zeolite filler

4.3.5 Swelling behaviour studies

Studies on the swelling behaviour of the PVA and zeolite-filled PVA films were carried out so as to ascertain the water-retention ability of the composites, which will serve as valuable information when discussing the metal-ion removal capacities of the different composites (**Chapter 5**). The results are reported in Table 4.2. The experiment was carried out in five replications and the mean values are reported.

Table 4.2: The swelling behaviour of PVA/Z composites measured as a function of change in mass. 'Wt' and 'abs' represent 'weight' and 'absorbed', respectively.

Comp. ratio (PVA/Z) wt (%)	*Wt. before abs. (g)*	*Wt. after abs. (g)*	*Swelling (%)*
100/0	0.820	1.096	33.7
95/5	0.728	1.234	69.5
90/10	0.874	1.495	71.1
85/15	0.859	1.548	80.2
80/20	0.864	1.571	81.8
70/30	0.861	1.634	89.7

From the results given in Table 4.2, it is observed that due to its hydrophilic nature, the pure PVA has a relatively high water absorption (retention) ability of 33.7%. This hydrophilicity is improved further with the introduction of the zeolite into the PVA matrix. Water-retention capacity increases from the initial 33.7% to 89.7% when there is 30% content of the zeolite in the composite. This suggests that the zeolite contributes immensely to the water-retention capacity, as evidenced by the degree of swelling. This is to be expected because the zeolite, apart from being hydrophilic due to its polar surface, also has a highly porous structure which enhances the flow of water molecules.[18] This enhanced water absorption capability could have positive implications for the removal of heavy-metal ions in solution.

4.4. Conclusions

PVA/Z nanocomposite films with varying zeolite content were prepared by melt intercalation. Results from the SEM showed good miscibility between the polymer and the filler, which results from hydrogen bonding. XRD results confirmed the preparation of PVA/Z nanocomposites with a partially intercalated and partially exfoliated structure. Thermal studies indicated that addition of the zeolite improved the thermal stability as confirmed by TGA and DSC data. The water-retention capacity was also enhanced with the addition of the zeolite into the polymer matrix, an occurrence that is expected to enhance the heavy-metal (in solution) removal capacities of the zeolite-filled PVA polymer nanocomposites.

4.5 References

1. Nawani P. Dissertation PhD Chemistry Thesis. The Graduate School, Stony Brook University, May 2008.
2. Sinha Ray S., Okamoto M. *Prog. Polym. Sci.* **28** (2003) 1539–1641.
3. Wang X.J., Gross R.A., McCarthy S.P. *J. Environ. Polym. Degrad*. **3** (1995) 161-167.
4. Lawton J.L. and Fanta G.F. *Carbohydr. Polym*. **23** (1994) 275-280.
5. Coffin D.R., Fishman M.L., L T.V. *J. Appl. Polym. Sci.* **61** (1996) 71-79.
6. Chiellin E., Cinelli P., Imam S.H., Mao L. *Biomacromolecules* **2** (2001) 1029-1037.
7. Tsukada M. Freddi G., Chrighton J.S. *J. Polym. Sci.* B*. Polym. Phys*.. **32** (1994) 243-248.
8. El-Khodary A., Oraby A.H., Abdelnaby M.M. *J. Magn. Mater.* **320** (2008) 1739.
9. Qian X.F., Yin J., Huang J.C., Yang X.X., Guo Y.F., Zhu Z.K. *Mater Chem. Phys*. **68** (2001) 95.
10. Lee J. Battacharyya D., Easteal A.J., Metson J.B. *Curr. Appl. Phys*. **8** (2008) 611.
11. Madejova J. *Vibrational Spectroscopy* **3** (2003) 1- 6.
12. Jayasekara R., Harding I., Bowater I., Christie G.B.Y., Lonergan G.T. *Polym. Test.* **23** (2004) 17.
13. Yang Y., Liu C., Wu H. *Polym. Test*. **28** (2009) 371-377.
14. Jia X., Li Y.F., Zhang B., Cheng Q., Zhang S. *J. Res. Bull.* **43** (2008) 611.
15. Peng Z., Kong L.X. *Polym. Degrad. Stabil.* **92** (2007) 1061-1071.

16. Peng Z, Kong LX, Li SD. *J. Appl. Polym. Sci.* **96** (2005) 1436.
17. Mbhele Z.H., Salemane M.G., Van Sittert C.G.C.E., Nedeljkovic T.M., Djokovic V., Luyt A.S. *Chem. Mater.* **15** (2003) 5019.
18. Kirschhock C., Hunger B., Martens J. and Jacobs P.A. *J. Phys. Chem*. **B104** (2000) 439-445.

CHAPTER 5

A COMPARATIVE STUDY ON THE ADSORPTION OF Cu(II), Pb(II) AND Co(II) ON CLINOPTILOLITE-FILLED EVA/PVA POLYMER NANOCOMPOSITE FILMS

5.1 Introduction

Adsorption, the most preferred method of heavy-metal recovery, was used to investigate the applicability of PVA/EVA-clinoptilolite films as adsorbent composite materials for the removal of Co^{2+}, Pb^{2+} and Co^{2+} from synthetic wastewater. The influence of factors such as pH, contact time, filler dosage, initial concentration of solutions and pretreatment of the filler on the overall metal removal capacity, was investigated. pH is one of the paramount factors to consider in adsorption studies, as metal uptake will vary under acid and basic media, particularly with ion exchangers. It has been reported that zeolites tend to alter the solution pH during ion exchange.[1] This is partly due to the H^+ in solution replacing exchangeable ions on the zeolite.[2]

The contact time allowed for interaction between the adsorbent and the sorbate is another important operational parameter in adsorption studies. This is particularly significant as it measures the efficiency and hence the cost effectiveness of the process for large-scale applications. Researchers have come up with different time scales for different metal ions ranging from minutes to several days.[3,4] The dependence of metal uptake on the concentration of the metal ions in solution has been widely investigated. This is critical in kinetic studies where the metal-adsorbent behaviour is observed over a concentration range. Studies have been reported in which the metal uptake increases with increasing concentration,[7] although this process is independent of contact time.[8]

Chemical conditioning of zeolites is often carried out in an attempt to remove cations that may hinder ion exchange from the framework, and replacing them with easily exchangeable cations.[9] It is also believed that exchangeable cations already existing on a zeolite framework are made more accessible with chemical

conditioning.[10] Some of the conditioning reagents include NaCl, $Ca(OH)_2$, KCl, HCl, $Mg(OH)_2$, etc.[11,12] NaCl has been the most frequently used, as it is reported to improve removal capacity,[2,13] while other conditioning reagents such as HCl have been reported to have destructive effects on the zeolite structure.[14]

From the optimum conditions thus obtained during the adsorption experiments, the sorption mechanisms of the metal ions in single and mixed solutions were studied in batch mode. The reusability (adsorption-desorption cycle) of the adsorbent material over a period of time was also evaluated.

5.2 Experimental procedure

5.2.1 Materials

Extruded EVA and PVA strips of an average thickness of 0.5 mm were used as the adsorbent materials. $Pb(NO_3)$, $CuSO_4 \cdot 5H_2O$ and $CoSO_4 \cdot 7H_2O$ were used as metal-ion sources for the preparation of synthetic solutions, while NaCl, KCl, and HCl were used as conditioning reagents for pretreatment of the filler. All reagents were of analytical grade of the highest purity available, and were supplied by Sigma Aldrich and Merck.

5.2.2 Adsorption studies

The sorption behaviour of the three metals on the adsorbent composite was studied using the batch technique at room temperature (approx. 25 ^{0}C). Synthetic stock solutions of Pb^{2+}, Cu^{2+} and Co^{2+} were prepared by dissolving $Pb(NO_3)_2$, $CuSO_4 \cdot 5H_20$ and $CoSO_4 \cdot 7H_2O$ in 1 000mL volumetric flasks, respectively, and then diluted accordingly to generate the required concentrations. In all experiments throughout the study, adsorbent strips of 40 mm by 20 mm length were placed in 50 mL of the synthetic solution during adsorption studies. All solutions were analyzed within 24 h to eliminate errors emanating from container plating or precipitation of the metal ions. Metal-ion content was quantified using atomic absorption spectroscopy (GBS Avanta 1.33), using an air-acetylene flame. All experiments were conducted in triplicate and mean values were reported. The

metal uptake degree (α) and the adsorbed metal amount per volume (q) were calculated as follows:

$$\alpha = \frac{Ci - Cf}{Ci} X\ 100\% \quad (5.1)$$

$$q = \frac{Ci - Cf}{Ci} X \frac{V}{m} \text{ (mg/g)} \quad (5.2)$$

where:

m is the mass of the adsorbent composite strip

V is the volume of the solution

C_i and C_f represent the initial and final concentrations, respectively

5.3 Results and discussion

5.3.1 Effect of zeolite loading

The amount of filler dosage in the composite is an important parameter because it is directly related to the adsorption capacity of an adsorbent under the given operating conditions. To evaluate the effect of zeolite loading on the adsorption behaviour, experiments were conducted with an adsorbent dose in the range of 0% to 30% of the filler at an initial concentration of 10 mg/L, at room temperature. Experiments were allowed to run overnight. The adsorption behaviour of clinoptilolite-filled EVA and PVA composites is shown in Figure 5.1 and Figure 5.2, respectively.

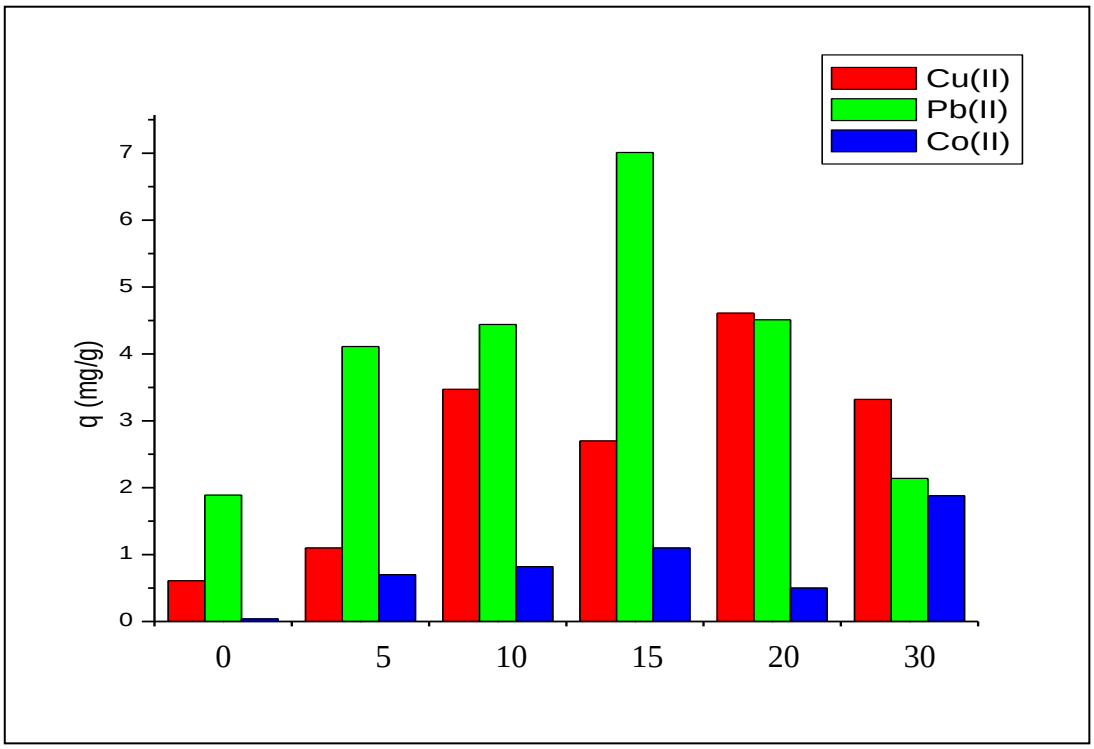

Figure 5.1: Adsorption studies of Pb, Cu and Co onto EVA-C composites with varying filler dosage (5% wt to 30% wt) at room temperature. Initial concentration was fixed at 10 mg/L.

For all metal ions, the removal efficiency increases with an increase in the amount of clinoptilolite in the composite. This is because increasing the loading of the adsorbent filler also increases the surface area and hence the number of active adsorption sites available in the composite films. However, as shown in Figures 5.1 and 5.2, the amount of metal removed per unit weight of the adsorbent *q*, decreases at higher dosages. The decrease in '*q*' at higher dosage can be attributed to the fact that some of the adsorption sites remain unsaturated during the adsorption process, whereas the number of available adsorption sites increase with increasing adsorbent.[15] The optimum dose values thus obtained were 15% zeolite loading for EVA-C composites and 10% for PVA-C composites, and were used in the subsequent adsorption experiments, unless otherwise indicated.

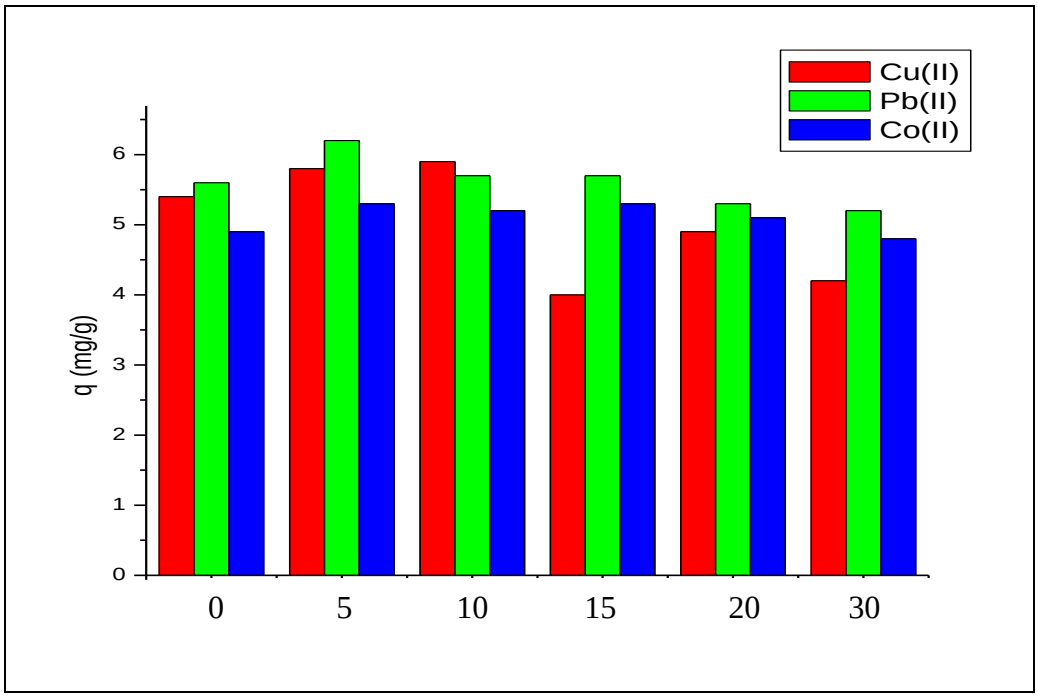

Figure 5.2: Effect of clinoptilolite (zeolite) loading onto PVA polymer matrix on the adsorption of Cu(II), Pb(II) and Co(II). C_i = 10 mg/ℓ; T = 25 ^{0}C

5.3.2 Effect of contact time

The effect of contact time on the metal-ion retention capacity was studied by varying the time from 2 h to 48 h for EVA-C and 2 h to 24 h for PVA-C, at a fixed initial concentration of 10 mg/ℓ. The results are presented in Figures 5.3 and 5.4, respectively. The effect of contact time on adsorption onto EVA-C (85/15) as shown in Figure 5.3, shows an increase in efficiency with an increase in time of contact. The metal-ion adsorption is rapid within the first 5 h, and then increases more slowly, and the adsorption process seems to have attained equilibrium after 24 h. However, for PVA-C (Figure 5.4), equilibrium was attained over a shorter period of 8 h, and again adsorption was rapid within the first 4 h. The initial metal-ion adsorption rate by EVA-C and PVA-C is very high as a large number of adsorption sites are available for adsorption. Once the available free sites are gradually filled up by the adsorbate species, adsorption slows down.

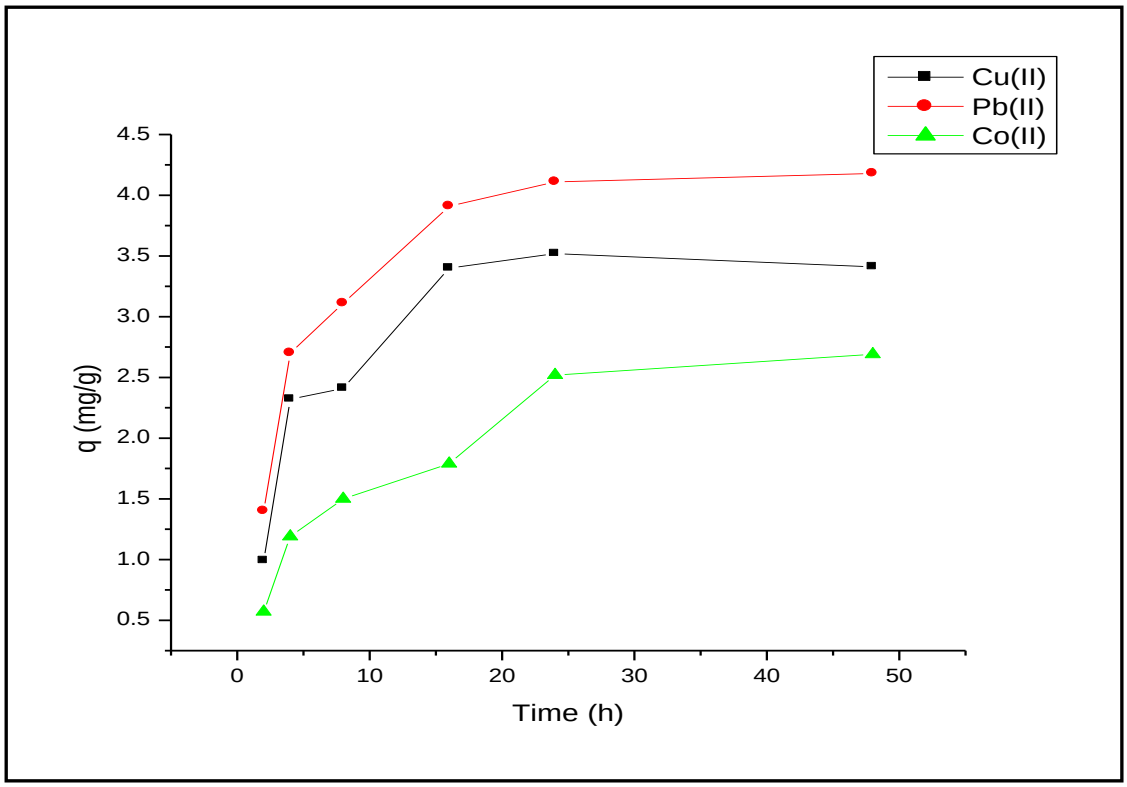

Figure 5.3: Adsorption of Pb^{2+}, Co^{2+} and Cu^{2+} onto EVA-C (85/15% wt) as a function of time

Also observed from Figures 5.3 and 5.4 is that equilibrium values of adsorbed amount (*q*) were higher for PVA-C than EVA-C, in all metal ions. This in essense suggests that PVA-C is more efficient than EVA-C, and hence equilibrium was reached earlier. For both composites, the metal-ion retention process is due to complex mechanisms of adsorption and ion exchange, but the chemical structure of the PVA-C accounts for the better efficiency. PVA is a three-dimensional structured polymer containing a large amount of super-hydrophilic carboxyl and carboxylate groups, which act as active adsorption sites for heavy metals.[16] Due to their super-hydrophilic characteristics, combined with the high cation exchange capacity (CEC) of the clinoptilolite, this composite would swell and expand quickly when in contact with aqueous solutions and the carboxyl and carboxylate groups present within the polymeric networks can capture metal ions in solution. This observation is in agreement with the assumption made in **Section 4.3.5**. In an attempt to improve the removal efficiency, the effect of pre-treatment of the filler

was investigated for the clinoptilolite-filled EVA composites, and the results are discussed below.

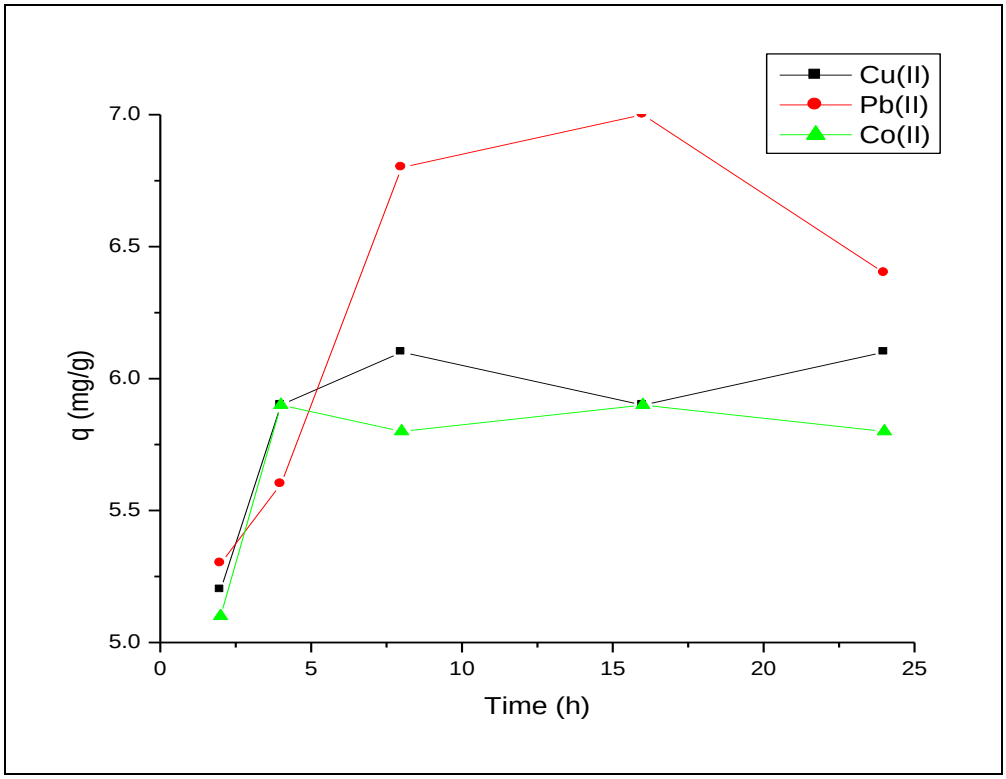

Figure 5.4: The effect of contact time on the adsorption of Cu(II) Pb(II) and Co(II) by PVA-C (85/15)

5.3.3 Effect of chemical conditioning of the filler in EVA-C composites

To investigate the influence of pretreatment, composites filled with 'as-received' clinoptilolite were compared with nanocomposites filled with NaCl-, HCl- and KCl-activated clinoptilolite. Portions of the filler material were soaked overnight in 100 mL of 2M of the conditioning reagent, with shaking at 160 rpm. Experiments were carried out at natural pH and the results are shown in Figure 5.5. The results show that pretreatment improves the adsorption efficiency of all three metal ions, compared to the composites filled with untreated clinoptilolite. However, this improvement is also a function of the conditioning reagent in the order HCl > NaCl > KCl, and this can be explained as follows: acid (HCl) activation of natural

clinoptilolite improves its ion-exchange capacity due to the dealumination, decatination and dissolution of amorphous silica fragments blocking the channels.[7,17] The relatively lower adsorption capacity shown by KCl-activated composites could be due to the resilience of K^+ to participate in ion exchange as compared to Na^+. This behaviour is attributed to sites on the zeolite that are occupied by K^+. It is proposed that K^+ is located at a specific M(3) site which is situated in an eight-member ring and has the highest coordination amongst all the cationic sites in the unit cells, resulting in strong bonding. Thus KCl-activated zeolite would have a higher proportion of K^+ moieties on the lattice, which will in turn determine the cation-exchange capacity. These observations are in accordance with research work done by Cincotti.[18]

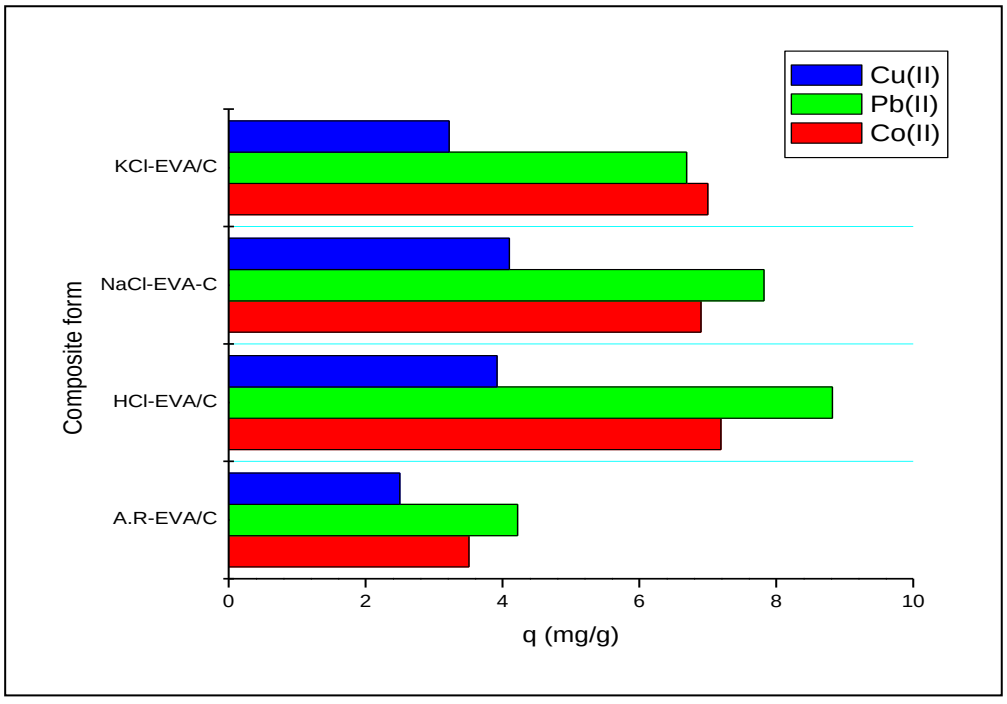

Figure 5.5: The influence of different conditoning reagents on the heavy-metal uptake onto EVA-C (85/10) after 24 h, at room tempererature. Initial concentration was kept constant at 10 mg/ℓ.

5.3.4 Influence of pH on adsorption

Solution pH is another controlling parameter that has a significant influence on the adsorption behaviour of an adsorbent, especially with metal cations. To optimize

the pH value for maximum efficiency, experiments were carried out using HCl-activated EVA-C (85/15) and PVA-C (90/10) at room temperature. The initial concentration was kept constant at 10 mg/L and the pH values varied from 2 to 12 for PVA-C and from 2 to 14 for EVA-C. The initial solution pH was set at less than pH 6 for all metal ions taking into account the possible metal precipitation. The results for adsorption onto EVA-C are shown in Figure 5.6. With increasing pH, metal-ion uptake increased initially, reaching a maximum level at between pH 4 and pH 5 for Pb(II) and Cu(II). For Co(II) on the other hand, a maximum level was attained at pH 7.

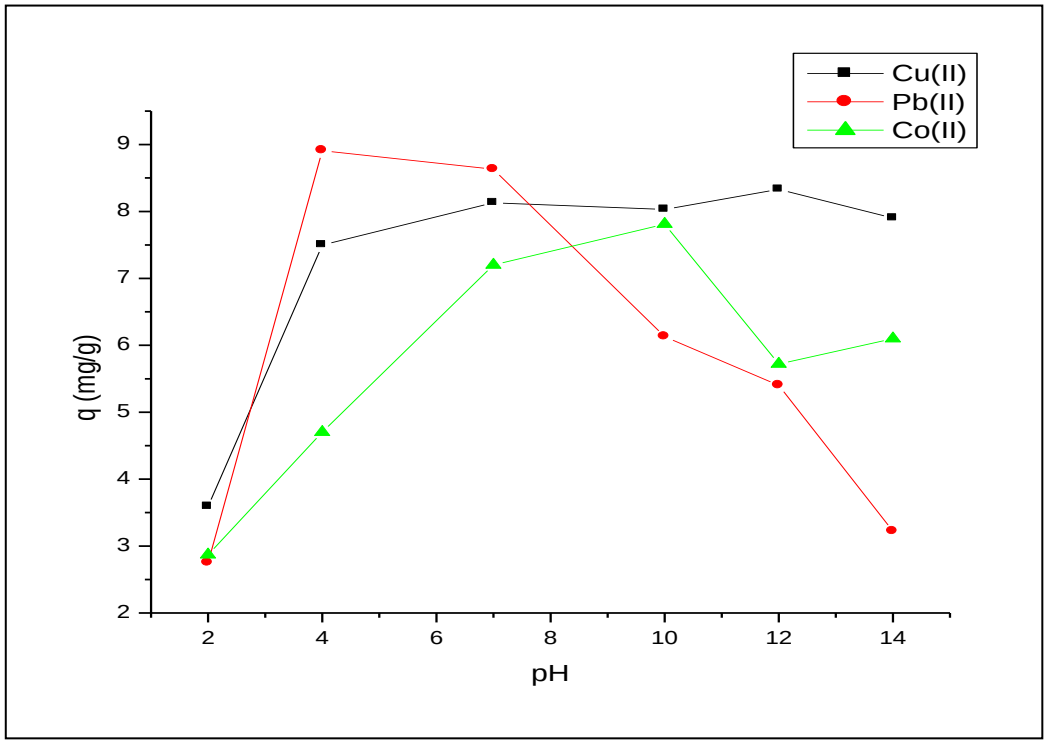

Figure 5.6: Influence of pH on the adsorption of Pb(II), Co(II) and Cu(II) onto HCl-activated EVA-C (85/15)

From the PVA-C adsorption values (Figure 5.7), adsorption capacity *q*, reached its maximum (pKa value) at pH 6 for Cu(II) and Co(II) and at pH 8 for Pb(II), then decreased at lower or higher pH values. This behaviour can be explained by both the change in ionic state of the acid functional carboxyl groups in the adsorbent as well as competition for the binding sites by the cations.[19,20] At low solution pH values, functional groups were protonated, and metal-ion uptake decreased while

at pH values higher than the pKa, carboxyl groups were negatively charged and the metal cations could bind to the negatively charged groups by electrostatic attraction.[15,21] On the other hand, the formation of aqua-metal species and hydroxo-complexes is also determined by the solution pH value.[22]

At very low pH values, the number of H_3O^+ significantly exceeds that of metal ions, and the latter can hardly compete with the H_3O^+ ions for the binding sites on the adsorbent. By increasing the pH, the surface charge of the adsorbent becomes more negative as the H_3O^+ concentration decreases and some sites become available to the metal ions. As the acidity decreases even further, more H_3O^+ ions on the surface of the adsorbent are replaced by metal ions such as $Cu(OH)^+$, $Pb(OH)^+$; and $Co(OH)_2$.[23-25]

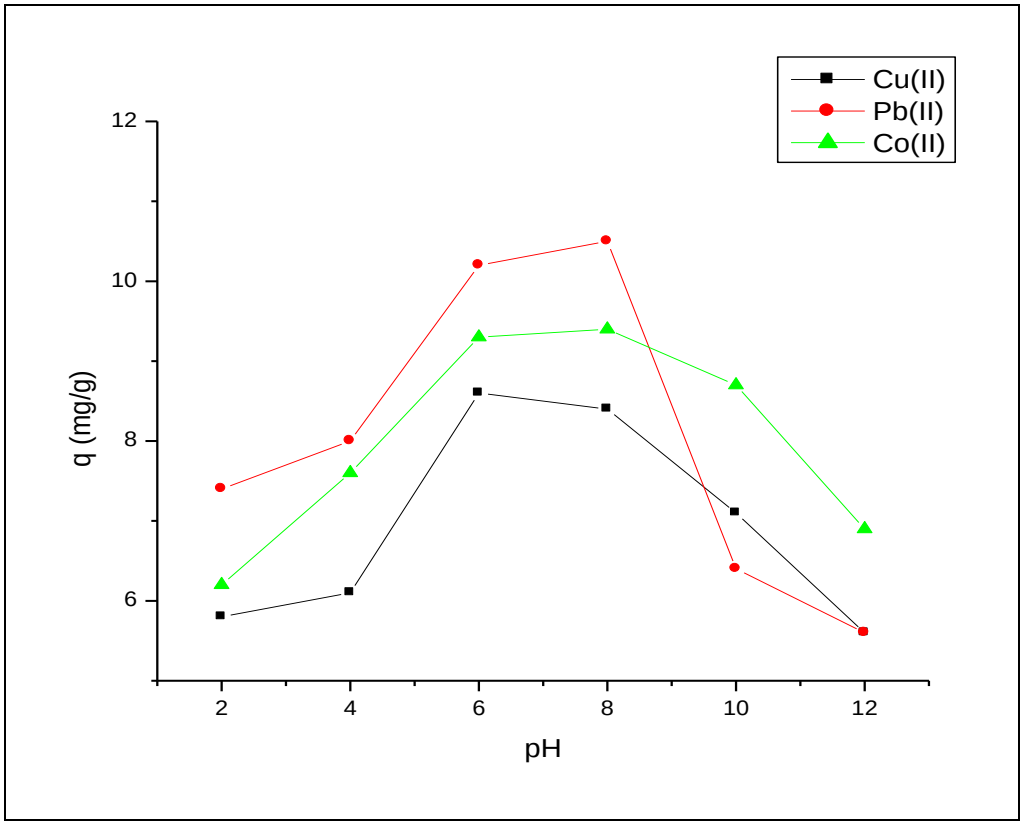

Figure 5.7: Effect of solution pH on the adsorption of Cu(II), Pb(II) and Co(II) onto PVA-C (90/10)

5.3.5 The effect of initial metal-ion concentration on adsorption

The adsorption capacity was investigated in correlation with the variation in the initial metal-ion concentrations in the range 0.5 mg/L to 20 mg/L at room temperature. The solution pH was fixed at pH = 6 and the adsorbent dose at 90/10 for both EVA/C and PVA/C. Figure 5.8 shows the percentage adsorption of Cu(II), Pb(II) and Co(II) as a function of the initial concentration. As observed in Figure 5. (a and b), the percentage adsorption of the three metal ions decreases with increasing metal concentration in solution. The high cation uptake at low initial concentration is due to the fact that there are more exchangeable sites available in the adsorbent at low M^{2+}/adsorbent ratios (M^{2+} = metal cation) while, as the ratios increase, exchangeable sites become saturated resulting in a decrease in the adsorption rate.[26]

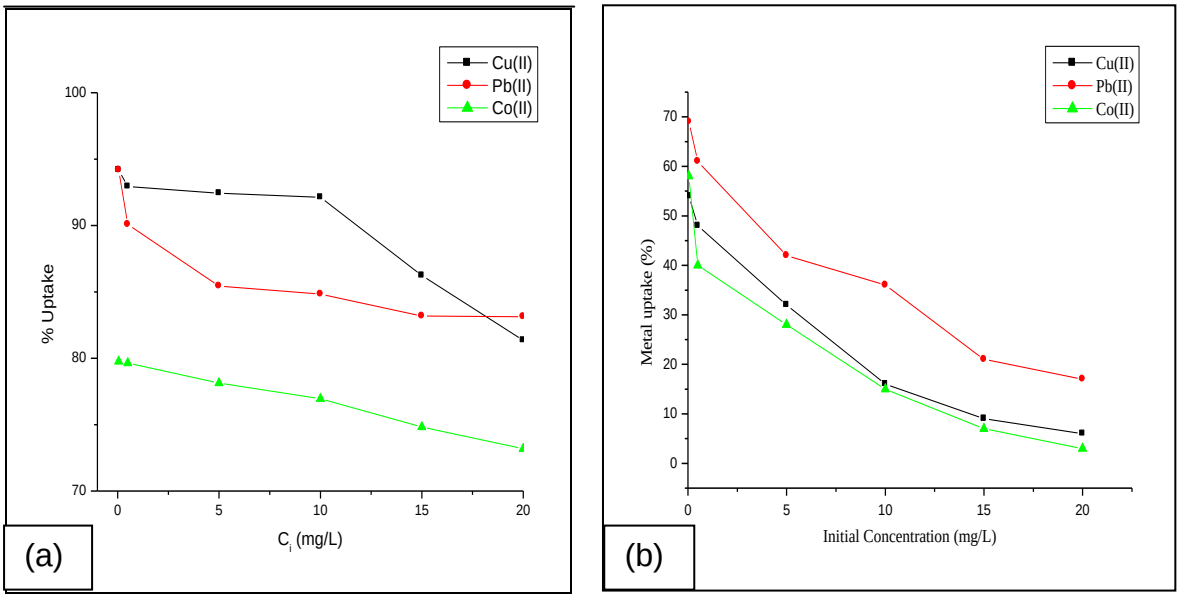

Figure 5.8: Percentage metal-ion adsorption as a function of initial concentration by (a) PVA/C and (b) EVA/C composite materials

In Figure 5.9, the amount of metal ion adsorbed per volume (*q*) is plotted as a function of the initial concentration. From these results, it is observed that adsorption capacity increases with an increase in initial concentration, and that the adsorption of ionic species occurs in two phases: an initial rapid phase and a slower second phase, whose contribution to the total adsorption is relatively slow.

The first phase is predominantly external surface adsorption while in the second phase adsorption seems to be controlled by intra-particle diffusion processes.[27] The observed results can be explained in two ways: Firstly, a higher initial concentration increases the driving force to overcome the mass-transfer resistance of the metal cations between the solid and aqueous phases. This then results in a higher probability of a collision between the metal cation and the adsorbent composite material.[28] Secondly, at higher initial concentration, there is bound to be more intense interaction between the metal ions and the adsorbent, resulting in an increase in metal-ion uptake with increasing initial concentration.

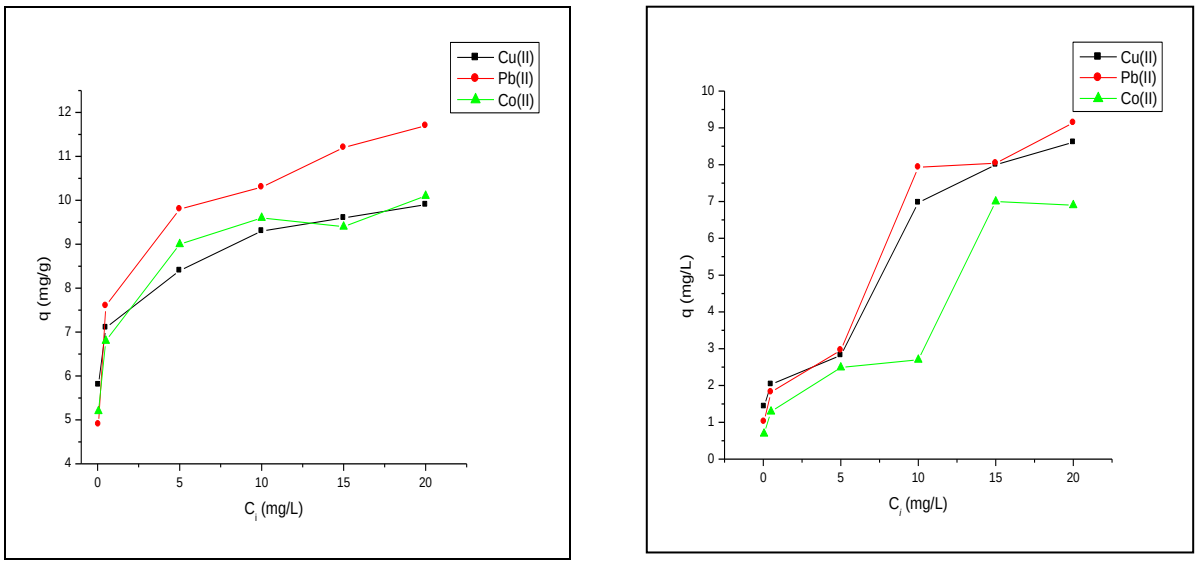

Figure 5.9: The amount adsorbed per unit mass of the adsorbent (*q*) is plotted as a function of the initial metal-ion concentrations, to illustrate adsorption behaviour on (a) PVA/C and (b) HCl-EVA/C (90/10). pH = 6; *t* = 8 h for PVA/C and 24 h for EVA/C.

Heavy-metal uptake is attributed to the diverse complex mechanisms of ion-exchange and adsorption processes. During the ion-exchange process, metal ions move through the pores and channels of the zeolite, in order to replace exchangeable ions. Diffusion was faster through the pores and was retarded when ions moved through the smaller channels of the microporous mineral. The adsorption phenomenon depends on the charge density of cations hence the diameter of the hydrate ions becomes important. Since the charges of all the cations studied are the same (+2), metal ions with the largest diameter will have

minimum adsorption while those with the least diameter will have maximum adsorption.[29] As seen in the adsorption studies discussed above, Pb^{2+} is the most preferred cation while Co^{2+} is the least adsorbed. Thus the selectivity trend is in the order: $Pb^{2+} > Cu^{2+} > Co^{2+}$, and this is in accordance with results obtained by Wang et al.[25] The consistent selectivity could perhaps be due to the high Si/Al ratio (5.7) of the clinoptilolite which results in a typical low anionic field that gives rise to good selectivity. These findings can be attributed to the dissimilar preferences of the clinoptilolite for various metal cations. Because of its high Si/Al ratio, clinoptilolite has a low charge density. Therefore, divalent cations with low hydration energies are sorbed preferentially compared to cations with high hydration energies. Thus a high concentration of Pb, with the lowest hydration energy, is expected to limit the uptake of Co and Cu.

5.3.6 Desorption and reusability studies

Although adsorption is a well-established technology for water purification, its success however, is largely dependent on the ability of the adsorbent to desorb the target contaminant for efficient reusability. To evaluate the reusability of the EVA/C and PVA/C adsorbent composites, four consecutive adsorption-desorption processes were carried out using the same adsorbent. Desorption studies were carried out with 2M solutions of NaOH and HCl, where the latter was found to be more efficient. This was expected because in acidic medium, the hydronium ions in solution replace the metal ions on the composite material while in basic medium, recovery was poor perhaps due to coordinating ligands being protonated, resulting in the metal cations being hardly detached from the adsorbent material.

Desorption studies for all three metal cations showed a similar trend, but only the results from the Pb(II) adsorption-desorption model are presented. Table 5.1 shows desorption results from EVA/C (85/15). Although the amount adsorbed in the subsequent cycles is less than that in the first cycle, there is still a significant amount of metal ion removed, an indication that the material can be reused over a significant period of time. The desorbed amounts were somewhat inconsistent, and although complete desorption could not be achieved, desorbed amounts of up

to 72% (2nd cycle) were still obtained. The incomplete desorption of metal cations could be attributed to interference by non-electrostatic forces between the metal and the composite material.[30]

Table 5.1: Adsorption-desorption cycle of Pb(II) onto HCl-EVA/C (85/15). 'Ads' and 'Des' represent the adsorbed and desorbed amounts (%), respectively. Conditions: t = 24h; pH = 6; C_i = 5 mg/L; T = 25^{0}C.

1st cycle		**2nd cycle**		**3rd cycle**		**4th cycle**	
Ads	*Des*	*Ads*	*Des*	*Ads*	*Des*	*Ads*	*Des*
78.46	66.42	75.13	72.38	70.32	64.15	59.26	51.78

Results from the adsorption desorption-desorption tests using PVA/C show that total adsorption capacity of the PVA/C for Pb(II) ions after four cycles decreased significantly by more than 50% from 89.34% to 43.79%. Although a relatively high amount of metal ion can be recovered from the PVA/C adsorbent when compared with the EVA/C, the significantly low adsorption capacity values after the second and subsequent cycles suggest that the reusability of the former is very poor. This could be due to the destructive nature of the acid (HCl) and perhaps the use of a different desorbing agent like EDTA[31,32] could produce better results.

Table 5.2: Adsorption-desorption cycle of Pb(II) onto PVA/C (90/10). Conditions: t = 8h; pH = 6; C_i = 5 mg/L; T = 25^0C.

1st cycle		**2nd cycle**		**3rd cycle**		**4th cycle**	
Ads	*Des*	*Ads*	*Des*	*Ads*	*Des*	*Ads*	*Des*
89.34	84.72	61.91	53.05	48.29	46.30	47.16	43.79

5.3.7 Adsorption isotherms

The adsorption data were fitted to the Langmuir and Freundlich isotherms. The Langmuir isotherm holds true for monolayer adsorption due to a surface of a finite number of identical sorption sites, and can be expressed in linearized form as:

$$C_e/q_e = b/Q_o + C_e/Q_o \qquad (5.3)$$

where:

C_e is the equilibrium concentration (mg/L) and

q_e is the amount adsorbed at equilibrium

Q_o and b are Langmuir constants representing the adsorption capacity (mg/g) and the heat of adsorption, respectively

Also important in the Langmuir isotherm studies is a constant, R_L, which is a parameter which predicts whether an adsorption system is favourable or not, and is calculated as:

$$R_L = 1/1 + bC_o \qquad (5.4)$$

where:

C_o is the initial concentration (mg/L)

For $0< R_L <1$ adsorption is favoured, and the higher the value of R_L, the greater the favourability.[33]

The Freundlich isotherm describes the heterogeneous surface energies by multilayer adsorption and is expressed in linear form as:

$$\ln q_e = \ln K_f + n \ln C_e \qquad (5.5)$$

where:

q is representative of the adsorption capacity (mg/g)

n is an empirical parameter related to the intensity of adsorption

If n is between 0.1 and 1, then adsorption is favourable.[30] The Langmuir and Freundlich parameters for Cu(II), Pb(II) and Co(II) adsorption onto PVA/C (90/10) under equilibrium conditions are listed in Table 5.3.

TABLE 5.3: Langmuir and Freundlich isotherm parameters for Pb(II), Cu(II) and Co(II) adsorption by HCl-EVA/C (85/15)

M^{2+}	Langmuir model				Freundlich model		
	R^2	Q_0	R_L	b	R^2	K_f	n
Pb	0.912	0.982	0.865	0.310	0.895	0.410	1.055
Cu	0.956	0.870	0.791	0.528	0.882	0.288	0.793
Co	0.910	0.717	0.865	0.310	0.887	0.139	0.776

From the Langmuir isotherm (Figure 5.10a), the R^2 values for Pb^{2+}, Cu^{2+}, Co^{2+} were 0.912, 0.956 and 0.910, respectively. From the Q_o values (Table 3) Pb(II) ions had the highest adsorption capacity, and the R values for all metal ions were >0, indicating that adsorption was favourable.

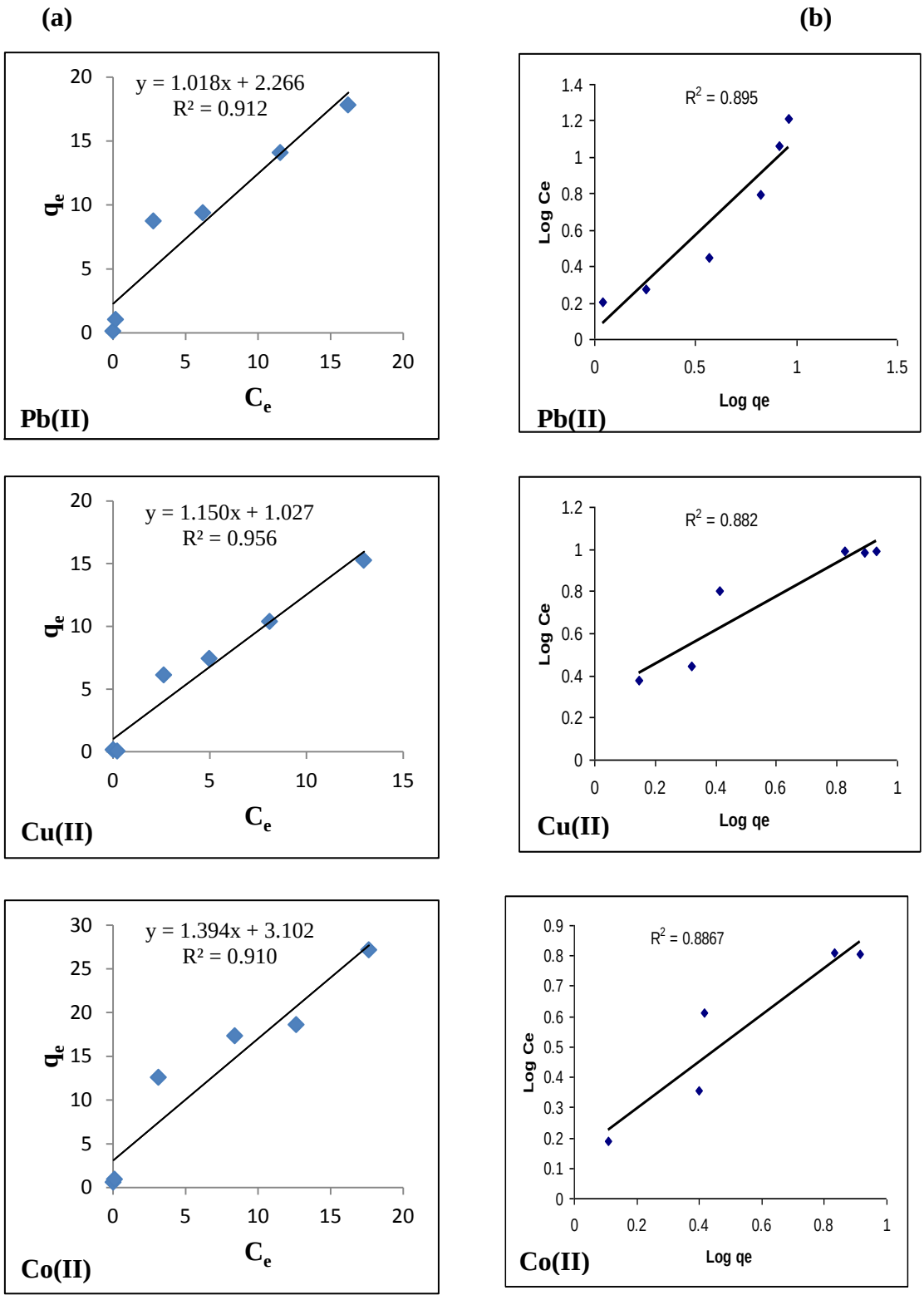

Figure 5.10: Langmuir (a) and Freundlich (b) adsorption isotherms for Pb(II), Cu(II) and Co(II) by PVA/C (90/10) under equilibrium conditions

The Freundlich constants K_f, were calculated to be 0.041 mg/g, 0.288 mg/g and 0.776 mg/g for Pb^{2+}, Cu^{2+}, Co^{2+}, respectively (Figure 5.10b). The R^2 values from the Freundlich isotherm plots are smaller than those obtained from Langmuir plots for all metal ions, suggesting that the Langmuir isotherm provides a better fit for the adsorption data. This is an indication that monolayer adsorption due to a surface area of a finite number of identical sorption sites is favoured over heterogeneous adsorption.

5.4 Conclusion

This chapter investigated the applicability of PVA/C and EVA/C extruded films in the removal of Pb(II), Cu(II) and Co(II) from synthetic wastewater. The results showed that removal capacity of the two adsorbent composites generally increases with an increasing amount of the filler. PVA/C exhibited better removal efficiency throughout the study when compared with EVA/C. However, pre-treatment of the filler in EVA/C was found to significantly improve the overall performance of the adsorbent composite, but was dependent on the conditioning reagent. Adsorption was also found to be influenced by such factors as time, pH and initial concentration of the solution. The Langmuir isotherm model provided a better fit for the adsorption data than the Freundlich isotherm model as evidenced by higher regression coefficient (R^2) values for the former. Consecutive adsorption-desorption experiments show that EVA/C composites can be used with high reusability when compared with PVA/C, although for both materials, complete desorption of the metal cation from the composite material could not be achieved. In a nutshell, the obtained results suggest that this simple but up-scalable methodology for the preparation of adsorbents has great potential for the preparation of similar nanocomposites for other environmental remediation applications.

5.5 References

1. Kesraoui-Ouki S. and M. Kavannagh M. *Waste Manage. Res.* **15** (1997) 383.

2. Sprynskyy M., Lebedynets M., Terzyk A. P., Kowalczyk P., Namiesnik J. and Buszewski B. *Journal of Colloid and Interface Science* **284** (2005) 408-415.

3. Sarioglu M. *Separation and Purification Technology* **41** (2005) 1–11.

4. Cagin V. PhD Dissertation (2006) The Graduate School of Natural and Applied Sciences of Middle East Technical University, Turkey.

5. Barrer R. M. and Klinowski J. *Faraday Trans*. I **66** (1974) 2080.

6. Helfferich F. *Dover Publications Inc.*, New York, 1995.

7. Tsitsishvili G. V., Andronikashvili T. G., Kirov G. N., Filizova L. D. *Natural Zeolites,* Ellis Horwood, New York (1992) 158.

8. Sun W., Wang Y. J., Yang L., Lu Y. C. and Luo G. S. *Solvent Extraction and Ion Exchange* (2008) 672 – 768.

9. Semmens M. J. and Martin W. P. *Water Research* **22** (5) (1988) 537-542.

10. Gradev G., Avramova A. and Stefanova I. *Occurrence, Properties and Utilization of Natural Zeolites* (1988) 463-470.

11. Zamzow M. J., Eichbaum B. R., Sandgren K. R. and Shanks D. E. *Sep. Sci. Technol.* **25** (1990) 13–15.

12. Milan Z., Sanchez E., Weiland P., de Las Pozas C., Borja R., Mayari R. and Rovirosa N. *J. Chem. Eng.* **66** (1997) 65-71.

13. Panayotova M. and Velikov B. *Journal of Environmental Science and Health* **38** (2003) 545-554.

14. Korkuna O., Leboda R., Skubiszewska-Zieba J., Vrublevs'ka T., Gun'ko V. M., Ryczkowski J. *Micropor. Mesopor. Mater.* **87** (33) (2006) 243-254.

15. Chen J.H., Li G.P., Qing Lin Liu Q.L., Ni J.C., Wu W.B., Lin J.M. *Chem. Eng. J.* **165** (2010) 465–473.

16. Zheng Y., Wang A. *Chem. Eng. J.* **162** (2010) 186-193.

17. Athanasiadis K., Helmreich B. *Water Research* **39** (2005) 1527-1532.

18. Cincotti, A., Lai, N., Orru, R., Cao, G. *Chemical Engineering Journal* **84** (2001) (3) 275-282.

19. Anirudhan T.S., Radhakrishnan P.G. *J. Colloid Interf. Sci.* **316** (2007) 268–276.

20. Lodeiro P., Fuentes A., Herrero R., Sastre de Vicente M.E. *Environ. Chem.* **5** (2008) 355–365.

21. Miretzky P., Fernandez Cirelli A. *J. Hazard. Mater.* **180** (2010) 1–19.

22. Barthomeuf D. *Studies in Surface Science and Catalysis* **105** (1997) 1677-1706.

23. Bosso S.T., Enzweiler J. *Water Research* 36 (2002) 4795-4800.

24. Taty-Costodes V.C., Fauduet H., Porte C., Delacroix A. *Journal of Hazardous Materials* B **105** (2003) 121-142.

25. Wang Y. H., Lin S.H., Juang R.S. *Journal of Hazardous Materials* B **102** (2003) 291-302.

26. Gunay A., Arslankaya E., Tosun I. *Journal of Hazardous Materials* **146** (2007) 362-371.
27. Zou W., Han R., Chen Z., Jinghua Z., Shi J. *Colloids and Surfaces* A: *Physicochemical and Engineering Aspects* **279** (2006) 238-246.
28. Barala S.S., Das N., Chaudhury G.R., Das S.N. *J. Hazard. Mater.* **171** (2009) 358–369.
29. Ederm E., Karapinar N., Donat R. *Journal of Colloid* and *Interface Science* **280** (2004) 309-314.
30. Singh V., Tiwari S., Sharma A.K., Sanghi S. *Journal of Colloid and Interface Science* **316** (2007) 224-232.
31. Wang X., Zheng Y., Wang A. *J. Hazard. Mater.* **168** (2009) 970–977.
32. Zhou Y.-T., Nie H.-L., Branford-White C., He Z.-Y., Zhu L.-M. J. *Colloid Interface Sci.* **330** (2009) 29–37.
33. Singh K.K., Talat M., Hasan S.H. *Bioresource Technology* **97** (2005) 125.

CHAPTER 6

GENERAL CONCLUSIONS AND RECOMMENDATIONS

6.1 General conclusions

The relatively new and simple melt-mixing technique provides a viable alternative for the preparation of PLSNs. Clinoptilolite-filled EVA and PVA polymer nanocomposites were successfully prepared and their application in metal ion recovery was explored. Based on the aims and objectives of the study, the following recommendations were drawn:

EVA/C composites prepared via the melt-intercalation technique exhibited uniform dispersion of the filler in the zeolite matrix, although at higher zeolite dose, agglomeration occurred, leading to the formation of voids on the surface of the films. As a result, the films become brittle resulting in reduced Young's modulus. Thermal characterization showed that addition of the zeolite retarded the onset of degradation of the EVA, but increased other degradation temperatures such as T_{max} and FDT, an indication of improved thermal stability.

PVA/C composites exhibited better miscibility between the polymer and the zeolite which was attributed to the enhanced hydrogen bonding taking place between the two phases. Results confirmed the preparation of composite materials with a partially intercalated and partially exfoliated structure. Addition of the zeolite was also found to improve both the thermal stability and water retention capacity. The latter observation was anticipated to enhance adsorption properties of the PVA/C composites.

Adsorption experiments showed that adsorption of Cu(II), Pb(II) and Co(II) by EVA/C and PVA/C was influenced by factors such as contact time, pH and initial concentration of the solution. The removal capacity of the two adsorbent composites was found to increase with increasing zeolite loading. Although PVA/C

exhibited a higher removal capacity and shorter equilibrium time when compared with EVA/C, pre-treatment of the filler in the latter was shown to significantly improve the removal efficiency of EVA/C, although this was dependent on the conditioning reagent. Better fitment of the adsorption data into the Langmuir isotherm was evidence that adsorption occurred on a monolayer of identical sorption sites. Although complete recovery of the metal ions from the adsorbent composites could not be achieved, EVA/C exhibited higher reusability of at least up to four times, when compared with PVA/C.

In view of the obtained results, conclusions were therefore drawn that indeed this simple, yet up-scalable melt-mixing technique has huge potential for the preparation of similar composites which could also be used in other environmental remediation applications.

6.2 Recommendations

Based on the results and conclusions drawn, and as a follow-up to this study, the following recommendations may be suggested:

- Although the melt-mixing technique is known to be simple and convenient, its effect on the properties of extruded films is not well established. Thus a comparative study on the properties of materials prepared using this method and one of the conventional methods should be undertaken.

- In this study, the dosage of the filler was in the range of 5% and 30%, since emphasis was on the physicochemical properties (adsorption and ion exchange) of the materials. However it has been reported in the literature that a filler dose of less than 5% can result in remarkable improvements in mechanical properties; a study should also be carried out to determine the effect of loading at less than 5% on the physicochemical properties of the materials.

- PVA/C composites materials exhibited poor mechanical properties, and perhaps the use of a compatibilizer or stabiliser such as vinyl acetate to improve compatibility, and hence the mechanical properties, could be explored in the future.

- Although PVA is a fully degradable polymer (depending on the degree of hydrolysis), EVA on the other hand is non-biodegradable. Therefore a study should be carried out to determine the extent to which the introduction of the zeolite enhances the biodegradability of the polymer.

- In the adsorption experiments, the introduction of impurities such as sulphate and chloride anions, which are often present in real wastewaters, could assist in ascertaining what effect they would have on the overall performance of the adsorbent composites.

- In this present study, pre-treatment of the filler was aimed only at inorganic cationic species. Thus a study in which the zeolitic filler is treated with larger ions such as alkylammonium for targeted organic pollutants should be explored.

APPENDIX

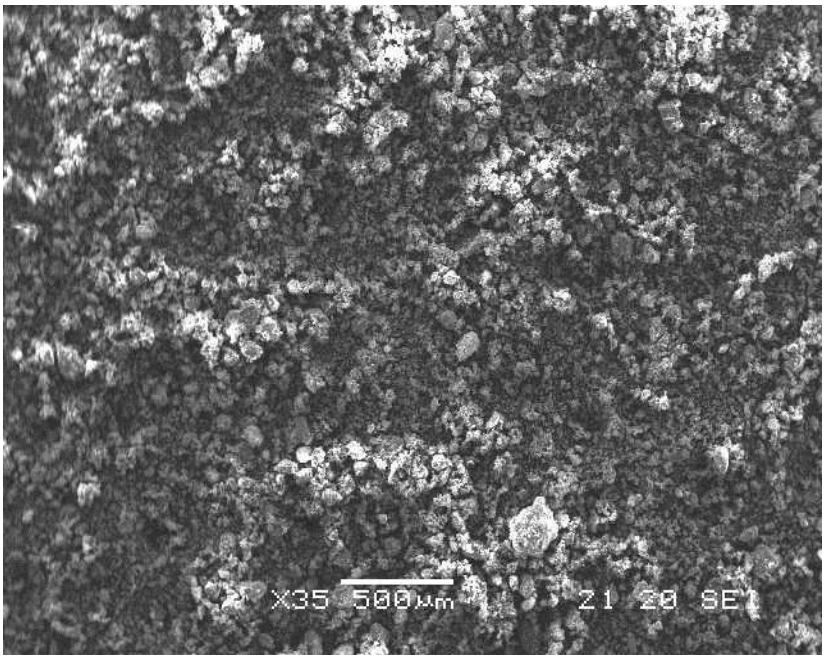

Figure 1: SEM micrograph for NaCl-treated clinoptilolite

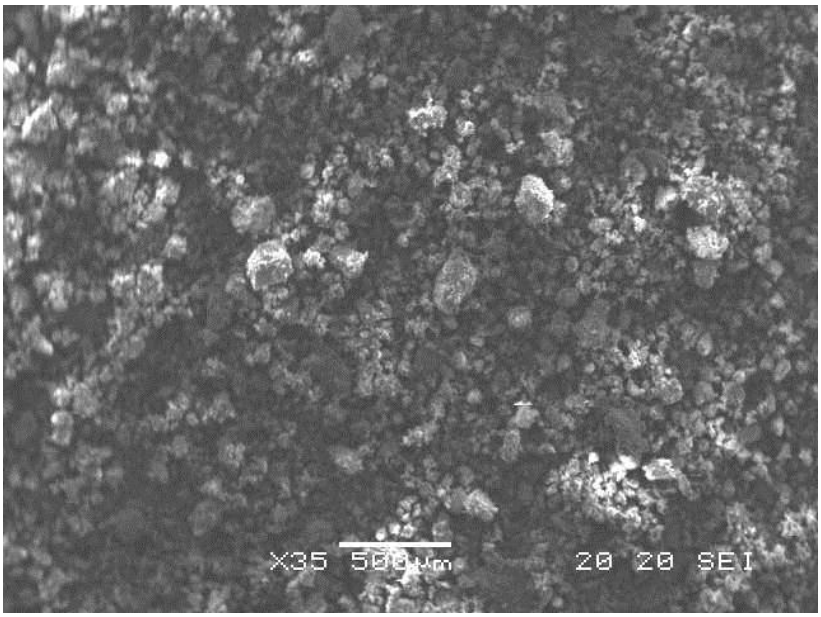

Figure 2: SEM image for KCl-conditioned clinoptilolite

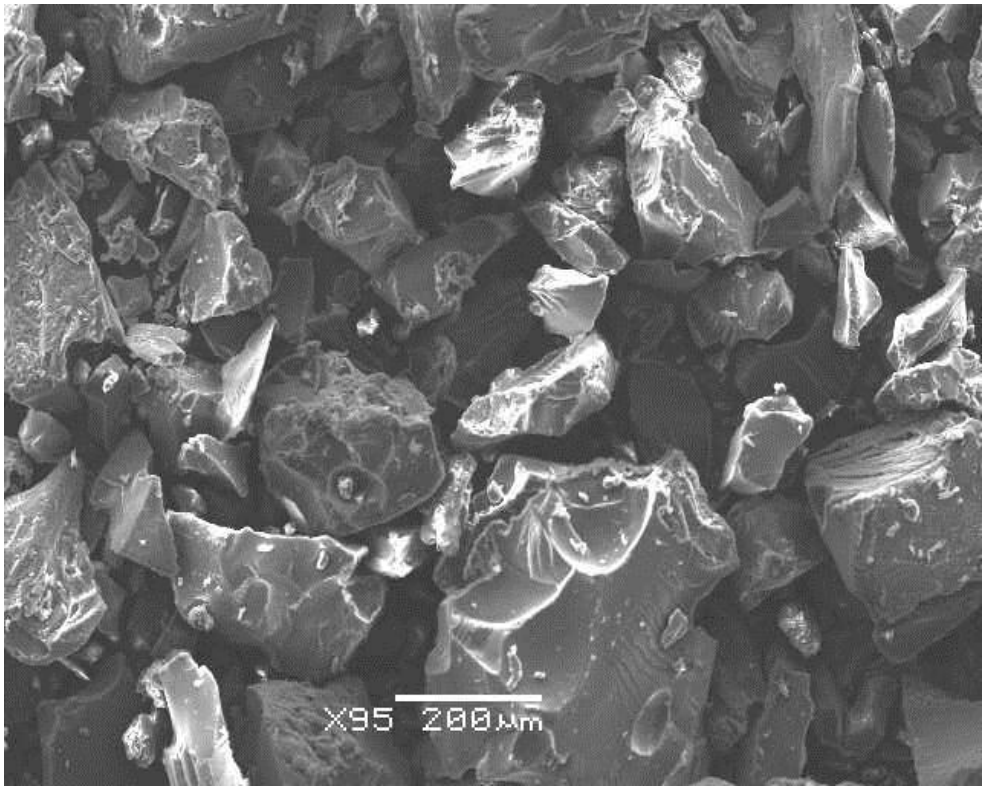

Figure 3: Plain PVA particles at low magnification (X90)

Table 1: BET analysis showing the effect of chemical conditioning on the surface area (SSA) and pore volume (PV) of clinoptilolite

Parameter	A.R.	KCl	NaCl	HCl
SSA (m^2/g)	15.96	16.44	19.50	20.24
PV (cm^3/g)	0.063	0.066	0.061	0.069

Table 2: XRF data showing the effect of NaCl and KCl pre-treatment on 'as received' (A.R.) clinoptilolite

Composition	**% Abundance**		
	A.R.	Na^+	K^+
Al_2O_3	12.42	12.62	12.14
CaO	1.29	0.31	0.14
Cr_2O_3	-	-	-
Fe_2O_3	1.22	0.42	0.17
K_2O	3.77	2.62	10.08
MgO	0.87	0.35	-
MnO	-	-	-
Na_2O	1.31	5.31	-
P_2O_5	-	-	-
SiO_2	71.37	71.11	70.62
SO_3	-	-	-
TiO_2	0.14	0.15	0.15
LOI (930^0C)	6.9	6.5	5.7
TOTAL	**99.29**	**99.13**	**99.23**

*Figures below 0.05 have been replaced with a dash (-)

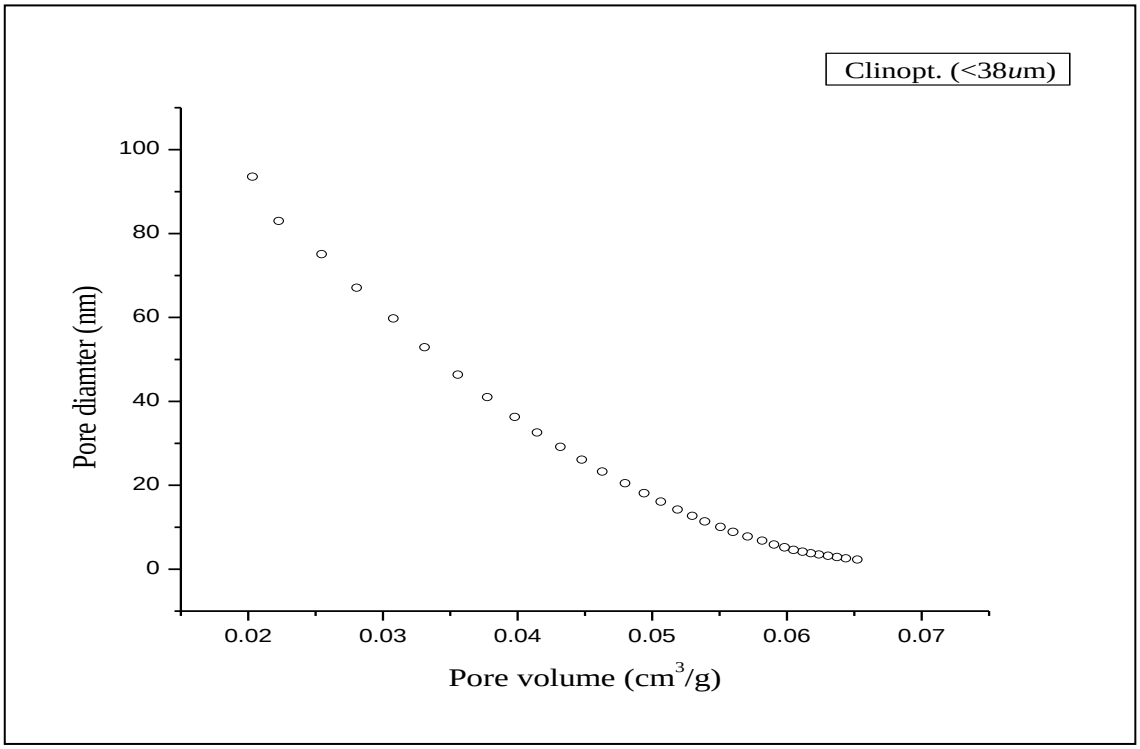

Figure 4: Pore-diameter distribution curve for 'as received' (A.R.) clinoptilolite

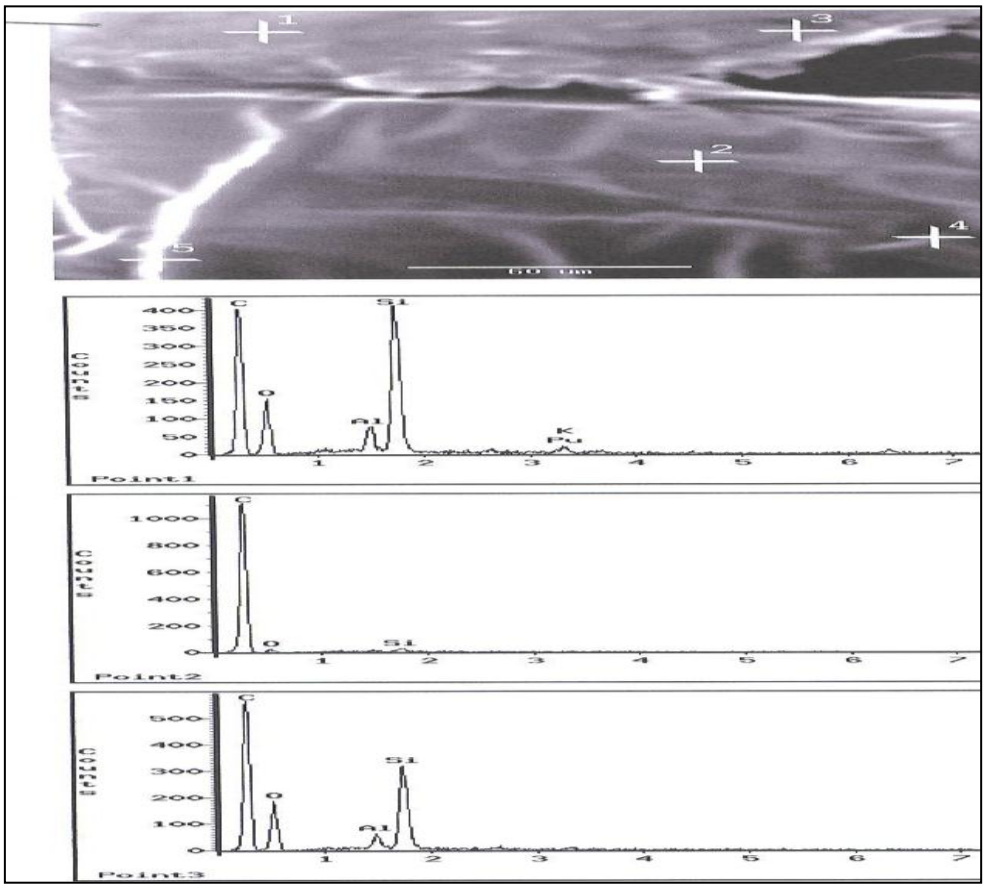

Figure 5: SEM-EDX scan showing the surface of EVA/C filled with A.R. zeolite

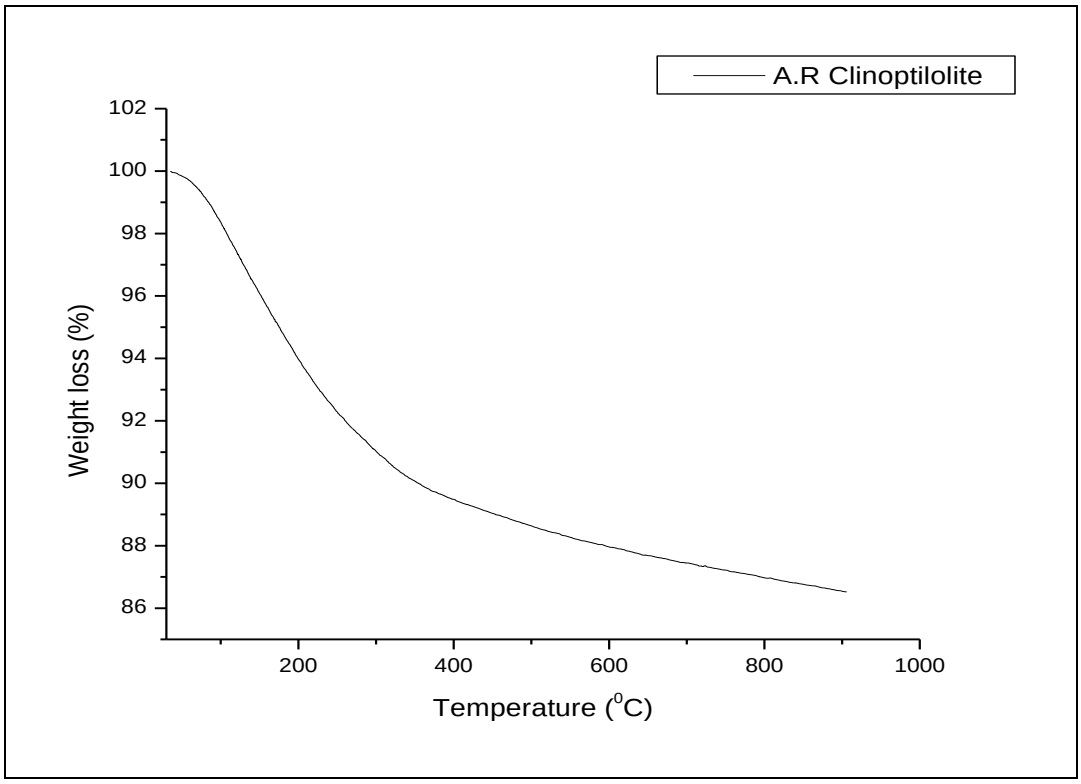

Figure 6: TGA curve for pristine zeolite (clinoptilolite)

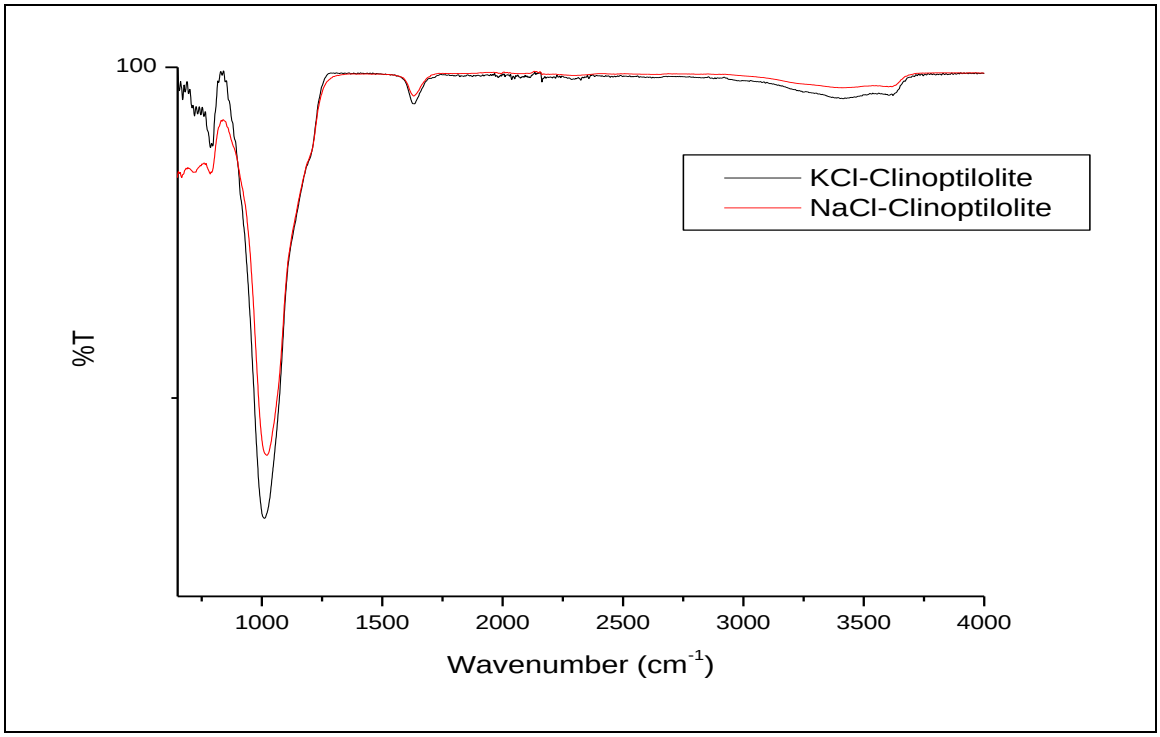

Figure 7: FT-IR spectra for KCl- and NaCl-treated clinoptilolite

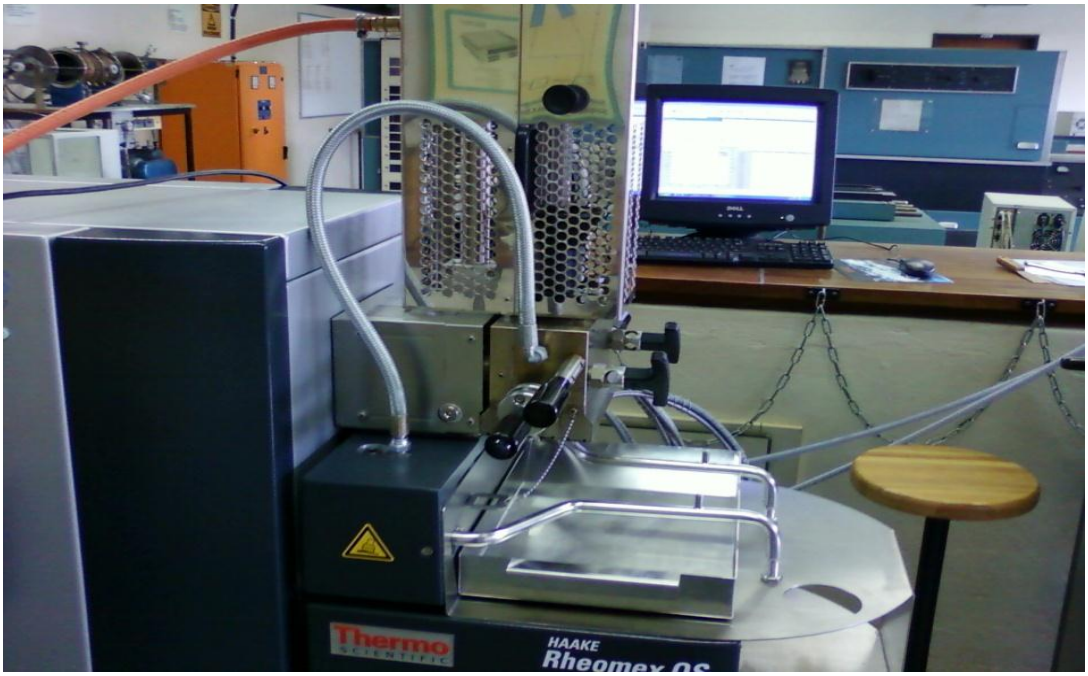

Figure 8: A side view of the Rheomixer (Haake Rheomex OS)

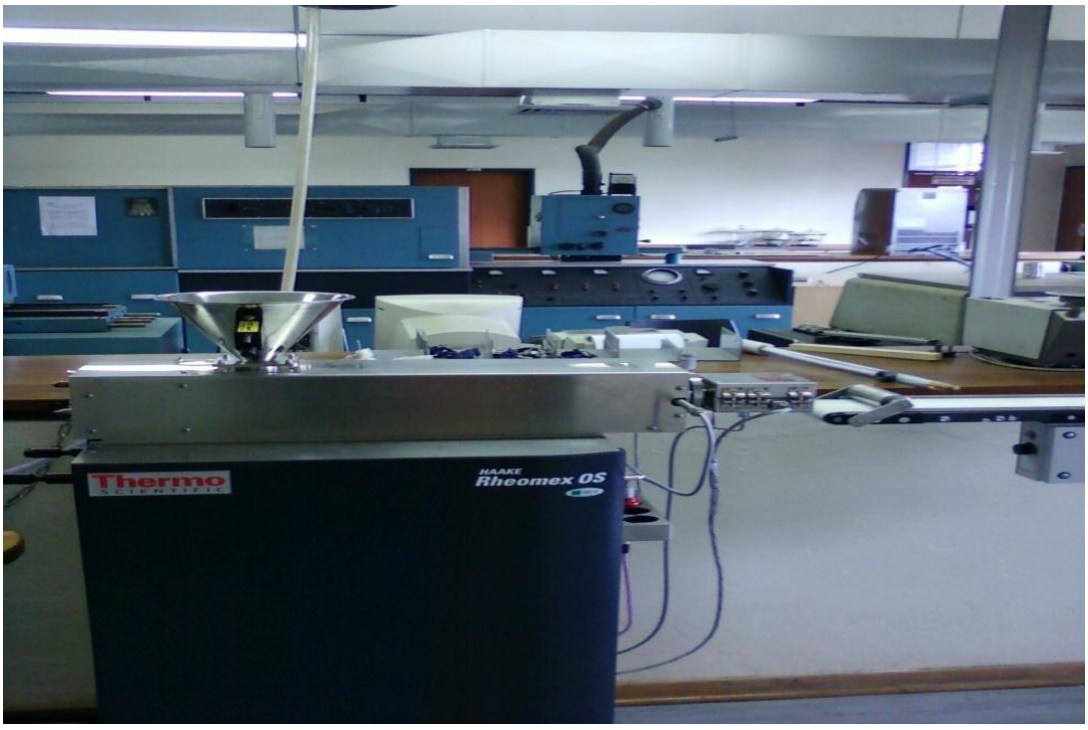

Figure 9: Sectional view of the Haake Rheomex OS single-screw extruder